

JAERI-Review
2002-035



JP0250516



TIARA Annual Report 2001

November 2002

Advanced Radiation Technology Center

日本原子力研究所
Japan Atomic Energy Research Institute

本レポートは、日本原子力研究所が不定期に公刊している研究報告書です。

入手の問合わせは、日本原子力研究所研究情報部研究情報課（〒319-1195 茨城県那珂郡東海村）あて、お申し越してください。なお、このほかに財団法人原子力弘済会資料センター（〒319-1195 茨城県那珂郡東海村日本原子力研究所内）で複写による実費頒布をおこなっております。

This report is issued irregularly.

Inquiries about availability of the reports should be addressed to Research Information Division, Department of Intellectual Resources, Japan Atomic Energy Research Institute, Tokai-mura, Naka-gun, Ibaraki-ken, 319-1195, Japan.

© Japan Atomic Energy Research Institute, 2002

編集兼発行 日本原子力研究所

TIARA Annual Report 2001

Advanced Radiation Technology Center

Takasaki Radiation Chemistry Research Establishment

Japan Atomic Energy Research Institute

Watanuki-cho, Takasaki-shi, Gunma-ken

(Received October 3, 2002)

This annual report describes research and development activities which have been performed with the JAERI TIARA (Takasaki Ion Accelerators for Advanced Radiation Application) facilities from April 1, 2001 to March 31, 2002. Summary reports of 109 papers and brief descriptions on the status of TIARA in the period are contained. A list of publications, the type of research collaborations and organization of TIARA are also given as appendices.

Keywords: JAERI TIARA, Ion Accelerators, Solid State Physics, Radiation Effects in Materials, Materials for Space, Semiconductors, Organic Materials, Inorganic Materials, Nuclear Fusion Reactor, Functional Materials, Radiation Chemistry, Radiation Biology, Nuclear Medicine, Biotechnology, Radioisotope Production, Nuclear Chemistry, Radiation Shielding, Materials Analysis, Microbeam Technology, Accelerator Technology, Safety Control

(Eds.) Masahiro SAIDOH, Yoshihiro OHARA, Hideki NAMBA, Hisayoshi ITOH, Shigeru TANAKA, Hiroshi NARAMOTO, Toshiaki SEKINE, Atsushi TANAKA, Yasuhiko KOBAYASHI, Kazuo ARAKAWA, Michiaki OTSUBO, Satoshi TAJIMA and Susumu TANAKA

原研イオン照射研究施設（T I A R A）平成13年度年次報告

日本原子力研究所高崎研究所
放射線高度利用センター

（2002年10月3日受理）

本年次報告は、原研イオン照射研究施設で、2001年4月1日から2002年3月31日までの間に行われた研究活動の概要をまとめたものである。1) 宇宙用半導体、2) バイオテクノロジー、3) 放射線化学及び有機材料、4) 無機材料、5) 材料解析、6) 核科学およびラジオアイソトープ製造、7) マイクロビーム応用、8) 加速器施設の放射線遮蔽、9) 加速器技術の9部門にわたる109編の研究報告に加えて、施設の運転保守・利用状況、公表された文献、企業・大学等との研究協力関係、研究開発・施設運営組織を収録する。

高崎研究所：〒370-1292 群馬県高崎市綿貫町 1233

編集委員：西堂雅博、小原祥裕、南波秀樹、伊藤久義、田中 茂、楢本 洋、関根俊明、
田中 淳、小林泰彦、荒川和夫、大坪道朗、田島 訓、田中 進

PREFACE

This report covers research and development activities which have been conducted with TIARA (Takasaki Ion accelerators for Advanced Radiation Application) during the period from April 2001 to March 2002, and also gives an outline of the operation of TIARA in the same period.

All accelerators in TIARA, the AVF cyclotron, the 3MV tandem accelerator, the 3MV single-ended accelerator and 400kV ion implanter, have been operated steadily since the construction were completed in 1993, and have supplied the beam-time to the research programs as had been recognized in advance by the Subcommittee of TIARA of Advisory Council for JAERI's Research Facilities. In the same time, available species and energy ranges of ions have been widened to meet requirements from users, and the quality of ion beams have been improved gradually.

In the semiconductor devices for space applications, the output characteristics of InGaP/InGaAs/Ge solar cells were examined with proton beam irradiation to characterize the radiation tolerance. The single event tolerance was investigated for SOI diodes using high-energy ion micro-beam system installed in a beam course of AVF cyclotron. New types of errors were also observed for the commercial 16 Mbit SRAM irradiated with heavy ion particles in addition to the usual single event phenomena. In the development of SiC devices, the radiation effects of SiC-based p-channel metal-oxide-semiconductor field-effect-transistors (MOSFETs) were examined and their radiation tolerance was discussed.

In the field of heavy-ion-microbeam application for biology, the microbeam cell irradiation system that provides precise-numbered heavy ions has been improved in its throughput. Using this system, it was demonstrated that gap junction intercellular communication may have an essential role in the radiation-induced bystander effect in normal human fibroblasts. For the positron emitting tracer imaging system (PETIS), the PETIS was applied to an experiment of iron uptake by an iron absorption maze mutant, and was found to be useful in testing quantitatively the ability of a mutant. For the mutation induction of plants by ion-beam irradiation, new carnation varieties 'Vital Ion series' were rapidly developed by a combination of carbon-ion mutagenization technique and in vitro cell and tissue culture technique.

In the field of radiation chemistry and organic materials, experimental studies of nano-wire formation along an ion trajectory, thin film dosimeter for ion beams, and shape control of etched pores have been continued. The single track gelation of polysilane based on the selective adhesion by the surface treatment is very useful for the positioning of the nano-wires on a substrate. With the aim of the application to nano-scopic electronic devices, it was confirmed that copper nano-wires grew upon the copper electrode through the pores of ion track membranes by the electrode position technique. The thin film dosimeter was applied to measure the dose distribution of 3-45 MeV/u ion beams. The functional nano-filters with a funnel shape were fabricated by using the two-step etching method, as this is a very unique technique. The LET dependence on primary process was investigated by measuring the G-value of oxides generated in aqueous phenol solution after heavy ion irradiation and by using the absorption spectroscopy system for ion beam pulse radiolysis in polystyrene-cyclohexane system.

In the field of nuclear fusion materials, various kinds of experiments were carried out. For simulating the neutron damage and the effects of He and H produced in transmutation reactions, dual or triple ion-beams were irradiated onto the candidate fusion materials (ferritic/martensitic steels, austenitic stainless steels, SiC/SiC composites, Li_2TiO_3 ceramics, etc.). Effects of implanted helium and dose rate on physical, chemical and thermo-mechanical properties (He embrittlement, hardness, high temperature strength) as well as microstructural evolutions (dislocation loops, swelling) during irradiation were investigated.

In the field of inorganic materials, electron radiation effects have been widely investigated. Electrical resistance of hydrogen-charged Pd alloys irradiated by 0.5MeV electrons at low temperatures was measured to study the effect of ordering/disordering of hydrogen isotopes. Change in resistivity of $\text{EuBa}_2\text{Cu}_3\text{O}_y$ irradiated with energetic electrons was also measured to investigate the process of defect production due to electron irradiation. In addition, Fe-Cu

alloys were irradiated by 2MeV electrons to clarify the mechanisms of radiation embrittlement. Structural changes in C_{60} molecules with 7-MeV $^{12}C^{2+}$ ions were investigated using Raman spectroscopy. As for highly efficient photocatalyst, Cr-doped TiO_2 film with concentration gradients was realized with 150keV Cr^+ ion implantation.

As the scientific activities in 2001, the continuing effort has been devoted to the surface modification of inorganic materials by employing the improved techniques. Especially a systematic approach to the modification of electronic structure in TiO_2 has been performed in combination with the calculation based on the first principle (F-LAPW). For the study of the interactions between energetic cluster ions and solid surface channeling experiment was performed by changing the number of atoms in clusters. From the view point of materials science, it should be noted that there appeared several papers treating the spontaneous structure formation or segregation in inhomogeneous systems.

In nuclear science and radioisotope production, the development of positron-emitting radioisotopes to be used in biology was continued. In particular, different materials of a target vial was tested to increase $^{13}NO_3^-$ ions and to decrease $^{13}NO_2^-$ ions in a proton-irradiated water. Using an isotope separator, energy dependence of the yield of endohedral ^{133}Xe fullerene was studied.

In the in-air micro-PIXE analysis, the success of elemental mapping for a slice of animal tissue samples in an atmospheric environment is worthy of one. To calculate the mass thickness and mass of each element for individual environmental samples, the method of quantitative analysis has been established by using a calibration curve of the standard sample. A large solid angle x-rays detector has been successfully developed for high-efficiency element analyses in the living cells.

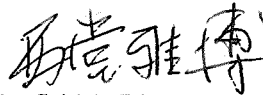
In the field of radiation shielding for accelerator facilities, three experiments have been performed aiming to contribute to the radiation safety of the accelerator facilities. The first one is on the formation of radioactive aerosols under high-energy radiation fields and the experimental results on the effects of neutron energy and added aerosol are discussed in terms of the attachment model. The second is on the successful development of a Bragg Curve Spectrometer (BCS) for fragment spectroscopy in neutron and proton induced reactions. The third one is on the response of personal dosimeters to high-energy neutrons and it was confirmed that the lead-converter was effective to improve the sensitivity of the bubble detector.

In the accelerator technology, a magnetic field of the AVF cyclotron was measured by the NMR magnetometer. A flat-top acceleration for the cyclotron has been designed to minimize the energy spread mainly for microbeam formation. A new feedback loop with a pair of the slits was effective to stabilize the voltage of the single-ended accelerator. A new sputter negative ion source was installed to the tandem accelerator. New emittance monitor with a multiple clearance, an illuminator and a CCD camera was developed. The submicron ion beam system was successfully achieved to produce the beam of 0.1 μm in diameter.

The reception of the users and the supports on utilizations for the experiments, safety management of the radiation controlled area, and other duties have been practiced smoothly.

The Eleventh TIARA Research Review Meeting was held on July 11 and 12, 2002 in Takasaki, of which subjects were reported in this issue. 12 oral and 83 poster papers, and two invited lectures were presented. 287 persons participated the meeting. Results of TIARA concerning to the microbeam technologies and their applications were also presented in occasion of the 8th International Conference on Nuclear Microprobe Technology and Applications which was held at Takasaki on September 8-13, 2002 organized by JAERI.

We owe the progress mentioned above to advices of the Consultative Committee for the JAERI-Universities Joint Research Project and Subcommittee of TIARA of Advisory Council for JAERI Research Facilities.



Masahiro Saidoh, Director
Advanced Radiation Technology Center
Takasaki Radiation Chemistry Research Establishment

Contents

1. Semiconductor for Space	1
1.1 Measurement of Single Event Transient Current Using Collimated Heavy-ion Micro-beam	3
1.2 Analysis of Single Event Error Mode in 16Mbit SRAMs	5
1.3 Radiation Effects on High-efficiency InGaP/InGaAs/Ge Terrestrial Triple-junction Solar Cells	8
1.4 Analysis of Failure Caused by Cosmic Rays in High-voltage High-power Semiconductor Devices (2nd Report)	11
1.5 Study of Charge Collection Mechanism using Multi Line Schottky Barrier Diode	14
1.6 Gamma-ray Irradiation Effects on p-channel 6H-SiC Metal- oxide-semiconductor Transistors	17
2. Biotechnology	21
2.1 Lethality of Single Tobacco Cells Irradiated with Heavy Ions	25
2.2 Mutation Generation in Protoplasts of Chrysanthemum with $^4\text{He}^{2+}$ and $^{12}\text{C}^{5+}$ Ion Beams	28
2.3 Effects of Ion Beams on Shoot Regeneration of Elatior Begonia (<i>B. \timeshiemalis</i>) . Leaf Cultures	31
2.4 Isolation of an Arabidopsis Mutant Defective in Damage Tolerance	33
2.5 Development of the Efficient Mutation Breeding Method using Ion Beam Irradiation	36
2.6 Development of Mutant Varieties "Vital Ion Series" in Carnation by Ion Beam Breeding	39
2.7 Mutation Generation in Chrysanthemum Plants Regenerated from Floral Organ Cultures Irradiated with Ion Beams	42
2.8 Effects of Ion Beam Irradiation on Chrysanthemum Leaf Discs and Sweetpotato Callus	44
2.9 RAPD Analysis of Xanta and Waxy Mutants Induced by Ion Beam Irradiation to Hinoki Cypress(<i>Chamaecyparis obtuse</i>)	47
2.10 Induction of Mutation in Garlic (<i>Allium Sativum L.</i>) by Ion Beam Irradiation	49
2.11 Characters of Tomato cv. First Mutant with Short Internode Induced by Irradiation of $^{12}\text{C}^{5+}$ Ion Beam to the Seeds	52
2.12 Mutation Breeding of Rice, Eggplant and Gloriosa by Ion Beam Irradiation	54
2.13 Regeneration of Variegated Plants From Ion-beam Irradiated Explants of <i>Ficus stipulata Thunb</i>	57
2.14 Effect of Ion Beam Irradiation on the Growth of Netted Melon	

(<i>Cucumis melo</i> L.)	60
2.15 Mutation Induction with Ion Beam Irradiation in <i>Solanum</i> Plants	62
2.16 Instability of Rice Chlorophyll Mutants Induced at M1 by Carbon Ion Beam Irradiation Is Inherited	64
2.17 Studies on Flower Color and Morphological Mutations from In Vitro Chrysanthemum Explants Irradiated with Ion Beams	68
2.18 Induction of Mutation in <i>Delphinium</i> L. by Ion-beam Irradiation	70
2.19 Isolation of Arabidopsis Mutants Defective in Root Hydrotropism	72
2.20 Single-hit Effects on Mammalian Cultured Cells with Heavy-ion Microbeams	74
2.21 Regeneration of Hemopoietic Organs in the Silkworm, <i>Bombyx mori</i> , After the Selective Irradiation of 100 Gy Carbon Ions	77
2.22 Mechanism of Bystander Effect Induced by Precise-numbered Heavy Ions	80
2.23 The Effect to Mammalian Nucleus by Irradiation of Heavy Ion Beams	83
2.24 Dynamical Study on Influence of the CO ₂ Enrichment to the Photoassimilate Transportation using Positron Imaging	86
2.25 Effect of Atmosphere Gas Conditions on Soybean (<i>Glycine Max</i> L.) ¹³ N ₂ Fixation Activity	89
2.26 Absorption and Transfer of the Iron (⁵² Fe) in the Iron Absorption Maize Mutant 'ys1'	92
2.27 Effects of Cold Stress on ¹¹ C Distribution in Rice Plants Detected by PETIS Detector	95
2.28 Water and Trace Element Behavior in a Plant	98
2.29 Positron Imaging Analysis of Assimilation and Translocation of Carbon and Nitrogen Sources in Rice Plant	100
2.30 Uptake of ¹⁸ FDG and ¹³ NO ₃ ⁻ in Tomato Plants	103
2.31 Utilization of Ion Beam-irradiated Pollen in Plant Breeding	105
2.32 Study on the Apoptosis Induction by a Local Damage using Penetration Controlled Ion-beam Exposure	108
3. Radiation Chemistry / Organic Materials	109
3.1 Preparation of Functional Nano-porous Membranes	111
3.2 Preparation of Copper Nanowires using Ion Track Membranes.	113
3.3 Nano-wire Formation and Selective Adhesion on Substrates by Single Track Gelation of Polysilanes	115
3.4 Oxidation Product Yields of Phenol along Heavy Ion Trajectory in Aqueous Solution : Differential G-value.	117
3.5 Crosslinking of Polymers in Heavy Ion Tracks	119
3.6 Primary Process of Radiation Chemistry Studied by Ion Pulse Radiolysis	121
3.7 Dosimetry for 3-45 MeV/u Ion Beams using Thin Film Dosimeters	123

4. Inorganic Materials	125
4.1 Effect of Helium on Ductile-brittle Transition Behavior in Reduced-activation 8Cr-2W Martensitic Steel	127
4.2 Swelling Behavior of F82H Steel Irradiated by Triple/Dual Ion Beams	130
4.3 Microstructure Change with Ion Beam Irradiation in Li_2TiO_3	133
4.4 Effect of Multi Ion-beams Irradiation on Mechanical Properties of Advanced SiC/SiC Composites for Fusion Systems	136
4.5 Damage Evolution in High Energy Multi Ion-irradiated BCC Metals and the Interaction between Gas Atoms (H and He) and Damage Defects	140
4.6 Effects of Dose Rate on Microstructural Evolution in Austenitic Alloys	143
4.7 Investigation of Irradiation-induced Hardening of F82H Steels Irradiated by Dual/Triple Ion Beams	146
4.8 Effect of Triple Ion Beam Irradiation on Mechanical Properties of High Chromium Austenitic Stainless Steel	149
4.9 Effect of Ion Irradiation on Mechanical Property of Materials Contact with Liquid Metal	152
4.10 Microstructure Evolution of the Advanced Fuel Cladding Material by Triple Ion Irradiation	155
4.11 Effects of Irradiation on Microstructure of Zircaloy-2	158
4.12 Effects of Initial Grain Boundary Segregation on Radiation-induced Segregation in SUS 316L Stainless Steel	161
4.13 Effect of an Electric Field on the Formation Process of Dislocation Loops in He^+ -irradiated $\alpha\text{-Al}_2\text{O}_3$	164
4.14 Photoluminescence Properties of Tb Implanted GaN	167
4.15 Formation Process and Stability of Radiation-induced Non-equilibrium Phase in Silicon (III)	170
4.16 Effect of Cr-ion Implantation in TiO_2 : Realization of Impurity Concentration Gradients	173
4.17 Modification of C_{60} Thin Films by 7-MeV $^{12}\text{C}^{2+}$ Ion Irradiation	176
4.18 Investigation of the Resonant Vibration Modes of Self Interstitial Atoms in Hcp Metals by Low Temperature Specific Heat Measurement	179
4.19 Hydrogen Migration in Electron Irradiated Pd-based Alloys	181
4.20 Electron Irradiation Effect in Oxygen-deficient $\text{EuBa}_2\text{Cu}_3\text{O}_y$	184
4.21 Interaction of Frenkel Pairs with Cu Atoms in Fe-Cu Alloys	186
4.22 Radiation Enhanced Copper Segregation Processes in Pressure Vessel Steel Model Alloys during Electron Irradiation	188
4.23 Radiation Effects on Li-vacancy Ordering in NaTi-type Li Compound	191
4.24 Elastic Property of Nanocrystalline Gold after Low-temperature 2 MeV	

Electron Irradiation	193
4.25 ESR Characterization of Activation of Implanted Phosphorus Ions in Silicon Carbide	195
5. Material Analysis	199
5.1 Fast Diffusion of Defect Clusters in Copper under Irradiation with 100-keV Carbon Ions	201
5.2 <i>In-situ</i> Observation of Growth Processes of Transition Metal Nitride Thin Films by Nitrogen-implantation	203
5.3 Preparation of Epitaxial Anatase TiO ₂ Films by Pulsed Laser Deposition	206
5.4 Fabrication of Titanium Dioxide Nanoparticles on Sapphire	208
5.5 Development of High Performance Buffer Materials -Sorption Mechanism of Europium by Smectite -	211
5.6 Electron Emission from Solids by Fast Cluster Impact	214
5.7 Improvement in Surface Roughness of Nitrogen-implanted Glassy Carbon by Hydrogen Doping II	217
5.8 <i>In-situ</i> Analysis on Adsorption and Desorption of Atoms at Liquid-solid Interface by Use of Rutherford Backscattering Spectroscopy	220
5.9 Percolation of Liquid Indium through Porous Media Composing of Ni and C ₆₀	222
5.10 AFM Observation of Nano-sized SiC Dots Prepared by Ion Beam Deposition Method	225
5.11 Encapsulated Structure in Co-C ₆₀ System	228
5.12 Structure and Optical Properties of Ge Implanted with Carbon Ions	231
5.13 Study of Improvement of Ion Irradiation Pd Using a Slow Positron Beam	234
5.14 Anomalous Chemical Bond Formation in Polycarbonate by Cluster Impact	237
5.15 Evaluation of Three Dimensional Microstructures on Silica Glass Fabricated by Ion Microbeam	240
5.16 Uptake of Heavy Metals by Synthetic Mica and Apatite	243
6. Nuclear Science and RI Production	247
6.1 ¹³ NO ₃ Yield in Proton-irradiated Water for Different Materials of a Target Chamber	249
6.2 Dose Effects of the Production Yield of Endohedral ¹³³ Xe-fullerene by Ion Implantation	251
7. Microbeam Application	253
7.1 Development of a High-energy Heavy Ion Microbeam & Single Ion Hit System	255

7.2	Simultaneous Mapping of Fluoride Both in the Tooth and in the Dental Material Filled in a Cavity of the Tooth using PIGE	258
7.3	Development of In-air Micro-PIXE Analysis System	261
	A. Tanaka, K. Ishii, Y. Komori, S. Matsuyama, H. Yamazaki, K. Kubota,	
7.4	Preliminary Study on Quantitative Elemental Analysis for Environmental Samples Using Micro-PIXE	264
7.5	Application of In-air Micro-PIXE Analysis System to the Study of Metabolic Function in the Cell	267
7.6	Development of a Large-solid-angle Multi-element Detection System for High-sensitivity Micro-PIXE Analysis	270
7.7	Analysis of Arsenic Around an Arsenic Mine by μ -PIXE	273
8.	Radiation Shielding for Accelerator Facilities	277
8.1	Effects of Neutron Energy and Added Aerosol on Radioactive Aerosol Formation under High Energy Neutron Irradiation	279
8.2	Development of a Bragg Curve Spectrometer (BCS) for Fragment Spectroscopy in Neutron and Proton Induced Reactions	282
8.3	Response of Personal Dosimeters to High-energy Neutrons	285
9.	Accelerator Technology/TIARA General	289
9.1	Measurement of Secondary Charged Particles with MeV Energy Cluster Ion Irradiation	291
9.2	Study of Secondary Ion Emission Processes from Solid Targets Bombarded by MeV Energy Cluster Ions	294
9.3	Development of a Magnetic Field Monitoring System for the JAERI AVF Cyclotron	296
9.4	Development of the Flat-top Resonator for the JAERI AVF Cyclotron	298
9.5	Present Status of JAERI AVF Cyclotron System	300
9.6	The Number of Operations for Auxiliary Safety Devices	303
9.7	Modification of the Vacuum System for AVF Cyclotron	305
9.8	Energy Stabilization of TIARA 3MV Single-ended Accelerator	308
9.9	Increase of a Negative Heavy Ion Source for the 3MV Tandem Accelerator	311
9.10	Development of Image Analysis Type Emittance Monitor	312
9.11	Improvement of the Injection Electrode System for Forming a Submicron Ion Beam	314
10.	Status of TIARA 2001	317
10.1	Utilization of TIARA Facilities	319
10.2	Operation of JAERI AVF Cyclotron System	321

10.3 Operation of the Electrostatic Accelerators	322
10.4 Radiation Control & Radioactive Waste Management in TIARA	323
Appendix	327
Appendix 1. List of Publication	329
Appendix 2. Type of Research Collaboration	358
Appendix 3. Organization and Personnel of TIARA	360

1. Semiconductor for Space

1.1	Measurement of Single Event Transient Current Using Collimated Heavy-ion Micro-beam	3
	S. Onoda, T. Hirao, J. S. Laird, H. Mori, H. Abe and H. Itoh	
1.2	Analysis of Single Event Error Mode in 16Mbit SRAMs	5
	H. Shindou, Y. Iide, T. Aburaya, S. Kuboyama, S. Matsuda, T. Hirao, T. Ohshima, M. Yoshikawa and H. Itoh	
1.3	Radiation Effects on High-efficiency InGaP/InGaAs/Ge Terrestrial Triple-junction Solar Cells	8
	M. Imaizumi, O. Anzawa, S. Kawakita, T. Ohshima, M. Yamaguchi, H. Itoh and S. Matsuda	
1.4	Analysis of Failure Caused by Cosmic Rays in High-voltage High-power Semiconductor Devices (2nd Report)	11
	H. Matsuda, I. Omura, Y. Sakiyama, S. Urano, S. Iesaka, H. Ohashi, T. Hirao, H. Abe, H. Itoh, H. Mori and S. Onoda	
1.5	Study of Charge Collection Mechanism using Multi Line Schottky Barrier Diode	14
	H. Mori, T. Hirao, J. S. Laird, S. Onoda and H. Itoh	
1.6	Gamma-ray Irradiation Effects on p-channel 6H-SiC Metal- oxide-semiconductor Transistors	17
	T. Ohshima, K. K. Lee, A. Ohi, M. Yoshikawa and H. Itoh	

This is a blank page.

1.1 Measurement of Single Event Transient Current Using Collimated Heavy Ion Micro Beam

S. Onoda*, T. Hirao**, J. S. Laird**, H. Mori*, H. Abe**, H. Itoh**

Graduate School of Engineering, Tokai University*

Department of Material Development, JAERI**

1. Introduction

Semiconductor devices used in space are irradiated with high-energy space radiations. The high dense electron-hole pairs are generated and lead to system failures, when these radiations path through the devices. Such kinds of phenomena are called Single Event Effect (SEE). In order to develop devices with high radiation tolerance, it is important to clarify the mechanisms of SEE. AVF cyclotron is useful tool in simulating SEE in space, because the energy of ions from the accelerator is similar to that of space radiations. In this work, we have measured the single event transient current using a collimated high-energy micro-beam that has been developed by the micro-collimator system and evaluated the single event tolerance of SOI diode.

2. Beam Formation

Heavy ions used in this study were 322 MeV Kr-ions accelerated with an AVF cyclotron at JAERI Takasaki. The range and Liner Energy Transfer (LET) of Kr with the energy of 322 MeV in silicon are 39.6 μm and 38.8 MeVcm^2/mg , respectively. The beam intensity was chosen as low as 100 ions/sec in order to reduce the effect of radiation damage. The beam intensity was reduced by using an attenuator installed on the beam line. The number of incident ions was monitored using a Faraday cup and a silicon surface barrier detector (SSD) placed in the target chamber. The energy

spectra were also measured with SSD and multi-channel analyzer (MCA) to estimate the beam quality. Figure 1 shows the energy spectra of 322 MeV Kr-ion beams passing through the micro-collimators with diameters of 20 μm . As shown in figure, the numbers of scattered ions were much smaller than that of non-scattered ions. Details of the procedure to form the collimated micro-beam and the estimation method of the beam quality have been described in the previous paper¹⁾

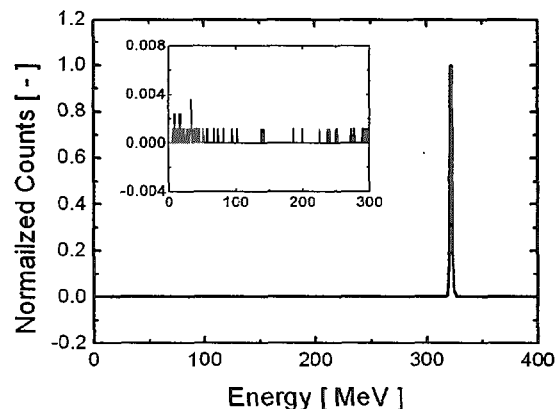


Fig. 1 Energy Spectrum of 322 MeV Kr-ion beams passing through micro-collimator of 20 μm in diameter. The inset figure is drawn with the magnified scale. The ordinate indicates the ion counts normalized by the peak count and abscissa indicates the ion energy, both two figures.

3. Sample

The silicon on insulator (SOI) n^+p diode was used in this study. The schematic diagram and SEM image of the sample are shown in figure 2. The top silicon layer,

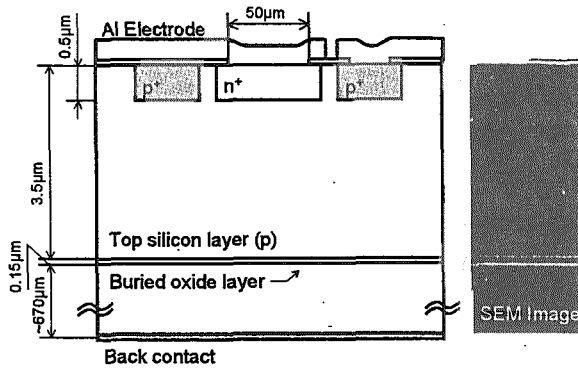


Fig.2 Cross sectional schema of the SOI n⁺p junction diode. SEM image is also displayed.

buried oxide layer and implanted n⁺ layer thickness are about 3.5, 0.15 and 0.5 μm, respectively. The sample was mounted on a chip carrier with 50 ohm double-ended micro striplines. Transient current induced in the sample was measured by using a 3 GHz oscilloscope under a bias voltage of +2 V.

4. Results and Discussion

Figure 3 shows the single event transient current induced by the irradiation of 322 MeV Kr-ions in the SOI diode. The obtained peak current, fall time and rise time are 630 μA, 160 ps and 6.3 ns, respectively. The collected charges, which is calculated from time integration of the waveform, is 1.1 ± 0.1 pC.

To examine the obtained value of charges for validity, the ion-induced charges (Q) are calculated by using the following simple equation,

$$Q = \frac{LET \cdot \rho \cdot q}{G} x, \quad (1)$$

where, LET , ρ , q and x are LET , the density of target material, elementary charge and length, respectively. The value of G is the energy of the electron-hole pair generation in the target material (3.6 eV for silicon). Assuming that the charge collection is

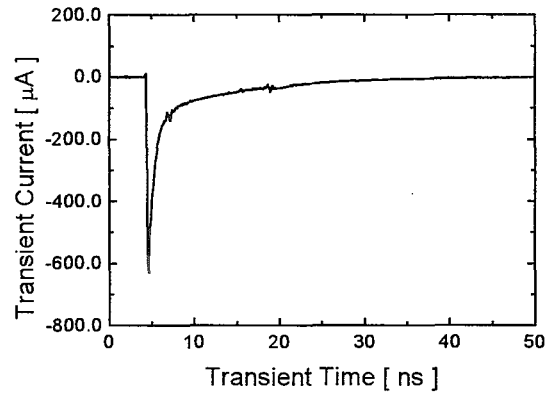


Fig.3 Single event transient current on n⁺/p SOI diode induced by Kr-322 MeV ion.

limited by the buried oxide layer, $x = 3$ μm (top silicon layer thickness) is applied for this calculation. The calculated value of the charges is 1.2 pC. The measured value is almost the same as the calculated charges in the top silicon layer. Although the ions path through the buried oxide layer, the charges are collected only from the top silicon layer. Therefore, it is obviously suggested that the buried oxide layer limits the charge collection of the n⁺p SOI diode. Similar results were also reported for p⁺n SOI diodes²⁾.

5. Summary

Transient current induced in n⁺p SOI diode by high-energy ions (Kr-322 MeV) was experimentally obtained. The collected charge of the n⁺p SOI diode is limited by the buried oxide layer like a p⁺n SOI diode.

Reference

- 1) H. Mori, T. Hirao, T. Ohshima, S. Onoda and H. Itoh, TIARA Annual Report 1999, 3-4.
- 2) T. Hirao, T. Hamano, T. Sakai and I. Nashiyama, Nucl. Inst. and Meth. B, (1999) 260-263.

1.2 Analysis of Single Event Error mode in 16Mbit SRAMs

H.Shindou*, Y.Iide*, T.Abura^y*, S.Kuboyama*, S.Matsuda*,
 T.Hirao**, T.Ohshima**, M.Yoshikawa** and H.Itoh**
 National Space Development Agency of Japan (NASDA)*
 Department of Materials Development, JAERI**

1. Introduction

Memory devices such as Static RAMs are widely used at the electronic systems loaded into the spacecraft. As the requirement of the space mission becomes more and more advanced, the high-density memory cells become indispensable to achieve the mission. But it is well known that many parameters that defining characteristic of a CMOS device are scaled as the technology is downsized, and that the radiation tolerance tends to decline as the technology generation progresses^{1), 2)}. Several new types of Single Event Effects, such as Multiple Bit upsets (MBU), Single Event Functional Interrupt (SEFI), Heavy ion induced snapback phenomena, can be observed and studied in state of art memory devices³⁾⁻⁶⁾. So it is very important to analyze the mechanism about these errors and to construct the effective error correction method in order to apply high-density memory devices to the system used in space.

This paper provides the heavy ion irradiation test results on 16Mbit Static RAMs. Some new types of Single event error were observed in addition to normal Single Event Upset (SEU).

2. Experimental

2.1 Sample Devices

The sample device used for this experiment is commercial 16Mbit Static Random Access Memory (TC55W1600FT) organized as 1,048,576 words by 16bits / 2,097,152 words by 8bits (two modes can be chosen) manufactured by TOSHIBA. The 0.18-micron CMOS process technology was applied to this. This device operates at power supply voltage of +2.3V to +3.1V. The chip is housed in a 48-pin thin-small outline package. In this experiment, the supply voltage was set to its minimum recommended.

2.2 Test Setup

Sample devices were controlled by a small microprocessor unit card. Specific data were written to the sample device prior to irradiation. The experiments were performed with mono energetic ions obtained from the heavy-ion accelerator at Japan Atomic Energy Research Institute (JAERI) Takasaki. The direction of the incidence is perpendicular to the chip surface. Memory cells were set all "0" state or all "1" state in this experiment.

3. Results and discussion

Table 1 shows the cross section value about normal Single Event Upset (SEU). It was possible to calculate the cross section only when irradiating N ion, because another error mode, "Stack Error" (mentioned later) occurred when irradiating Ne, Ar and Kr ion, and we cannot collect enough data to calculate the cross section. The significant difference of tolerance between all "0" state and all "1" state wasn't observed.

The representative examples of the irradiation test result were shown in Table 2. Two types of the error were identified besides the normal SEU. One is the "Multiple bit Upset (MBU)" ("Mode II" in Table 1). Figure 1 shows the typical pattern of the MBU cluster. We used the physical bit-map analysis method⁷⁾ in order to investigate the shape of the error cluster. Most of the errors form clusters when irradiating Ne, Ar and Kr ion. But some normal cells are also intermittently included in the error cluster. The size of these clusters tends to increase with the increase of LET. It is considered that these MBU clusters are directly occurred by the ion incidence on the memory cell. Further investigation about the physical memory cell size and the arrangement

of the cell is necessary to obtain the collect shape of the cluster. Now we are investigating about this.

The other type of the error is the "Stuck error" ("Mode III" and "IIIa" in Table 2). Stuck error means that the error data could not be corrected even if a correct value was re-written to the memory cell unless turn off the power supply. The occurrence of the stuck error is always accompanied by the increase of the I_{dd} value. This error always occurred suddenly. And while the I_{dd} value was keeping normal, no sign about this error was observed. In some case, the number of errors increases even if it stops irradiation. From this point, it is possibly said that the snapback phenomena⁵⁾ occurred. Representative error pattern of this mode is shown in Figure 2. This error is composed of the line error and a lot of cluster error. After re-written the collect data to the memory cell, some cluster errors were disappeared, but most of the errors are stuck. In all cases, when turning on again after switching off the power, all of the bit work normally. In this chip, the V_{dd} is supplied only from the right side of the chip in Figure 2.

From the result, it is thought that the Latch-up current generated at the cross point of the line error by the incidence of heavy ion, and the irregular supply voltage drop occurred at the left side of the chip. So, many of the memory cell which located on this irregular region cannot work normally and stuck. Further studies are necessary to clarify the mechanism about the

stuck error.

4. Conclusion

The analysis result of the Single Event Error mode in the commercial 16Mbit SRAM is shown. Some new types of error were observed in addition to normal SEU.

References

- 1) P. E. Dodd, et al., "Impact of Technology Trends on SEU in CMOS SRAMs," IEEE Trans. Nucl. Sci. 43 (1996) 2797-2804.
- 2) L. W. Massengill, "Cosmic and Terrestrial Single-Event Radiation Effects in Dynamic Random Access Memories," IEEE Trans. Nucl. Sci. 43 (1996) 576-593.
- 3) O. Musseau, et al. "Analysis of Multiple Bit Upsets (MBU) in a CMOS SRAM," IEEE Trans. Nucl. Sci. 43 (1996) 2879-2888.
- 4) R. Koga, et al., "Single Event functional interrupt (SEFI) sensitivity in microcircuits," Proceedings of RADECS97 (1997) 311-318.
- 5) R. Koga, et al., "Heavy ion induced snapback in CMOS devices," IEEE Trans. Nucl. Sci. 36 (1989) 2367-2374.
- 6) A. Makihara, et al., "Analysis of Single-Ion Multiple-Bit Upsets on High Dencity DRAMs," IEEE Trans. Nucl. Sci. 47 (2000) 2400-2404.
- 7) N. Nemoto, et al., "A Nondamaging Beam Blanking SEM Test Method and its Application to Highly Integrated Devices," IEEE Trans. Nucl. Sci. 48 (2001) 2187-2192.

Table 1: SEU cross section

Ions	SEU Cross Section [cm^2/bit]
N	4.79×10^{-9} (at all "0"), 4.72×10^{-9} (at all "1")
Ne, Ar, Kr	Cannot obtain enough data to calculate (Stuck error occurred immediately.)

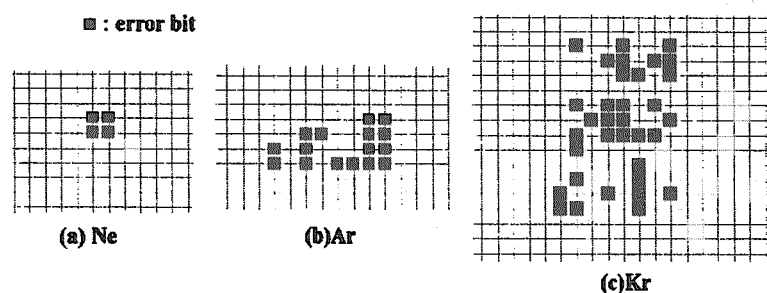
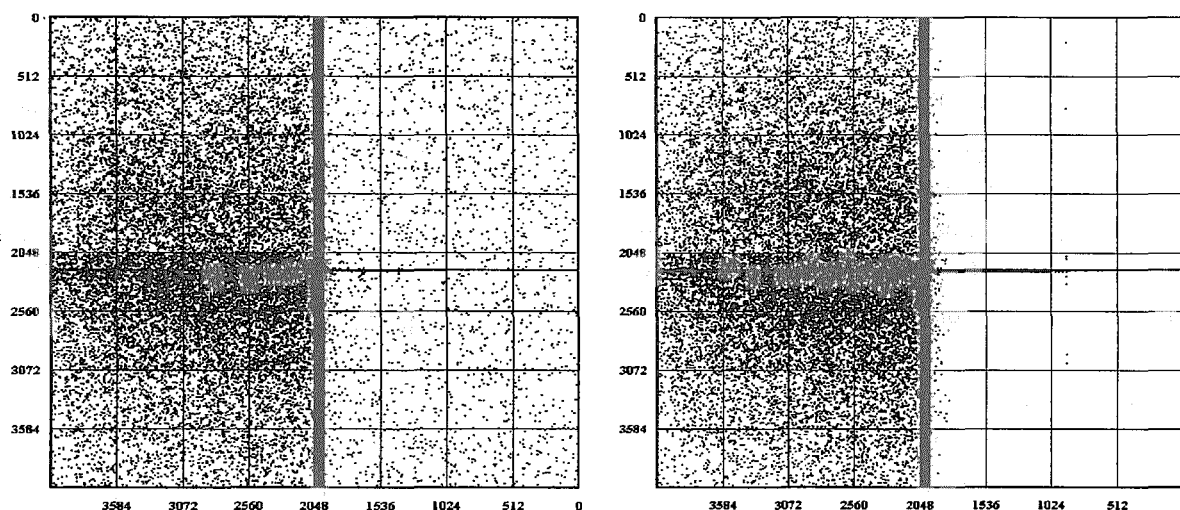


Fig. 1: The typical pattern of the SEU cluster (Physical Bit Map).

Table 2: The representative example of the Error mode in 16Mbit SRAMs

Ions	Fluence [particles/cm ²]	Idd [mA] when after irradiation ^{(*)1}	No. of Error [bit]	No. of Stuck Error ^{(*)3} [bit]	Error mode ^{(*)4}
N	3742	Initial ^{(*)2}	286	0	I
N	45972	4.4	5587	1956	II
N	51206	20.0	51692 ^{(*)5}	58692 ^{(*)6}	IIIa
Ne	16.7	Initial	20	0	II
Ne	20.7	14.4	23442	23302	III
Ne	23.4	23.0	56736	65324	IIIa
Ar	11.5	Initial	54	0	II
Ar	23.5	2.7	2122	2083	III
Ar	23.5	12.9	26467	27525	IIIa
Kr	10.5	Initial	48	0	II
Kr	10.5	2.6	1881	1837	III
Kr	10.5	20.9	20941	21384	IIIa

^{(*)1} At all cases, Idd increases like a step function, not gradually. In this experiment, if the increase of Idd was observed, irradiation was stopped immediately at the point. ^{(*)2} "Initial" means that Idd was the same as the initial (about 0.6mA) when ending irradiation. ^{(*)3} "Stuck Error" means that the error data could not be corrected, even if rewrite a correct value. ^{(*)4} The classification of the "Error mode" is as follows. Mode I : Normal SEU, Mode II : Normal SEU + MBU, Mode III : Normal SEU + Stuck error, Mode IIIa : Stuck error occurs. And the number of errors increases even if it stops irradiation unless turn off the power supply. ^{(*)5} ^{(*)6} See also Fig. 2.



(a) The error bit map immediately after N ion irradiation ending. (This data corresponds to the data of ^{(*)5} in Table 2.)

(b) The error bit map after rewriting correct data (after (a)). (This data corresponds to the data of ^{(*)6} in Table 2.)

Fig. 2: The typical pattern of the physical error bit map when the stuck error occurs.

1.3 Radiation Effects on High-Efficiency InGaP/InGaAs/Ge Terrestrial Triple-Junction Solar Cells

M. Imaizumi*, O. Anzawa*, S. Kawakita*, T. Ohshima**, M. Yamaguchi***,
H. Itoh**, and S. Matsuda*

Department of Research and Development, NASDA*, Department of Material
Development, JAERI**, Toyota Technological Institute***

1. Introduction

Despite that developing special electronic devices for space use costs very high, the market of such devices is not sufficiently large for business. Therefore, using commercial devices, which are supposed to be durable in space environment, for space application has been considered recently. Meanwhile, for space solar cells, InGaP/GaAs/Ge triple-junction cells have shown excellent performance and now become the majority of space solar cells^{1,2)}.

In Japan, National Space Development Agency of Japan (NASDA) has concentrated only on development of Si space solar cells so far, while a triple-junction cell with high efficiency over 30% (AM1.5) were achieved by Japan Energy Corp. (JE) as a terrestrial cell under one of the NEDO projects³⁾. In this report, irradiation effects upon the terrestrial triple-junction cell are shown and durability of the cell in space, namely, radiation tolerance and its dependency of output parameters on the fluence of radiation particles is discussed.

2. Experimental

High-Efficiency terrestrial triple-junction solar cells produced by JE were adopted for this study. The design of the cell utilizes InGaAs with indium content of 1% as a middle cell material. Since the cell is optimized for AM1.5D spectrum, the thickness of the InGaP top cell is relatively thick compared to that of triple-junction space cells. Efficiency of as high as 31.3% with the cell area of 25 cm² has been

realized under 1sun condition³⁾, but the cell size for this study is 1cm×1cm.

Irradiations of 1 MeV electrons and 3 and 10 MeV protons onto the cells were performed. In the case of 10 MeV proton irradiation, AM0 simulated light was illuminated to a cell in the irradiation chamber during the irradiation, and the irradiation was interrupted at each designated fluence and a current-voltage (I-V) characteristic of a test cell was measured. Therefore, the change in I-V parameters of a cell can be collected immediately during irradiation experiment (simultaneous method). On the other hand, in the case of 1 MeV electron and 3 MeV proton irradiations, the particles of designated fluences were irradiated to different cells under dark condition, and the I-V curve of each cell was measured after the irradiation experiment (sequential method).

Protons with various energies (30 keV-10 MeV) were irradiated to the terrestrial triple-junction cells. According to TRIM calculation, protons with energy of 30 keV, 50 keV, 100 keV, 150 keV, 380keV, 1 MeV, and 3 MeV are supposed to stop at approximately the top cell junction, the top cell base region, the top/middle cell interface, the middle cell junction, the middle cell base region, the vicinity of the bottom cell junction (several microns under the epitaxial layer/Ge substrate interface), and the bottom cell base region, respectively; and 10 MeV protons pass through entire the cell. The fluence was kept at 1×10^{12} cm⁻². The I-V characteristics were measured by the sequential method described above.

3. Results and Discussion

Typical photovoltaic performance was measured under Xe-lamp single light source AM0 solar simulator (1sun), and the values were short circuit current density (J_{sc}) of 16.0 mA/cm², open circuit voltage (V_{oc}) of 2.54 V and conversion efficiency (η) of 25.3%. A typical I-V curve of the cell under AM0 is shown in Fig. 1.

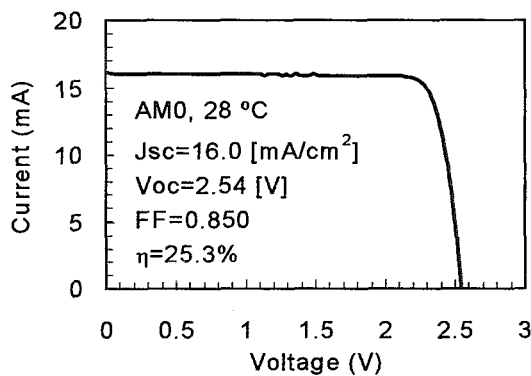
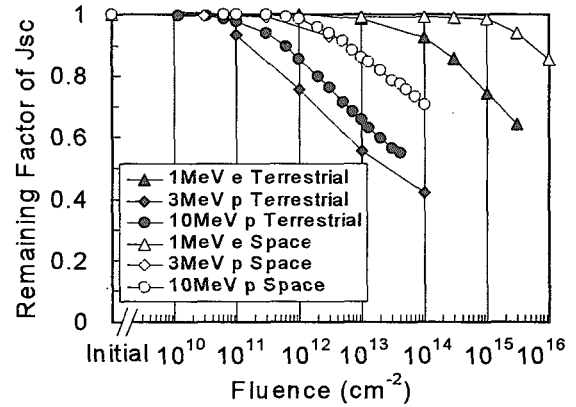


Fig. 1 Typical Current-voltage characteristic of the InGaP/InGaAs/Ge terrestrial triple-junction solar cell.

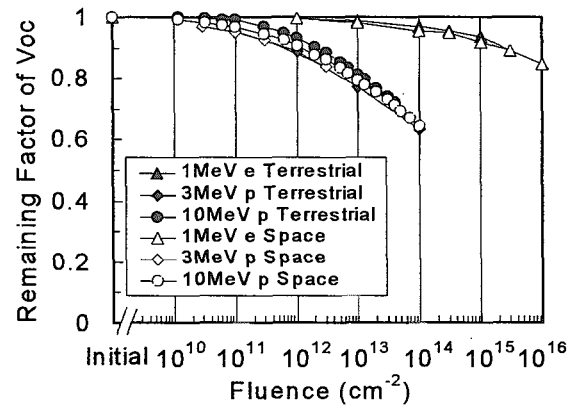
Degradation trend in J_{sc} , V_{oc} and maximum power (P_{max}), which corresponds to η , expressed as the remaining factor are shown in Fig. 2 (a), (b) and (c), respectively (solid symbols). For reference, the degradation characteristics of one of the best triple-junction space cell are shown in the figures as well (open symbols)¹⁾.

For J_{sc} , the fluence for the terrestrial cell is one order (10 MeV protons) or one and half order (1 MeV electrons and 3 MeV protons) of magnitude lower than that for the space cell. This is because of the difference in a current limiting sub-cell, top cell for the space cell and middle cell for the terrestrial cell. For V_{oc} , regardless to the irradiated particles, there is almost no difference in degradation between the terrestrial cell and the space cell. This should be because the photovoltage is mainly determined

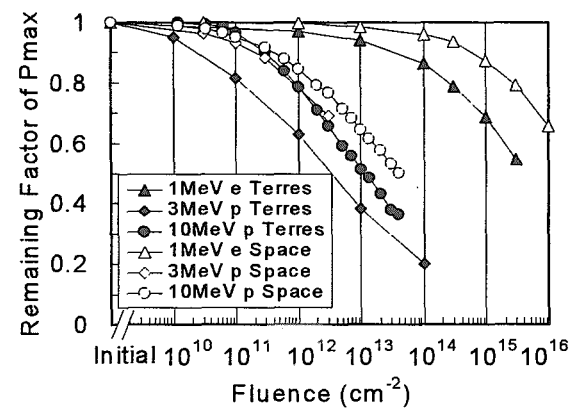
by a combination of materials of sub-cells. Consequently, for P_{max} , the terrestrial cell degrades a half order (10 MeV protons) or an



(a) Short-circuit current density



(b) Open-circuit voltage



(c) Maximum power (Efficiency)

Fig. 2 Degradation in (a) J_{sc} , (b) V_{oc} and (c) P_{max} (η) of the terrestrial triple-junction cell due to 1 MeV electron, 3 MeV proton and 10 MeV proton irradiations (solid symbols). For a reference, the degradation characteristics of a space triple-junction cell are shown as well (open symbols).

order (1 MeV electrons and 3 MeV protons) of magnitude faster in fluence in comparison with the space cell. Indeed distinct difference in radiation tolerance of output power is observed between the terrestrial cell and the space cell, but the radiation tolerance of the terrestrial cell is equivalent to that of GaAs single junction cells⁴⁾. Therefore, the terrestrial cell can be applied to space missions of which radiation environment is predicted to be moderate.

The relation between the remaining factor of performance parameters (J_{sc} , V_{oc} , P_{max} and fill factor (FF)) and proton energy is indicated in Fig. 3. This characteristic is a sort of the relative damage coefficient,

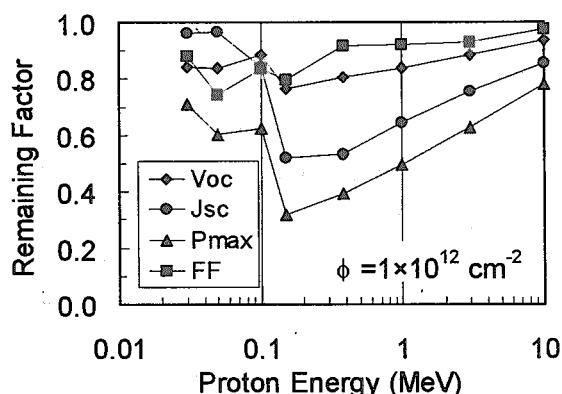


Fig. 3 Relation between the remaining factor of J_{sc} , V_{oc} , P_{max} and FF and irradiated proton energy.

Among the protons with the variety of energies, protons with energy of 30 keV, 150 keV and 1 MeV are considered to damage mainly the top, the middle and the bottom cell junctions, respectively. Therefore, local minimums are expected to be observed on remaining factor of cell parameters at these energies. In Fig. 3, the parameters except J_{sc} show local minimum not at 30 keV but at 50 keV. This shift is likely to derive from an error in the TRIM calculation or depth distribution of defects. At 150 keV, there observed greatest degradation for the terrestrial cell, especially for

J_{sc} , in the energy range. This should be because the InGaAs middle cell has the least radiation tolerance among the three sub-cells and the cell is current limiting in the design of the terrestrial cell.

Observation of change in quantum efficiency of the top cell and the middle cell due to the proton irradiations confirmed that not only the InGaAs middle cell but also the top InGaP cell is degraded greatly in the case of 150 keV. In the case of 10 MeV, only the middle cell significantly degrades, while almost no degradation is observed for the top cell.

In the energy region of >150 keV, however, degradation becomes smaller in proportion to the energy and no minimum appears at 1 MeV. The reasons of the proportional tendency are thought to be as follows: first, the contribution of the Ge bottom cell is basically small, second, the Ge junction characteristic is originally poor in the triple-junction cell so that the radiation damage does not influence so much on the performance.

An increase of reverse bias leak current due to the irradiation showed similar trend to Fig. 3. This implies that the proton irradiation generates defects which act as recombination center of minority-carriers (current pass under reverse bias), and increase in concentration of the center leads degradation of J_{sc} , as well as the degradations of V_{oc} and FF.

References

- 1) N. S. Fatemi et al., *Proceedings of 17th EU PVSEC*, Munich, (2001) in press.
- 2) R. R. King et al., *Proceedings of 28th IEEE PVSC*, Anchorage, (2000) 998-1001.
- 3) T. Takamoto et al., *Proceedings of 28th IEEE PVSC*, Anchorage, (2000) 976-981.
- 4) B. E. Anspaugh, *GaAs Solar Cell Radiation Handbook*, JPL Publication 96-9, NASA, 1996.

1.4 Analysis of Failure Caused by Cosmic Rays in High-Voltage High-Power Semiconductor Devices (2nd Report)

Hideo Matsuda*, Ichiro Omura*, Yoko Sakiyama*,
Satoshi Urano*, Susumu Iesaka*, Hiromichi Ohashi**,
Toshio Hirao***, Hiroyuki Abe***, Hisayoshi Itoh***,
Hideki Mori****, Shinobu Onoda****

Toshiba Corporation, Semiconductor Company *

Toshiba Corporation, R&D Center **

Department of Material Development, JAERI***

Graduate School of Engineering, Tokai University****

1. Introduction

High power semiconductor devices have been widely used in key industries, for instance, traction, transmission, etc. A failure of such power devices induced by cosmic rays at the sea level has been recently observed ¹⁾. At the present stage it is considered that high power devices fail or breakdown by interaction between Si and cosmic rays, e.g., high energy neutrons and protons.

The aims of this work is (1):to verify the equivalence between the failure rates obtained by proton irradiation and those by actual cosmic rays and (2):to examine the failure rates for various devices at their nominal voltage, which are quite useful for designing high power devices having high performance as well as high reliability. In order to clarify the failure mechanisms, we have investigated the failed areas in tested devices.

2. Experiments

2.1 Proton irradiation

An AVF-cyclotron at TIARA has been used for proton irradiation. Parameters are proton energy and fluence. The failure rate of high power devices was derived from the number of failures divided by

proton fluence. The block diagram of test system is schematically shown in Fig.1.

2.2 Heavy ion irradiation

An 3MV-tandem-accelerator has been used for heavy ion irradiation. A micro-beam of 15MeV carbon ion was scanned on the test devices at 2 microns per pitch. The block diagram of test system is shown in Fig.2.

3. Results and discussion

3.1 Proton irradiation

The test devices suddenly failed by proton irradiation during voltage supplied. The phenomenon is very similar to the failure caused by actual cosmic rays. Fig.3 shows the failure rate as a function of supplied electric field. The horizontal axis represents the maximum electric field in the devices. The vertical axis represents the failure rate divided by irradiated particle fluence. The failure rate increases as irradiation energy or electric field increases. The slope of the failure rate obtained in this test is similar to that of the failure rate by actual cosmic rays or by neutrons irradiation²⁾. The test results reflected the failure by actual cosmic rays.

3.2 Heavy ion irradiation

The charges in tested devices have been generated by micro beam formed using 15MeV carbon ion. Fig.4 shows the generated charges. The horizontal axis represents the time. The vertical axis represents the current. Left side shows the current at 800V voltage supplying and right side shows the current at 850V voltage supplying. The generated charges have been calculated by integrating the current. The generated charges, which value is around 100pC at 800V, have been multiplied up to 100nC as applied voltage increase up to 850V. As applied voltage increases still more, multiplied charges increase still more, avalanche breakdown occurs and the device will fail.

4. Conclusion

A preliminary examination of failures in high power devices due to proton and heavy ion irradiation has been performed. The test results obtained by proton irradiation are similar to those reported previously²⁾. The propriety of our measurements for device failure has been verified. The device will fail by avalanche multiplication of generated charge.

References

- 1) H.Matsuda, et al, "Analysis of GTO Failure Mode During DC Voltage Blocking", Proc. of the 6th ISPSD, (1994) pp221-225.
- 2) H.R.Zeller, "Cosmic Ray Induced Failures in High Power Semiconductor Devices", Microelectron. Reliab., 37, (1997)pp1711-1718.

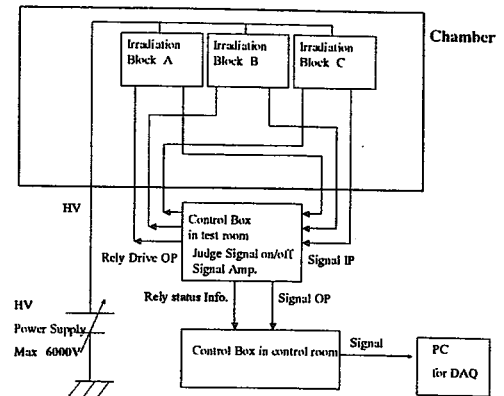


Fig.1 Diagram of Proton Irradiation Test System

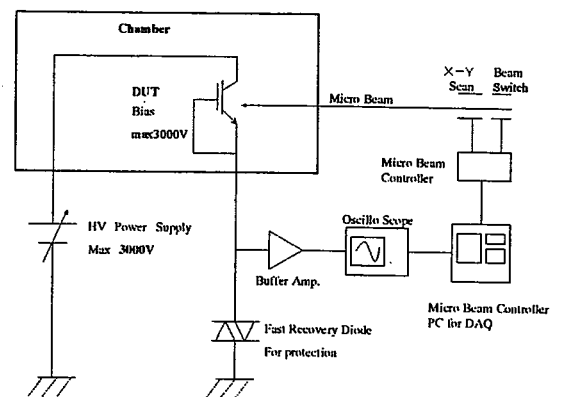


Fig.2 Diagram of Heavy Ion Irradiation Test System

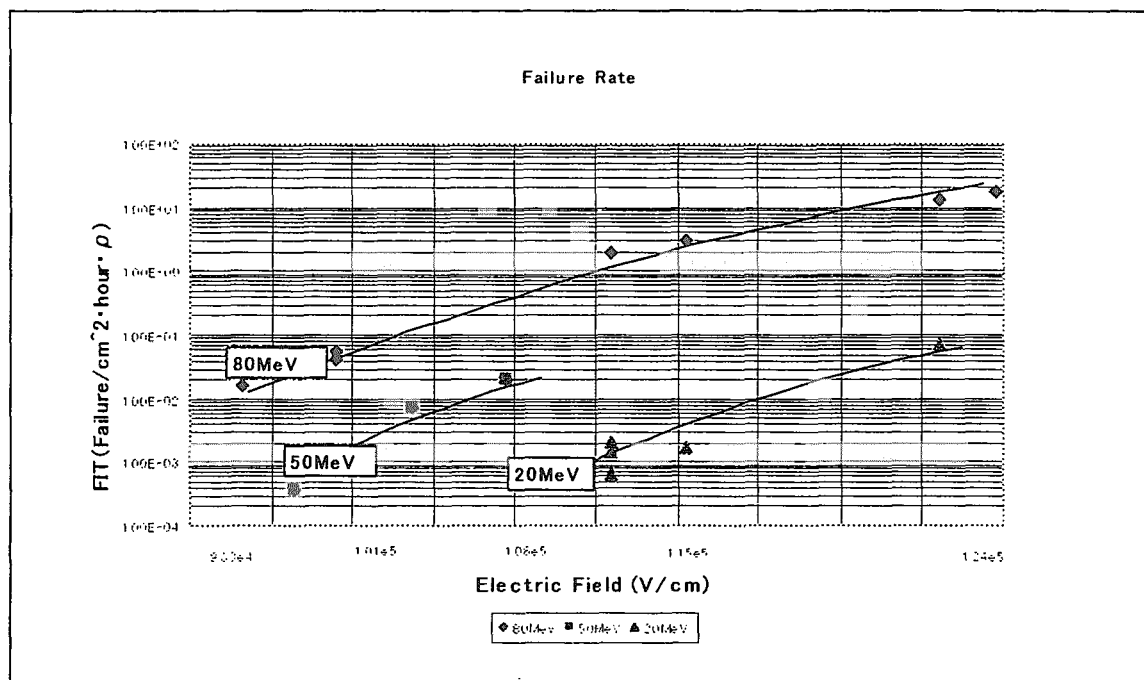


Fig.3 Dependence of Failure Rate on Electric Field

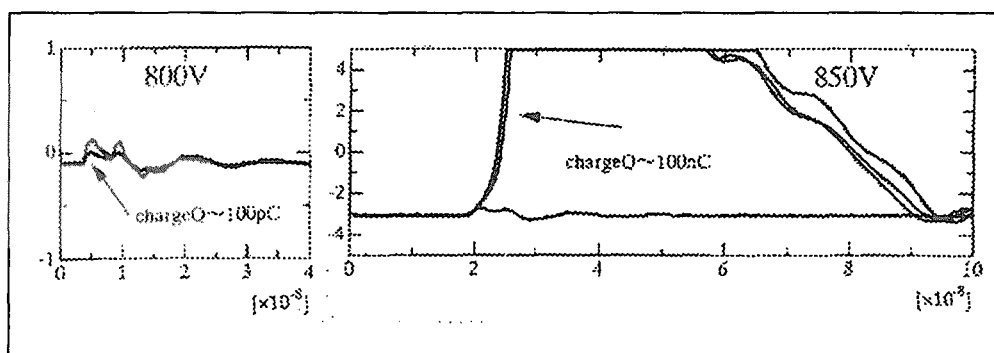


Fig.4 Generated Charges by Micro Beam of Carbon Ion

1.5 Study of Charge Collection Mechanism using Multi Line Schottky Barrier Diode

H. Mori*, T. Hirao, J. S. Laird, S. Onoda* and H. Itoh

*Graduate School of Engineering, Tokai University
Department of Materials Development, JAERI

1. Introduction

Single-Event Phenomena (SEP) are common occurrences in electronic devices used in high radiation fields such as the space environments. SEP are primarily caused by an interaction between the ionization track generated by a high-energy heavy ion and the sensitive region of a device. Among SEP, Single-Event Upset (SEU) is a major concern for DRAM and SRAM devices. As a device manufacturing processes have progressed, Large Scale Integration (LSI) of devices has lead to general lowering of the threshold Linear Energy Transfer (LET) for SEU. A serious new problem for Ultra LSI devices is the Multiple-Bit Upset (MBU), that occurs when a single high LET ion passes through and generate electron-hole plasma which subsequently extends over a region comprising more than one memory cell. However, the fundamental processes of MBU have not yet been fully clarified. In this paper, we investigate MBU from the point of view of the relationship between the collected charge and the angle of the incident ion.

2. Experimental

The heavy ions used in this study were 18 MeV oxygen ions, of which linear energy

transfer (LET) and the projected range in silicon are $6.75 \text{ MeV} / (\text{mg}/\text{cm}^2)$ and $11 \mu\text{m}$ respectively. For ion irradiation, a microbeam of about $1 \mu\text{m}$ in diameter was formed using a heavy ion microbeam system connected to a 3 MV tandem accelerator at JAERI Takasaki TIARA facility.

The test device was the Schottky barrier diode with a substrate doping level of $5 \times 10^{15} \text{ cm}^{-3}$ (phosphorus donors). The schematic structure of the test device is shown in Fig.1.

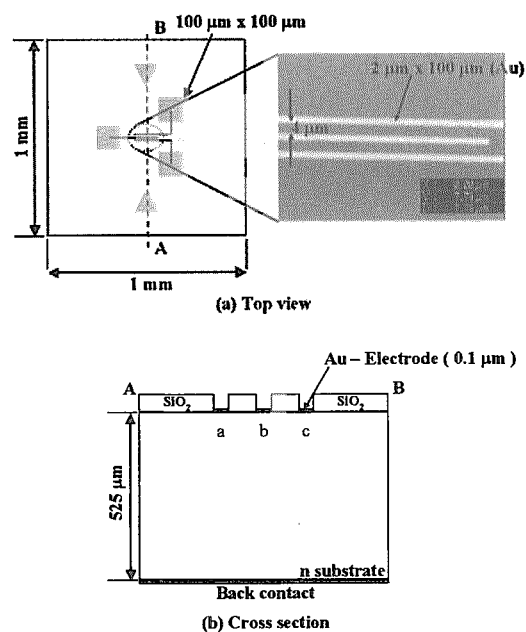


Fig.1 Schematic design of the test device. The device has the three electrode, which were named the a-, b- and c-electrode.

As shown in Fig.1, the device has the three Schottky contacts, which were named the a-, b- and c-electrode. The contact has the size of $2\ \mu\text{m} \times 100\ \mu\text{m}$ and has a thickness of 10 nm. The distance between the contacts is $4\ \mu\text{m}$. At an applied bias of -5 V, the depth of the depletion region for the test device is about $1\ \mu\text{m}$. The test devices were mounted on a chip carrier with $50\ \Omega$ double-ended micro strip lines. They were fixed at an angle of 0° and 45° to the incident ion.

When a single ion hits on the c-electrode, collection charges are measured on each electrode from the waveform of the transient current. The transient current measurements were made with the Transient Ion Beam Induced Current (TIBIC) system¹⁾. TIBIC system consists of the electronic scanner, the fast beam switch and the oscilloscope (Tektronix model TDS 694C). All signal were delayed for every 2.5 ns by the difference in the length of a signal cable.

3. Results and Discussion

Fig.2 shows the Ion Beam Induced Current (IBIC) image. As shown in Fig.2, every depletion region on the electrodes did not overlap each other at an applied bias of -5 V.

Fig.3 shows the waveforms of the transient current induced by an 18 MeV oxygen ion in the test device at an applied bias of -5 V. The ion hit on the c-electrode. Its incident angle was 45° . As shown in Fig.3, the hole current was acquired from c-electrode where the ion hit. For the waveform of the hole current, the peak current, the charge collection time and the

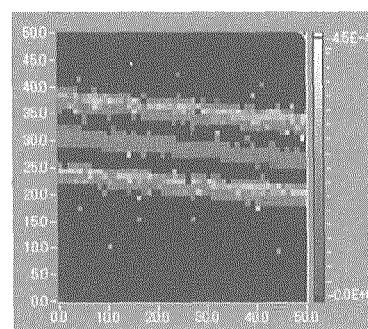


Fig.2 IBIC image on the test device induced by 18 MeV oxygen ion at an applied bias of -5 V.

amount of collected charge are approximately $400\ \mu\text{A}$, 3 ns and 240 fC, respectively. By comparison of the incident ion angle 0° , the amount of collected charge is 1.4 times as many as 170 fC. It accounts for the results that the amount of the collected charge is in proportion to the inverse cosine laws for the incident angle of ion²⁾. On the other hands, the electron current was acquired from both the a-electrode and the b-electrode. These signals may be

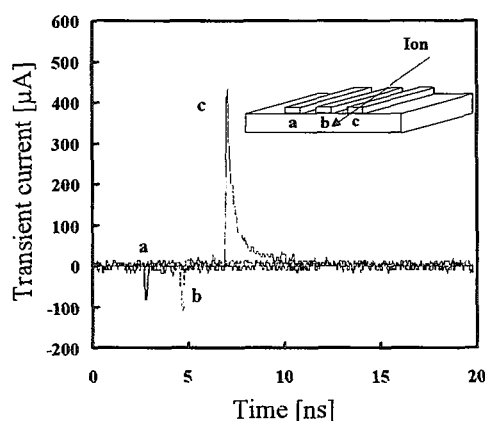


Fig.3 Waveforms of the transient current induced by 18 MeV oxygen ion. The hole current was acquired from the c-electrode, The electron current was acquired from both the a- and b-electrode.

caused by the flow of the electron current that the ion generated on the depletion region under the c-electrode. To support this assumption, we are analyzing the transient current with the equivalent circuit and the ISE-TCAD device simulator.

4. Summary

We had the single ion irradiation experiments in order to investigate MBU from the point of view of the relationship between the collected charge and the angle of the incident ion. As the results, the hole current was detected from the electrode where the ion hit, the electron current was detected from other electrode

Acknowledgements

The authors would like to thank Dr. T. Ohshima for his advice to make the test device and an Electrostatic Accelerator group at JAERI Takasaki for their cooperation in the present experiments.

Reference

- 1) J.S.Laird, et al., JAERI-Review 2000-204, (2000) 11-13
- 2) H. Mori, et al., Extended Abstracts (The 62nd Autumn Meeting, 2001); JSAP, No.2, 12p-E-18 (2001) 595

1.6 Gamma-ray Irradiation Effects on p-Channel 6H-SiC Metal-Oxide-Semiconductor Transistors

T. Ohshima, K. K. Lee, A. Ohi, M. Yoshikawa and H. Itoh

Department of Material Development, JAERI

1. Introduction

Silicon carbide (SiC) electronic devices are expected to be used in harsh radiation environments, such as in space and nuclear reactor facilities, due to its excellent physical properties¹⁾ and radiation resistance²⁾. For developing radiation resistant devices based on SiC, it is important to understand the radiation response of electrical characteristics of both n-channel and p-channel metal-oxide-semiconductor (MOS) field effect transistors (FETs). In previous studies^{3,4)}, Ohshima et al. reported that n-channel SiC MOSFETs show extremely strong radiation resistance compared to silicon (Si) MOSFETs. However, there is no report on the irradiation effects of p-channel SiC MOSFETs because the fabrication process of p-channel SiC MOSFETs with excellent electrical characteristics has not yet been realized. Recently, we established the fabrication process of p-channel SiC MOSFETs using a combination of hot ion implantation and high-temperature annealing. In this paper, we report the influence of gamma-ray irradiation on the electrical characteristics of p-channel SiC MOSFETs.

2. Experimental

The p-channel MOSFETs used in this study were fabricated on n-type 6H-SiC epitaxial layer (thickness: 5 μm) grown on n-type 6H-SiC substrates (3.5° off Si-face). The net donor concentration in the epitaxial layer is $5 \times 10^{15} \sim 1 \times 10^{16} / \text{cm}^3$. The source and drain of the MOSFETs were formed using

aluminum (Al) ion implantation at 800 °C and subsequently annealed at 1800 °C for 1 min in an Ar atmosphere. The gate oxide was fabricated by pyrogenic oxidation ($\text{H}_2:\text{O}_2 = 1:1$) at 1100 °C for 30 min. The thickness of the gate oxide (33 nm) was determined by atomic force microscopy observation. The gate length and width of the MOSFETs are 10 μm and 200 μm , respectively. The source and drain contacts were formed using Al evaporation and subsequent alloying at 850 °C for 5 min in Ar. Gamma-ray irradiation was performed up to 1 MGy (SiO_2) at a rate of 8.8 kGy/h at room temperature (RT) in air. During the irradiation, no electrical bias was applied to the gate, drain and source of the MOSFETs.

The electrical characteristics were measured at RT under dark conditions. The channel mobility (μ) of the MOSFETs was derived from the linear region of the drain current (I_D) versus drain voltage (V_D) curves. The threshold voltage (V_T) was determined as the value at the intersection between the V_G axis and the line extrapolated from the curve of the square root of the drain current (I_D). Details in the procedure are described in ref. 4.

3. Results and Discussion

Figure 1 shows I_D - V_D curves for a typical p-channel SiC MOSFET before irradiation. The I_D - V_D characteristics can be controlled by bias applied to gate and the linear and saturation regions are exhibited. The value of μ derived from the linear region is 5 cm^2/Vs .

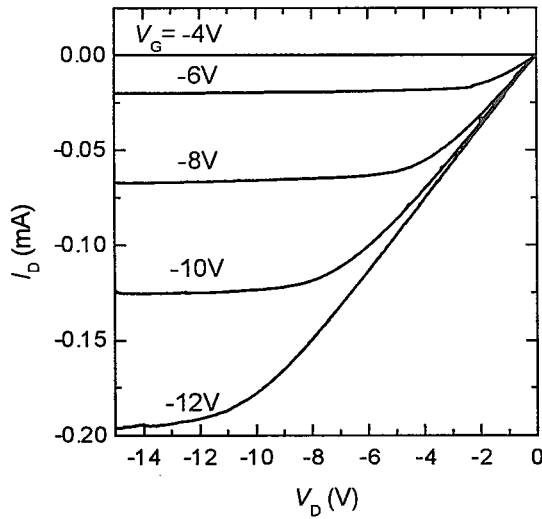


Fig. 1 I_D - V_D curves for a typical p-channel SiC MOSFET before irradiation. The values of gate voltage (V_G) are represented in the figure.

The V_T for the MOSFET is 3.82 V.

Figure 2 shows absorbed dose dependence of μ for p-channel SiC MOSFETs. The result for n-channel SiC MOSFETs and Si MOSFETs⁵⁾ are also shown in the figure for comparison. The value of μ is normalized to the pre-irradiated value (μ_0). For p-channel SiC MOSFET, μ decreases above 5×10^4 Gy(SiO_2) and becomes 65% of μ_0 after irradiation at 1×10^6 Gy(SiO_2). For n-channel SiC MOSFETs, no significant change in μ is observed at doses below 1×10^6 Gy(SiO_2). This result indicates that p-channel SiC MOSFETs have approximately 300 times higher radiation resistance than Si MOSFETs whereas their resistance is low compared to n-channel SiC MOSFETs.

In the case of Si MOSFET, it was reported that the degradation of their electrical characteristics such as channel mobility occurs by the generation of interface traps⁵⁾. Interface traps generated due to irradiation were estimated from subthreshold curves. According to McWhorter and Winokur⁶⁾, V_T

is affected by the generation of oxide trapped charges and interface traps. The shift of V_T (ΔV_T) due to irradiation is expressed as $\Delta V_T = \Delta V_{\text{OX}} + \Delta V_{\text{IT}}$, where ΔV_{OX} and ΔV_{IT} are the voltage shift due to the generation of oxide trapped charges and interface traps, respectively. ΔV_{OX} and ΔV_{IT} can be extracted from the change in V_{MID} which is the voltage correspond to mid-gap condition (See ref. 6). Figure 3 shows the radiation induced interface traps (ΔN_{IT}) and oxide trapped charges (ΔN_{OX}) for p-channel SiC MOSFETs as a function of absorbed dose. The values of ΔN_{IT} and ΔN_{OX} are estimated from the following relation⁶⁾,

$$\Delta N_{\text{IT, OX}} = |\Delta V_{\text{IT, OX}}| C_{\text{OX}}/q \quad (1),$$

where C_{OX} and q are the oxide capacitance and the elementary charge, respectively. The value of ΔN_{IT} increases with increasing absorbed dose. Considering the result

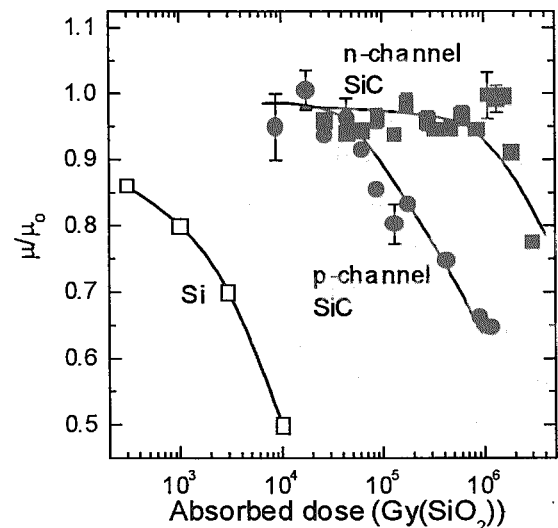


Fig. 2 Absorbed dose dependence of μ for p-channel SiC MOSFETs. The result for n-channel SiC MOSFETs and Si MOSFETs⁵⁾ are also shown in the figure for comparison. The value of μ is normalized to the pre-irradiation value (μ_0).

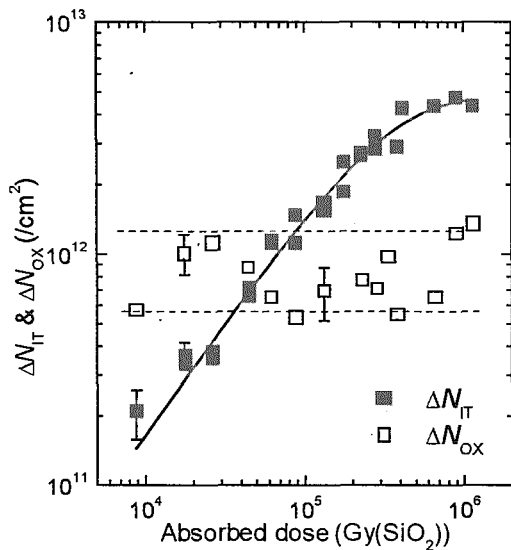


Fig. 3 Radiation induced interface traps (ΔN_{IT}) and oxide trapped charges (ΔN_{OX}) for p-channel SiC MOSFETs as a function of absorbed dose.

obtained in Fig. 2, this suggests the channel mobility for p-channel SiC MOSFETs is degraded by interface traps generated due to irradiation as well as Si MOSFETs. On the other hand, ΔN_{OX} is almost constant throughout irradiation up to 1×10^6 Gy(SiO_2). This might indicate that positive oxide-trapped charge generated above 1×10^{12} /cm² are immediately neutralized. Based on the result of Si MOS studies^{7, 8)}, neutral electron traps are capable of capturing electrons and as a result, they are negatively charged.

4. Summary

The p-channel SiC MOSFETs were fabricated using Al ion implantation at 800 °C and high temperature annealing at 1800 °C. Gamma-ray irradiation effects on the electrical characteristics of p-channel SiC MOSFETs were studied. The channel mobility estimated from I_D - V_D curves decreases above 5×10^4 Gy(SiO_2) and

becomes 65 % of initial value at 1×10^6 Gy(SiO_2). The radiation resistance of p-channel SiC MOSFETs is demonstrated to be approximately 300 times stronger than that of the Si MOSFETs.

References

- 1) W. E. Nelson, F. A. Halden and A. Rosengreen: J. Appl. Phys. **37** (1966)333.
- 2) H. Itoh, M. Yoshikawa, I. Nashiyama, S. Misawa, H. Okumura and S. Yoshida: IEEE Trans. Nucl. Sci. NS37 (1990) 1732.
- 3) T. Ohshima, M. Yoshikawa, H. Itoh, Y. Aoki and I. Nashiyama, Materials Science & Engineering B **61-62** (1999) 480.
- 4) T. Ohshima, H. Itoh and M. Yoshikawa, J. Appl. Phys **90** (2001) 3038.
- 5) F. W. Sexton and J. R. Schwank, IEEE Trans. Nucl. Sci. **32** (1985) 3975.
- 6) P. J. McWhorter and P. S. Winokur, Appl. Phys. Lett. **48** (1986) 133.
- 7) A. J. Leis, T. R. Oldham, H. E. Boesch Jr. and F. B. McLean, IEEE Trans. Nucl. Sci. **36** (1989) 1808.
- 8) M. Walters and A. Reisman, J. Electrochem. Sci. **138** (1991) 2756.

This is a blank page.

2. Biotechnology

2.1	Lethality of Single Tobacco Cells Irradiated with Heavy Ions	25
	Y. Yokota, Y. Hase, N. Shikazono, S. Kitamura, A. Tanaka and M. Inoue	
2.2	Mutation Generation in Protoplasts of Chrysanthemum with $^4\text{He}^{2+}$ and $^{12}\text{C}^{5+}$ Ion Beams	28
	H. Ikegami, H. Murakami, K. Hirashima, T. Nakahara, Y. Hase and A. Tanaka	
2.3	Effects of Ion Beams on Shoot Regeneration of Elatior Begonia (<i>B. \times hiemalis</i>) . Leaf Cultures	31
	M. Iizuka, N. Kudo, Y. Kimura, Y. Hase and A. Tanaka	
2.4	Isolation of an Arabidopsis Mutant Defective in Damage Tolerance	33
	A. Sakamoto, V.T.T. Lan, N. Shikazono, Y. Hase, H. Watanabe and A. Tanaka	
2.5	Development of the Efficient Mutation Breeding Method using Ion Beam Irradiation	36
	H. Yamaguchi, T. Morishita, K. Degi., A. Tanaka, Y. Hase and N. Shikazono	
2.6	Development of Mutant Varieties "Vital Ion Series" in Carnation by Ion Beam Breeding	39
	M. Okamura, N. Yasuno, M. Ohtsuka, A. Tanaka, N. Shikazono and Y. Hase	
2.7	Mutation Generation in Chrysanthemum Plants Regenerated from Floral Organ Cultures Irradiated with Ion Beams	42
	M. Okamura, N. Yasuno, M. Takano, A. Tanaka, N. Shikazono and Y. Hase	
2.8	Effects of Ion Beam Irradiation on Chrysanthemum Leaf Discs and Sweetpotato Callus	44
	K. Ueno, S. Nagayoshi, K. Shimonishi, Y. Hase, N. Shikazono and A. Tanaka	
2.9	RAPD Analysis of Xanta and Waxy Mutants Induced by Ion Beam Irradiation to Hinoki Cypress(<i>Chamaecyparis obtuse</i>)	47
	K. Ishii, Y. Yamada, Y. Hase, N. Shikazono and A. Tanaka	
2.10	Induction of Mutation in Garlic (<i>Allium Sativum L.</i>) by Ion Beam Irradiation	49
	T. Tashiro, Y. Yamamoto, A. Tanaka, N. Shikazono and Y. Hase	
2.11	Characters of Tomato cv. First Mutant with Short Internode Induced by Irradiation of $^{12}\text{C}^{5+}$ Ion Beam to the Seeds	52
	M. Masuda, K. Murakami, S. G. Agong, T. Yuasa, A. Tanaka and Y. Hase	
2.12	Mutation Breeding of Rice, Eggplant and Gloriosa by Ion Beam Irradiation	54
	M. Mizobuchi, M. Okada, M. Matsumoto, A. Iwasaki, A. Tanaka and Y. Hase	
2.13	Regeneration of Variegated Plants From Ion-beam Irradiated Explants of <i>Ficus stipulata Thunb</i>	57
	M. Takahashi, S. Kohama, K. Kondo, M. Hakata, Y. Hase, N. Shikazono, A. Tanaka and H. Morikawa	
2.14	Effect of Ion Beam Irradiation on the Growth of Netted Melon (<i>Cucumis melo L.</i>)	60

	M. Taneishi, H. Katai, H. Yamada, H. Otsuka, Y. Hase, N. Shikazono and A. Tanaka	
2.15	Mutation Induction with Ion Beam Irradiation in <i>Solanum</i> Plants	62
	N. Matsuzoe, T. Umeda, Y. Hase and A. Tanaka	
2.16	Instability of Rice Chlorophyll Mutants Induced at M1 by Carbon Ion Beam Irradiation Is Inherited	64
	M. Maekawa, Y. Hase, N. Shikazono and A. Tanaka	
2.17	Studies on Flower Color and Morphological Mutations from In Vitro Chrysanthemum Explants Irradiated with Ion Beams	68
	T. Sato, H. Naganoma, Y. Hase and A. Tanaka	
2.18	Induction of Mutation in <i>Delphinium</i> L. by Ion-beam Irradiation	70
	T. Kimura, S. Tsuzuki, S. Kondo, Y. Tsuchiya, Y. Hase and A. Tanaka	
2.19	Isolation of Arabidopsis Mutants Defective in Root Hydrotropism	72
	K. Koizumi, G. Takata, K. Nakaya, N. Negishi, Y. Sasuga, Y. Sakata, Y. Oono, Y. Kobayashi, H. Takenaga and S. Tanaka	
2.20	Single-hit Effects on Mammalian Cultured Cells with Heavy-ion Microbeams	74
	Y. Kobayashi, T. Funayama, S. Wada, M. Taguchi and H. Watanabe	
2.21	Regeneration of Hemopoietic Organs in the Silkworm, <i>Bombyx mori</i> , After the Selective Irradiation of 100 Gy Carbon Ions	77
	K. Kiguchi, E. Ling, K. Fukamoto, S. Xu, K. Shirai, R. Kanekatsu, Y. Kobayashi, Z.-L. Tu, T. Funayama and H. Watanabe	
2.22	Mechanism of Bystander Effect Induced by Precise-numbered Heavy Ions	80
	Y. Furusawa, C. Shao, M. Aoki, S. Wada, T. Funayama and Y. Kobayashi	
2.23	The Effect to Mammalian Nucleus by Irradiation of Heavy Ion Beams	83
	S. Wada, M. Natsuhori, N. Ito, Y. Kobayashi, T. Funayama and K. Yamamoto	
2.24	Dynamical Study on Influence of the CO ₂ Enrichment to the Photoassimilate Transportation using Positron Imaging	86
	S. Matsushashi, S. Watanabe, N. S. Ishioka, C. Mizuniwa, T. Ito and T. Sekine	
2.25	Effect of Atmosphere Gas Conditions on Soybean (<i>Glycine Max</i> L.) ¹³ N ₂ Fixation Activity	89
	N. Ohtake, T. Ohyama, K. Sueyoshi, H. Fujikake, N. S. Ishioka, S. Matsushashi, S. Watanabe, T. Sekine, H. Uchida and A. Tsuji	
2.26	Absorption and Transfer of the Iron (⁵² Fe) in the Iron Absorption Maize Mutant 'ys1'	92
	T. Tsukamoto, S. Kiyomiya, H. Nakanishi, H. Uchida, S. Watanabe, N. S. Ishioka, S. Matsushashi, T. Sekine and S. Mori	
2.27	Effects of Cold Stress on ¹¹ C Distribution in Rice Plants Detected by PETIS Detector	95
	H. Hayashi, H. Mano, N. Suzui, S. Matsushashi, C. Mizuniwa, T. Ito, N. S. Ishioka, T. Watanabe, T. Sekine, H. Uchida and A. Tsuji	

2.28	Water and Trace Element Behavior in a Plant	98
	T. M. Nakanishi, J. Furukawa, K. Tanoi, M. Yokota, S. Ueoka, N. Ikeue, Y. Hayashi, N. S. Ishioka, S. Watanabe, T. Sekine, T. Ito, T. Mizuniwa, S. Matsuhashi, H. Uchida and A. Tsuji	
2.29	Positron Imaging Analysis of Assimilation and Translocation of Carbon and Nitrogen Sources in Rice Plant	100
	S. Otsuki, Y. Sonoda, S. Saiki, S. Matsuhashi, S. Watanabe, N. S. Ishioka, T. Sekine and J. Yamaguchi	
2.30	Uptake of ^{18}F FDG and ^{13}N O ₃ ⁻ in Tomato Plants	103
	A. Tsuji, H. Uchida, T. Yamashita, S. Matsuhashi, T. Ito, C. Mizuniwa, N. S. Ishioka, S. Watanabe and T. Sekine	
2.31	Utilization of Ion Beam-irradiated Pollen in Plant Breeding	105
	S. Kitamura, Y. Yokota, M. Inoue, Y. Hase and A. Tanaka	
2.32	Study on the Apoptosis Induction by a Local Damage using Penetration Controlled Ion-beam Exposure	108
	Y. Hase and S. Wada	

This is a blank page.

2.1 Lethality of single tobacco cells irradiated with heavy ions

Y. Yokota*, Y. Hase**, N. Shikazono**, S. Kitamura**, A. Tanaka**
and M. Inoue*

Faculty of Agriculture, Kyoto Prefectural University*
Department of Ion-beam Applied Biology, JAERI**

1. Introduction

Biological effects of ionizing radiations are dependent on the linear energy transfer (LET). In mammalian cells irradiated with carbon ions having different LETs, relative biological effectiveness (RBE) on reproductive death peaked at a LET range of 137 to 157 keV/μm^{1),2),3),4)}. Also in plants, biological effects of radiations depend on LET^{5),6),7),8)}. Hase et al. (2002) reported that the RBE on survival reduction of tobacco seeds irradiated with carbon ions reached the maximum at 230 keV/μm⁹⁾. LET value giving maximal biological effect in plant cells might be higher than that in mammalian cells. To our knowledge, there is no report about LET-dependence on biological effect in single plant cells.

In this study, we examined the lethality of single tobacco cells irradiated with helium and carbon ions with different LETs, and compared with that in mammalian cells.

2. Materials and Methods

Tobacco (*Nicotiana tabacum* L.) protoplasts were isolated from BY-2 cell line, and embedded (thickness of 299 ± 15 μm) in the modified LS medium. They were irradiated with carbon and helium ions and gamma-rays within 24 hours after plating. Nickel plates with different thickness were used to make a given LET of the ions on the cell irradiated. Physical parameters of ion beams used here were calculated by the ELOSS M computer program¹⁰⁾, and are shown in Table 1. The particle fluence of ion beams was determined using CR-39 track detectors. Doses of ion beams were calculated by the formula of
Dose (Gy) = LET (keV/μm) × particle-fluence (number of particles/cm²) × 1.6×10^{-9}
Irradiation was done at room temperature.

After the irradiation, cells were incubated at 27°C in the dark condition. Two weeks after the irradiation, colonies over 16 cells were counted as survivors derived from the cells irradiated. The surviving fraction was calculated as a ratio of the colony-forming

efficiency in the cells irradiated to the unirradiated cells from the same cell population. It was always around 10%. Dose-response curves for the surviving fractions were approximated by the formula of

$$SF = 1 - [1 - e^{-D/D_0}]^M$$

where SF is the surviving fraction, D is the dose, and D_0 and M are constants to be experimentally determined by a least-squares method using a computer program (KaleidaGraph version 3.09, Synergy Software). Inactivation cross sections were determined by the formula of

$$\text{Inactivation cross section } (\mu\text{m}^2) = \text{LET (keV/\mu m)} \times D_0^{-1} (\text{Gy}^{-1}) \times 0.16$$

Twenty-four hours after plating, the cross-sectional area of the cell nucleus stained with DNA-specific dye (DAPI) was measured under a fluorescence microscope.

Table 1 Physical parameters of ion beams used here.

Radiation	Energy ^a (MeV/u)	Penetration depth ^b (mm)	LET (keV/μm) ^b	
			Mean	Range
Gamma-rays	—	—	0.2	0.2
Helium ions	24.8	6.2	8.9	8.83-8.97
	6.63	0.58	30.8	26.4-36.8
Carbon ions	25.9	2.3	78.6	76.0-81.0
	17.3	1.1	115	107-124
	11.4	0.53	180	152-221
	9.17	0.37	247	181-386
	8.30	0.31	309	196-712

^a at the surface of the medium.

^b in the medium as a water equivalent.

3. Results and Discussion

Dose-response curves for the surviving fraction are shown in Figure 1. All curves had clear shoulders. The D_{10} values in gamma-rays and carbon ions of 247 keV/μm were 47.5 and 10.4 Gy, respectively. D_{10} values in mammalian cells irradiated with X-rays and carbon ions with a LET giving the maximal RBE were in the range of 6.6 to 7.8 and 1.6 to 2.3 Gy, respectively^{1),2),3)}. Radiation-sensitivity of single tobacco cells was much lower than that of mammalian cells.

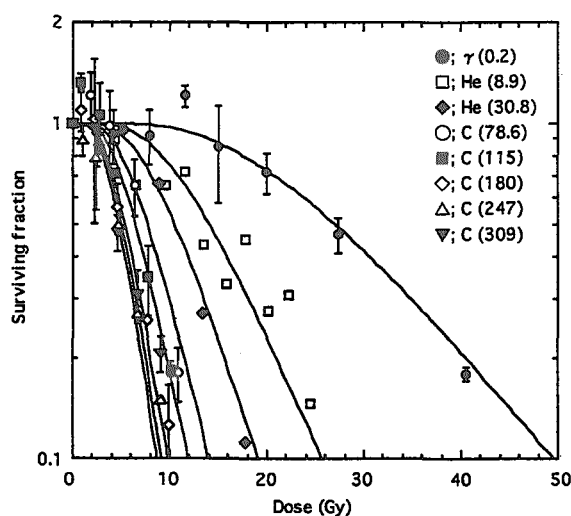


Figure 1 Survival curves of single tobacco cells irradiated with carbon and helium ions and gamma-rays. LET values (keV/ μ m) are shown in the parentheses. In gamma-rays and carbon ions, each plot shows mean \pm S.E. of 3 separate experiments; in helium ions, mean in single experiment.

Relationship of LET and RBE based on the D_{10} values is shown in Figure 2. RBE clearly depended on LET. The RBE value reached the maximum by the irradiation of carbon ions of 247 keV/ μ m, resulting in 5.72. LET value of carbon ions giving the maximal RBE in single tobacco cells is higher than that in mammalian cells (137 to 157 keV/ μ m)^{1),2),3),4)}, and similar to that in tobacco seeds (230 keV/ μ m)⁹⁾.

The cross-sectional area of cell nucleus was $149 \pm 19 \mu\text{m}^2$. Number of ion particles per cell nucleus area was obtained from the particle-fluence determined by the CR-39 track detector. Relationship of the surviving fraction and number of ion particles per cell nucleus is shown in Figure 3. The values of the apparatus threshold-dose (D_q) for 8.9, 30.8, 78.6, 115, 180, 247, 309 keV/ μ m were 1620, 351, 100, 58, 31, 20 and 17 ion-particles per cell nucleus, respectively.

As shown in Figure 4, Inactivation cross sections calculated from the final slopes of dose-response curves increased with increasing LET. Inactivation cross sections for the carbon ions with 180, 247 and 309 keV/ μ m were 11.9, 18.5 and 21.9 μm^2 , respectively, suggesting that they reach a plateau over the LET of 247 keV/ μ m.

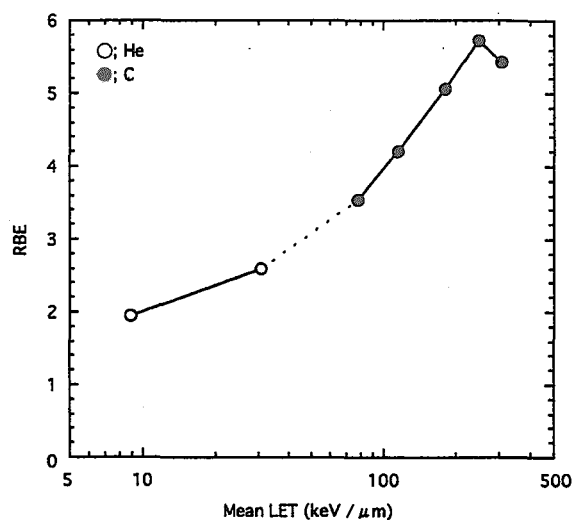


Figure 2 LET-RBE relationship based on the D_{10} in single tobacco cells.

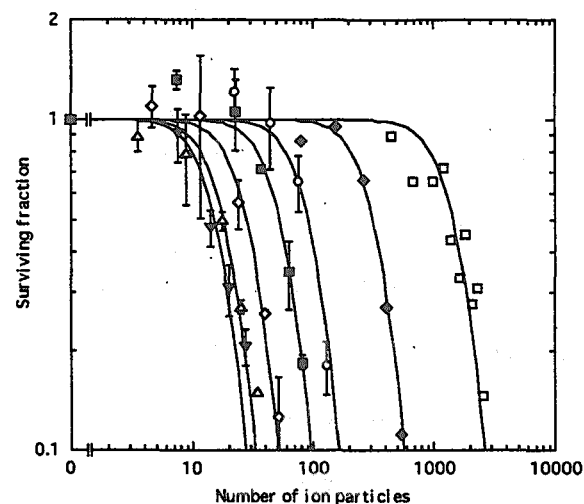


Figure 3 Relationship between surviving fraction and number of ion particles penetrated a cell nucleus. Symbols are the same as shown in Figure 1.

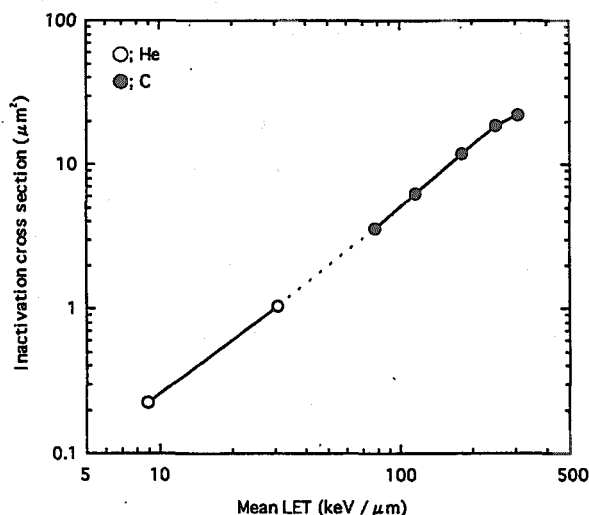


Figure 4 Inactivation cross section in single tobacco cells irradiated with different LETs.

References

- 1) W. K. Weyrather, S. Ritter, M. Scholz and G. Kraft (1999) *Int. J. Radiat. Biol.*, **75**, 1357-1364
- 2) M. Aoki, Y. Furusawa, T. Yamada (2000) *J. Radiat. Res.*, **41**, 163-175
- 3) Y. Furusawa, K. Fukutsu, M. Aoki, H. Itsukaichi, K. Eguchi-Kasai, H. Ohara, F. Yatagai, T. Kanai and K. Ando (2000) *Radiat. Res.*, **154**, 485-496
- 4) J. Kiefer, P. Schmidt and S. Koch (2001) *Radiat. Res.*, **156**, 607-611
- 5) Y. Hirono, H. H. Smith, J. T. Lyman, K. H. Thompson and J. W. Baum (1970) *Radiat. Res.*, **44**, 204-223
- 6) M. Mei, H. Deng, Y. Lu, C. Zhuang, Z. Liu, Q. Qiu and T. C. Yang (1994) *Adv. Space Res.*, **14**, 363-372
- 7) A. Tanaka, N. Shikazono, Y. Yokota, H. Watanabe and S. Tano (1997) *Int. J. Radiat. Res.*, **72**, 121-127
- 8) N. Shikazono, A. Tanaka, S. Kitayama, H. Watanabe and S. Tano (2002) *Radiat. Environ. Biophys.*, in press
- 9) Y. Hase, M. Yamaguchi, M. Inoue and A. Tanaka (2002) *Int. J. Radiat. Biol.*, in press
- 10) S. Tanaka, M. Fukuda, K. Nishimura, H. Watanabe and N. Yamano (1997) JAERI-Data/Code, 97-019

2.2 Mutation Generation in Protoplasts of Chrysanthemum with $^4\text{He}^{2+}$ and $^{12}\text{C}^{5+}$ Ion Beams

H.Ikegami*, H.Murakami*, K.Hirashima*, T.Nakahara*, Y.Hase** and A.Tanaka**
Fukuoka Agricultural Research Center*, Department of Ion-Beam-Applied Biology,
JAERI*

1. Introduction

Ion beams have high LET(linear energy transfer) and are applied to induce various mutations to many plants¹⁾. It is also known that wide range of somaclonal mutations happened in protoplast culture. Thus a high mutation rate is expected when these techniques described above are combined. In addition, protoplast method is useful in a point that we can prevent chimera from emerging and acquire numerous regenerated plants.

We had already grown 660 mutants of chrysanthemum by irradiating protoplasts and culturing them. In this work, we investigated the phenotypes of the regenerants and selected 21 lines, comparing the differences among those plants irradiated with several different doses.

2. Experimental methods

Chrysanthemum variety, 'Syuhounochikara' (white flower) was used for the experiment. Isolation and embedding of mesophyll protoplasts were conducted by the modified method²⁾. The protoplasts were irradiated with 50 MeV $^4\text{He}^{2+}$ or 220 MeV $^{12}\text{C}^{5+}$ ion beams from the AVF cyclotron in JAERI. Those irradiated protoplasts were cultured, regenerated and grown in a field of Fukuoka Agricultural Research Center. Mutation phenotypes were investigated after flowering.

3. Results and Discussion

Various types of mutations were observed. The mutants showed different traits especially in height, flowering day, the number of petals, flower

type, and flower color. Among 660 mutants we chose 21 lines in the first selection and are growing them for the second selection.

Regenerants derived from protoplasts were about 85% height of control (data not shown). Irradiated plants totally exhibited dwarf characteristics, extent of which increase according to a dose (Table 1). However some of irradiated plants were superior in height to 0Gy line.

Day of flowering distributed from October 6th to December 10th. The average day of flowering was about October 20th in all doses (Table 1). On the other hand, the fact that both the earliest day of flowering and the latest day were found in high dose irradiated lines shows ion beams irradiation might have broaden the limits.

Though the rate of ray petals in total petals was higher in $^4\text{He}^{2+}$ ion 10Gy line than in low dose lines (0, 2, 5Gy), there was no significant difference among the number of ray petals in each plot as well as the number of total petals (Table 1). It is interesting that one of the irradiated plants had 385 ray petals and others had more tubular petals than ray petals.

High frequent mutations also occurred in flower type (Table 2). Among those mutations, twisted or different length petals are frequently observed and there were some exposed center or square, too. The mutation rate of irradiated lines was more than two times higher than that of 0Gy line.

Flower-color change happened to one of 101 plants in $^4\text{He}^{2+}$ ion with 2Gy, one of 204 in $^4\text{He}^{2+}$ ion with 5Gy and two of 91 in $^{12}\text{C}^{5+}$ ion with 5Gy (Table 3). The rate of color change was especially

high in $^{12}\text{C}^{5+}$ ion with 2Gy. Though there is a difference in the number of plants of each plot, the fact that no flower color mutation occurred in non-irradiated lines suggests that ion beams could induce flower color mutation at higher frequency than somaclonal mutation.

Summery

It can be said that various types of mutations were induced by irradiating ion beams in protoplasts of chrysanthemum. It is consequent for us to build up and use such groups that has a wide range of mutation spectrum for breeding. In the case of aiming at a practical trait, however, we should remember the fact that strong

mutation pressure could cause extreme unfavorable traits. It was not determined in this experiments whether one mutation is due to somaclonal mutation or ion beams. This result suggests that we need more data to reveal the differences between those mutating methods.

References

- 1) S.Nagatomi, A.Tanaka, A.Kato, H.Yamaguchi, H.Watanabe and S.Tano, TIARA Annual Report 6:41-43 (1998)
- 2) T.Nakahara, K.Hirashima, M.Koga, A.Tanaka, N.Shikazono and H.Watanabe, TIARA Annual Report 7:28-29 (1999)

Table 1. The characteristics of regenerated plants

Radiation	Energy(MeV)	Dose(Gy)	No. of plants	Height rate(%)	No. of total petals	No. of ray petals	Rate of ray petals(%)	Flowering day
$^4\text{He}^{2+}$	50	2	107	90.8	184	150	81.5	10/20
		5	297	87.8	214	176	82.2	10/19
		10	67	81.5	193	142	73.6	10/20
$^{12}\text{C}^{5+}$	220	2	25	-	173	122	70.5	-
		5	105	-	164	100	61.0	10/21
control		0	59	100.0	191	151	79.1	10/19

1) height rate = (average height of 50 plants/ average height of control line) \times 100 (%)

2) rate of ray petals = (No. of ray petals/No. of total petals) \times 100 (%).

3) -: no data.

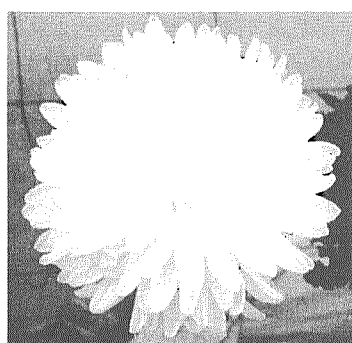
Table 2. Flower type mutation

Radiation	Energy(MeV)	Dose(Gy)	No. of plants	Flower type					Mutation rate(%)
				normal	twist petals	exposed center	twist petals and exposed center	non-flowering	
$^4\text{He}^{2+}$	50	2	95	33	57	0	5	0	65.3
		5	239	84	121	6	24	4	64.9
		10	46	15	25	4	2	0	67.4
control		0	49	34	11	0	2	2	30.6

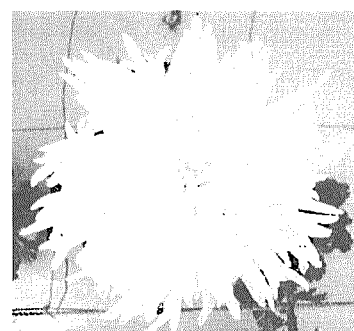
1) Mutation rate = { (twist+exposed center+twist and exposed center+non-flowering)/total plants} \times 100 (%)

Table 3. Flower color mutation

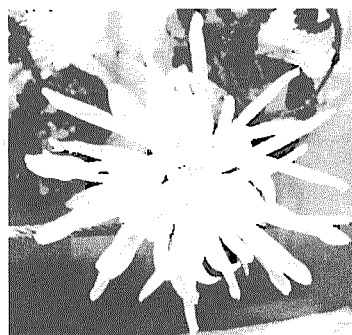
Radiation	Energy(MeV)	Dose(Gy)	No. of plants	Flower color	
				white	yellow
$^4\text{He}^{2+}$	50	2	101	100	1
		5	264	263	1
		10	54	54	0
$^{12}\text{C}^{5+}$	220	2	12	12	0
		5	91	89	2
control		0	52	52	0



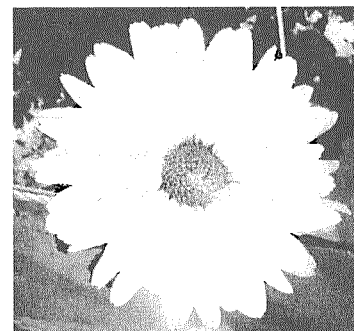
Normal



Twist petals



Long and thin petals



Exposed center

Figure1. Flower type of mutants induced by $^4\text{He}^{2+}$ ion-beam irradiations

2.3 Effects of Ion Beams on Shoot Regeneration of Elatior Begonia (*B. × hiemalis*) Leaf Cultures

Masahide IIZUKA*, Nobuhiro KUDO*, Yasuo KIMURA*,
Yoshihiro HASE** and Atushi TANAKA**

Gumma Horticultural Experiment Station*,

Department of Radiation Research for Environment and Resources, JAERI.**

Introduction

Ion beams, which have a higher linear energy transfer (LET) than X and gamma rays, is one of efficient mutagenic agents, applicable to mutation breeding of many horticultural crops. However, there have been few studies on the effects of ion beam irradiation on induction of mutation in vegetables and ornamental crops. The lethal dose of the $^4\text{He}^{2+}$ and $^{12}\text{C}^{5+}$ ion beam irradiation to strawberry, hydrangea and spiraea seed became clear^{1),2),3)}

We have the mutation breeding of the Elatior Begonia (*B. × hiemalis*) is important pot cultures. An ion beam was irradiated in Elatior Begonia for the purpose of variation of the flower color. We examined effects of ion beam irradiation on germination of Elatior Begonia.

Materials and Methods

Elatior Begonia (*B. × hiemalis*) cv. Line in greenhouse were used as plant materials. Young leaves were excised, surface sterilized by immersing in 70% ethyl alcohol for 1 min, followed in 1%(W/V) sodium hypochlorite solution for 15 min and then rinsed three times in distilled water. The leaf segments were cultured on modified Murashige and Skoog's (MS) medium supplemented with 0.5 mg/l NAA and 1mg/l BA. The

samples covered with Kapton film were irradiated with carbon ion beam (220 MeV $^{12}\text{C}^{5+}$ and 320 MeV $^{12}\text{C}^{6+}$) at various doses (2 to 150 Gy). After irradiation the leaf segments were transferred to the fresh medium and cultured at 20 °C and 16 hr-photoperiod. Regeneration rate was investigated after 40-50 days of culture.

Results and Discussion

When the dosage of irradiation increased, the regeneration rates of the leaf segments decreased. At the dose of more than 10Gy in $^{12}\text{C}^{5+}$ ion beams, the regeneration rate decreased rapidly (Fig.1). And at the dose of more than 20Gy in $^{12}\text{C}^{6+}$ ion beams, the regeneration rate decreased rapidly (Fig.2).

We are performing cytological studies to investigate horticultural values of the mutants and are screening mutants of flower color variation in the growing plants.

References

- 1) N. Kudo et al. TIARA Ann. Rep., 16:62-64. (1998)
- 2) M. Iizuka et al. TIARA Ann. Rep., 2.3:30-31. (1999)
- 3) M. Iizuka et al. TIARA Ann. Rep., 2.7:45-46. (2001)

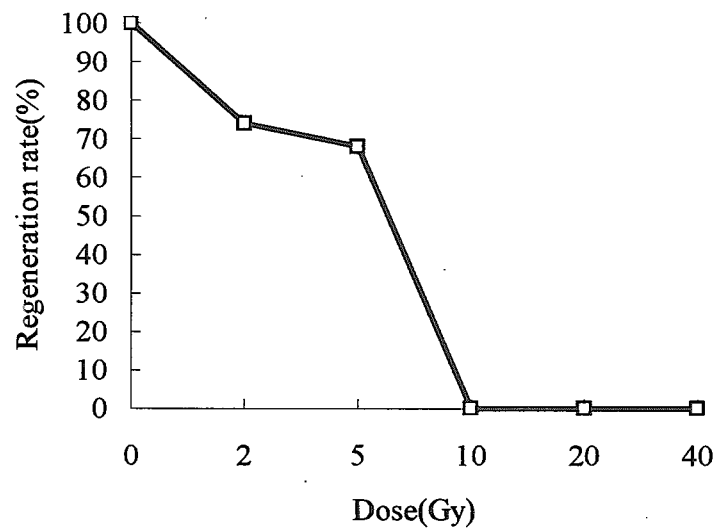


Fig.1.Effect of $^{12}\text{C}^{5+}$ ion beam on the regeneration of Elatior Begonia

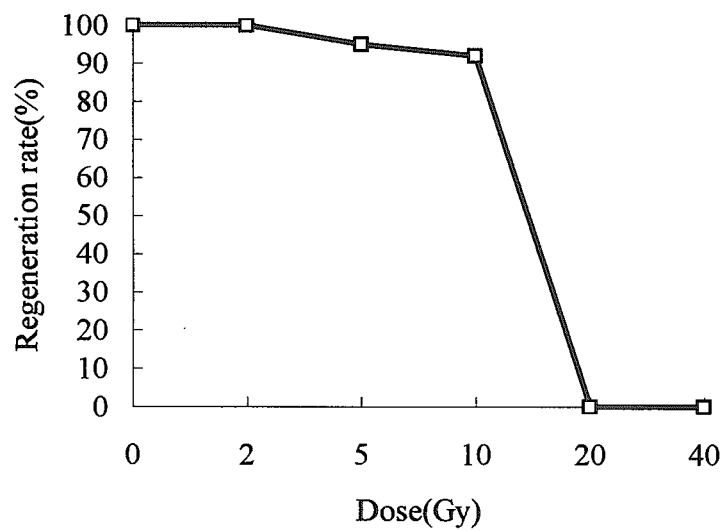


Fig.2.Effect of $^{12}\text{C}^{6+}$ ion beam on the regeneration of Elatior Begonia

2.4 Isolation of an *Arabidopsis* mutant defective in damage tolerance

Ayako Sakamoto*, Vo Thi Thuong Lan*, Naoya Shikazono*, Yoshihiro Hase*, Hiroshi Watanabe** and Atsushi Tanaka*

Department of Ion-Beam-Applied Biology, JAERI*

JAERI**

1. Introduction

Plants require sunlight for photosynthesis, thus are destined to expose themselves to harmful UV radiation for many hours. Even in such a hard environment, however, plants grow vigorously and breed. The reason why plants are resistant to UV has been studied for years. Most known factor is the presence of UV-absorbing compounds such as flavonoid¹⁾. In addition, plants have enzymes to repair damaged DNA²⁾ and the mechanisms by which plants extinguish the active oxygen³⁾. The presence of other unknown system(s) has also been predicted to regulate the response to UV.

To isolate a novel gene involved in UV-response in plant, we have tried to isolate UVB-sensitive mutants. As a result, we successfully isolated six new mutants named *suv* (sensitive to UV). Among these mutants, here we report the identification and characterization of *suv1*.

2. Materials and Methods

2.1 Mutagenesis and Screening

Arabidopsis thaliana ecotype Columbia seeds were irradiated with carbon ions with a dose of 150 Gy as previously described⁴⁾. The M1 seeds were grown and self-pollinated, preparing M2 seeds. The offspring seeds derived from M2 were harvested in each plant, preparing 3000 lines of seed stocks. UVB sensitivity of all M2 lines was examined by root bending assay as described previously⁵⁾. In brief,

seedlings were vertically grown on nutritive agar plates under continuous white light for three days. After exposed to 0.5kJ/m² of UVB, seedlings were incubated another three days under the dark condition. The line that showed a reduced root growth was picked up as a candidate of UVB sensitive mutant.

2.2 Mapping

Candidates of UVB-sensitive mutants were crossed to the Landsberg *electa* ecotype. F2 plants from this cross were grown and one leaf was removed and stored for DNA preparation. Then the plants allowed to self-pollinate, the seeds were harvested in each plant and preparing F2 line seeds. The F2 lines were screened for UVB sensitivity by root bending assay. DNA was extracted from the leaf stocks of UVB sensitive homozygous lines and analyzed by SSLP⁶⁾ or CAPS⁷⁾ method.

3. Results and Discussion

To study the mechanisms of UV-tolerance in higher plants, we have isolated UVB sensitive mutants. About 3000 of M2 lines derived from ion beam-irradiated seeds were screened for UVB sensitivities under non-photoreactivating conditions. Thirteen M2 lines, whose growths were inhibited by UVB irradiation, were selected as candidates of UVB sensitive mutants. These lines were mapped on six different positions on chromosomes. We named the six mutants as *suv* (sensitive to

UV) 1 to *snv6* and analyzed *snv1* further.

To characterize the *snv1* mutant, we applied several DNA damaging treatment to *snv1* and analyzed the responses. First, we irradiated various doses of UVB to the *snv1* and wild type seedlings and measured the root growth in non-photoreactivating (dark) or photoreactivating (light) condition. The result showed that the *snv1* was more sensitive to UVB than wild type plant in both conditions.

To know whether *snv1* mutant is also sensitive to other type of DNA damage, we applied several agents inducing different type of DNA damage. When we exposed to γ -rays, the *snv1* seedlings showed hypersensitivity compared to the wild type. On the other hand, seedlings transplanted on the agar plates containing methylmethane-sulfonate (MMS, alkylating agent) showed slightly reduced growth compared to the wild type. Surprisingly, *snv1* was also inhibited to grow on the plate containing mitomycin C (MMC). Since MMC is thought to cause intra- or inter-strand cross-links on double strand DNA, our results suggested a diverse function of *SUV1* gene.

To identify the *snv1* gene, we performed fine mapping using 268 chromosomes prepared from the cross of *snv1* with Ler. However, we found that there was no recombination over 15cM region in the bottom of chromosome I. We assumed that this strange recombination rate in *snv1* might be due to a chromosome inversion induced by ion beam irradiation. To identify the mutation, we tried to find the ends of inverted region. We utilized the sequences of bacterial artificial chromosome (BAC) corresponding to the boundaries of no-recombination region. The DNA probes prepared from seven BACs were used to detect the restriction enzyme-

digested patterns of *snv1* DNA. Using the probe of T2K10 (left side) or T1F15 (right side, overlap with F7B5), we found that some fragments were lost in the *snv1*/DNA. Next, we designed 14 pairs of PCR primers covering the missing 14.5kb (left) and 6.6kb (right) fragments. By PCR analyses, we found that the subfragment 11 in the 14.5kb fragment and the subfragment 3 in the 6.6kb fragment were not amplified in *snv1*. Then we performed TAIL-PCR to analyze the missing regions in *snv1*. Sequencing of the TAIL-PCR fragments revealed that the sequence of T1F15 was broken in the middle and rejoined to the sequence of T2K10. Moreover, when we read the another half of T2K10, this sequence was rejoined to the DNA corresponding to the F8A5 located about 200kb downstream to T2K10. Finally, we found that the *snv1* mutant involves quite complicate rearrangements including chromosome inversion and translocation (Fig.1A).

Owing to the chromosomal rearrangements, at least two genes were disrupted in *snv1* (Fig.1B). One gene encoded the protein that has a homology to the large GTP binding protein family. The other gene encoded the catalytic subunit of DNA polymerase ζ (*AtREV3*). In yeast or animal cells, *REV3* has shown to be involved in the translesion synthesis, a pathway to overcome the stalled replication at the DNA lesion⁸⁾. Therefore, we hypothesized that in the *snv1* damaged DNA interrupts DNA replication because of mutation of *AtREV3*, leading to the inhibition of cell division and root elongation.

REV3 is known to concern with the error-prone TLS and to cause most of UV-induced mutations in yeast and animal cells⁸⁾. Our finding suggests that there are error-prone TLS activities in plants. However, since

plants do not have a specialized germ line, error-prone TLS seems to enhance the risk to leave a mutated gene to the next generation. Do plants have a special system to avoid a mutation in reproductive cells or don't they care about the mutation? It would be necessary to study the plant system maintaining the genome. We are now planning to analyze the mutation rate in somatic cells with or without error-prone TLS by using *suv1* mutant.

References

- 1) G. I. Jenkins, G. Fuglevand, J. M. Christie, in *Plants and UV-B* (P. J. Lumsden ed.) Cambridge University Press (1997) pp. 135-156,
- 2) A. B. Britt, *Trends Plant Sci.* 4 (1999) 20-25.
- 3) K. Asada, *Annu. Rev. Plant Physiol. Plant Mol. Biol.* 50 (1999) 301-339.
- 4) A. Tanaka, N. Shikazono, Y. Yokota, H. Watanabe and S. Tano, *Int. J. Radiat. Biol.* 72 (1997) 121-127.
- 5) A. B. Britt, J.-J. Chen., D. Wykoff, D. Mitchell, *Science* 261 (1993) 1571-1574.
- 6) C. J. Bells and J. R. Ecker, *Genomics* 19 (1994) 137-144.
- 7) A. Konieczny and F. M. Ausubel, *Plant J.* 4 (1993) 403-410.
- 8) C.W. Lawlence, P. E. M. Gibbs, R. S. Murante, X.-D. Wang, Z. Li, T. P. McManus, W. G. McGregor, J. R. Nelson, D. C. Hincle and V. M. Maher, in *Biological Responses to DNA Damage*, Cold Spring Harbor Laboratory Press (2000) pp. 61-69.

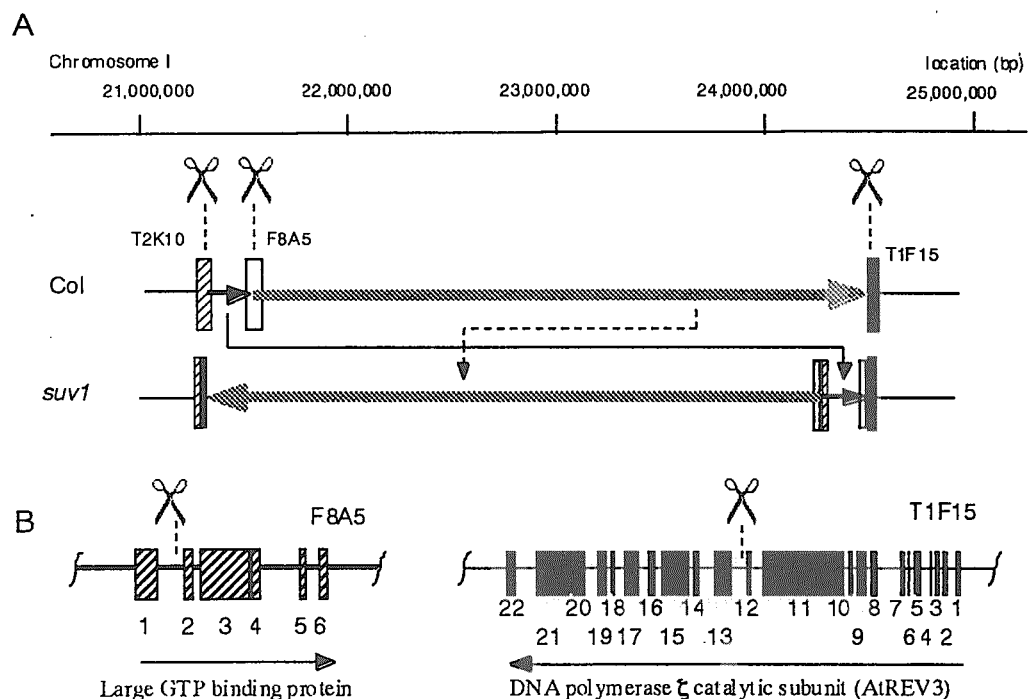


Fig.1 Chromosome rearrangement in *suv1* mutant

A. Chromosome rearrangement taken place in *suv1*. The chromosome I of *suv1* was broken at three point (scissors) and one was inverted and the other was translocated as shown with arrows. The BACs positioned under broken sites are shown as rectangles. B. Structure of two genes disrupted in *suv1*. Arrows indicate directions of ORF, rectangles and numbers indicate exons.

2.5 Development of the efficient mutation breeding method using ion beam irradiation

H. Yamaguchi, T. Morishita, K. Degi,
A. Tanaka*, Y. Hase* and N. Shikazono*

Institute of Radiation Breeding, NIAS,

Department of Radiation Research for Environment and Resources, JAERI *

1. Introduction

Most mutagens used for registered crop mutant varieties in the world are gamma rays and X rays. Ion beams are expected to be widely utilized as new mutagens, because they have very high linear energy transfer (LET) and relative biological effectiveness (RBE) in comparison with gamma rays and X rays. By ion beam irradiation, specific flower mutants that were not obtained with gamma rays were induced in chrysanthemum¹⁾. However, the differences among ion beams and gamma rays in the effect of mutation and in the spectrum of induced mutant are not evident.

On the other hand, it is the problem in mutation breeding that the mutation occurs not only in the trait aimed to improve, but also in other traits and the infection by irradiation. It was reported that some shoots produced after gamma ray irradiation had lower chromosome number than the control plants and the reduction of chromosome number was correlated with the size of inflorescence in chrysanthemum²⁾. It is also indicated the nuclear DNA content measured with the flow cytometry was related to the plant size in sugar cane³⁾. Therefore, we considered that the nuclear DNA content might be available for the index of infection by irradiation.

In this study, to develop the efficient mutation breeding method using ion beams, we investigated the effect of mutation and the influence of carbon ion beam irradiation on nuclear DNA content of plants regenerated from irradiated leaf explants in

chrysanthemum.

2. Materials and Methods

The chrysanthemum cultivar 'Taihei' was used for this study. Leaf explants were plated on callus induction media (MS media supplemented with 4 μ M BA, 1 μ M NAA, 2 % sucrose and 0.9 % agar). They were irradiated with various doses of accelerated $^{12}\text{C}^{5+}$ (220 MeV, 0.02 nA) ion and $^4\text{He}^{2+}$ (100 MeV, 20 nA) particles using an AVF Cyclotron in JAERI and with various doses of gamma rays in IRB. After irradiation, the explants were plated on new media, and then plated on regeneration media (MS media supplemented with 4 μ M BA, 0.5 μ M NAA, 2 % sucrose and 0.9 % agar) three weeks later. The regeneration rate was investigated six weeks later. The regenerated plants were established and the flower color was investigated.

In C ion beam irradiation with 1 Gy, 2 Gy and 3 Gy and in gamma ray irradiation with 10 Gy, 20 Gy and 30 Gy, the nuclear DNA contents of regenerated plants were measured with flow cytometric analysis. Leaf of garden pea (*Pisum sativum* cv. Narikoma Sanjunichi) was used as standards and the ratio of nuclear DNA content in a sample to that in garden pea was calculated. The measurements were repeated two times using two different leaves of a plant in 50 plants of each irradiation dose.

3. Results and Discussion

The influences of C ion beam, He ion beam

and gamma ray irradiation on the regeneration from leaf explants were shown on Fig 1. The dose of 50 % regeneration was 3 Gy with C ion beams, 8 Gy with He ion beams and 25Gy with gamma rays, respectively.

Mutants in flower color over 10 types emerged in this experiment. The effects of mutation induction with C ion beams, He ion beams and gamma rays were compared from the relationship between the regeneration rate and the mutation rate in flower color (Fig.2). This data indicated that in the dose in which the regeneration rate was over 80 % the effect on mutation induction was higher in C ion beams than in gamma rays. Besides, below 80 % of regeneration rate, the effect was higher in gamma rays than in C ion beams. The He ion beams were less effective than C ion beams and gamma rays.

Figure 3 shows that the influences of C ion beam and gamma ray irradiation on nuclear DNA content. In gamma rays, the plants that

have the less DNA contents than the original plant increased as the irradiation dose increases. On the average, the decrease in nuclear DNA contents is 0.9 % with 10 Gy, 1.8 % with 20 Gy and 2.6 % with 30 Gy. On the other hand, in C ion beams, the DNA contents decreased drastically with 1 Gy irradiation, such as dose, which almost did not affected regeneration. But, the increase of irradiation dose did not affect the decrease of the nuclear DNA contents so much as gamma rays.

References

- 1) S. Nagatomi et al., TIARA Ann. Rep 6 (1997)48-50.
- 2) S. Ichikawa, et al., Radiation Botany 10 (1970)557-562.
- 3) S. Nagatomi, et al., Breed. Sci. 48 Supple.2(1998)334.

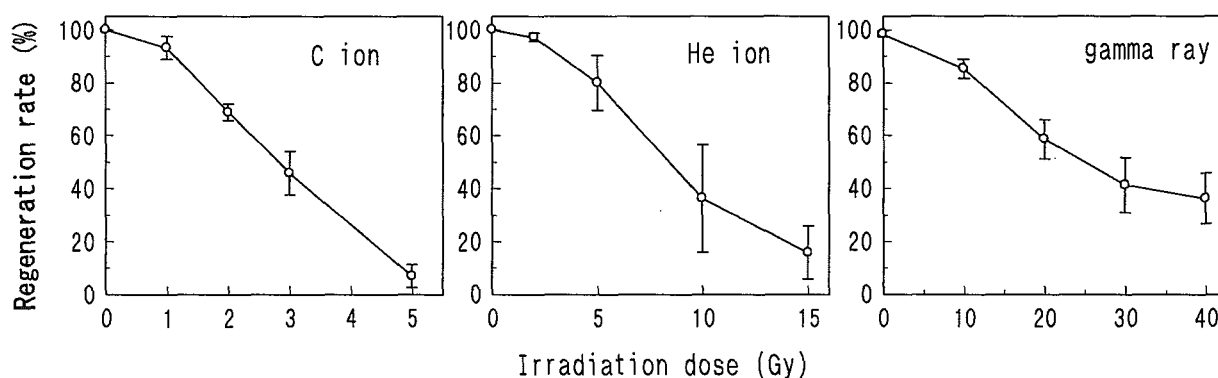


Fig.1 The influence of C ion beam, He ion beam and gamma ray irradiation on the regeneration from leaf explants in chrysanthemum.

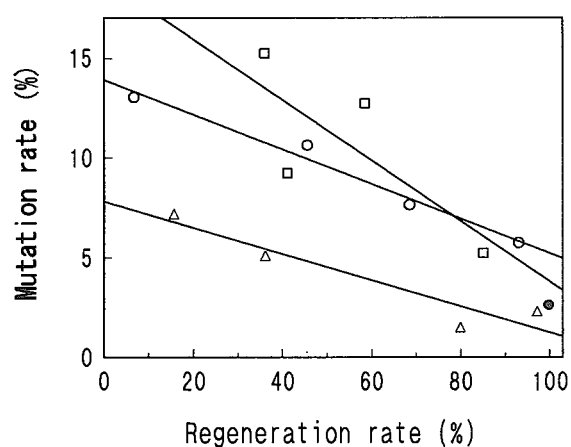


Fig.2 The relationship between the regeneration rate and the mutation rate in flower color in chrysanthemum.

○ : C ion △ : He ion
□ : gamma ray ● : 0 Gy (Somaclonal variation)

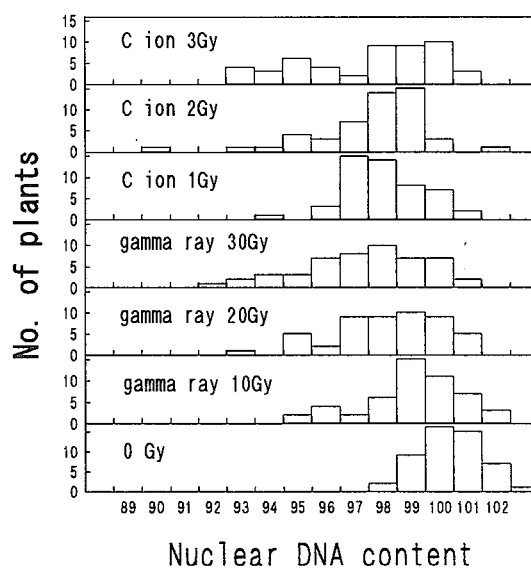


Fig. 3 The influence of C ion beam and gamma ray irradiation on nuclear DNA content in chrysanthemum.

2.6 Development of Mutant Varieties "Vital Ion Series" in Carnation by Ion Beam Breeding

M.Okamura*, N.Yasuno*, M.Ohtsuka*, A.Tanaka**, N.Shikazono**, and Y.Hase**

Plant Laboratory, Agribio business company, Kirin Brewery Co., Ltd.*

Department of Ion-Beam-Applied Biology, JAERI**

1. Introduction

Ion beams are expected to be utilized widely as new mutagens, because they deposit high energy on a target densely and locally as opposed to low linear energy transfer (LET) radiation such as electrons, X-rays and gamma rays. Takasaki Ion Accelerators for Advanced Radiation Application (TIARA) has been established as the first facility of ion beams only for the material and biological use in the world in 1993 and the research on the biological effects and the mutation induction of ion beams started¹⁾. In a series of research, the characteristics of ion beams have been made clear that novel mutants were induced such as resistance to ultraviolet, flower with serrated petals and sepals in *Arabidopsis*¹⁾, specific flower color in chrysanthemum²⁾ and in carnation³⁾, and mutation frequencies by carbon ions were 8 fold to 33 fold higher than those of electrons¹⁾.

In 2002, we have developed the carnation new varieties "Vital Ion series", that is the first success in the world to commercialize the new variety series by ion beam breeding. In this report, we describe the characteristics of the varieties and mutants by the combined method of ion beam irradiation with in vitro cell (Fig.1) and tissue culture³⁾.

2. Materials and Methods

Spray carnation variety, 'Vital' (cherry pink, serrated petals), was used for the experiment. The leaf segments were placed in petri dish containing Murashige and Skoog medium supplemented with 2mg/l Zactin, 30g/l sucrose and 7g/l agar (MSZ medium). The samples covered with Kapton film were irradiated with 220 MeV carbon ion beams from the TIARA AVF cyclotron (JAERI, Takasaki). After irradiation, the leaf segments were transferred onto fresh MSZ medium and cultured in the

growth room. The frequency of adventitious shoot regeneration was examined two months after irradiation. The regenerated plants were acclimatized in the greenhouse and their flower color and shape were investigated (Fig.2). The frequency of adventitious shoot regeneration from the leaf cultures irradiated by gamma rays was examined as well and the flowers derived from gamma irradiation were investigated as comparison.

3. Results and Discussion

1) Biological effect of ion beams

The dose response curve of adventitious shoot regeneration by ion beam irradiation showed that the regeneration frequency decreased with increasing dose and the median regeneration dose (RD50) was estimated at 15 Gy. In gamma rays, RD50 was around 60Gy. The RBE of ion beams relative to gamma rays was estimated to be 4.

The mutants of flower color and shape in the plants irradiated by ion beams were shown in Table 1, and that by gamma rays in Table 2. The mutation rates of flower color are 2.8% and 2.3% in ion beams and gamma rays, respectively. In ion beam breeding, pink and red mutants were obtained at the dosages of 5Gy to 10Gy that is 20 to 40 tracks to the cell. On the other hand, the dosages of gamma ray irradiation to obtain pink and red mutants were 30Gy to 50Gy that is 60,000 to 100,000 spurs. These results suggest that ion beams can induce mutations at low dosages of irradiation, resulting in the effective induction of the mutants with one or a few point mutations that have no or very few undesired mutations.

2) Characteristics of mutants by ion beams

Flower color mutants such as pink, pale pink and red were obtained by gamma ray

irradiation, whereas those by carbon ion beam contained pink, dark pink, light pink, salmon, red, complex and striped types of flower color (Fig.3).

The mutation spectrum of the flower color and shapes was the widest in ion beam breeding. Qualitative mutants such as salmon, red, striped color, etc. as well as quantitative mutants such as dark pink, pink, light pink, bi-colored etc. have been obtained in carnation. Wide variety of flower shape mutants have been obtained such as round petals, wild *Dianthus* type flowers etc (Fig.4).

3) Development of varieties "Vital Ion series"

From among the new color mutants derived from ion beam breeding of cv. Vital, three mutant varieties, dark pink, red and bi-colored type had been developed and applied for registration and commercialized (Fig.5). The other mutants such as salmon, pink, pearl and yellow will be registered and commercialized as "Vital Ion series" in 2002. The original variety Vital is Kirin's superior variety that has resistance to Fusarium disease, high

productivity, long vase life etc. By ion beam breeding, we have succeeded in the breeding of cv. "Vital" color family and rose type flowers (Fig.6) as well within two years that retained the superior characteristics of the parent.

The expected distribution amount of "Vital Ion series" cut flowers in Japan is to be more than several ten millions, that is about ten billion yen. The "Vital Ion series" are tested in Europe as well, therefore more economic impact is expected. Higher energy ion beams that have deeper penetration depth to the plant tissue and organ will make it possible to broaden the target crops and materials, resulting in the progress of commercialization of ion beam breeding.

References

- 1) A. Tanaka, Gamma Field Symposia, No.38 (1999), 19-28
- 2) S. Nagatomi, et al., JAERI-Review 98-016 (1998), 41-43
- 3) M. Okamura et al., JAERI-Review 2001-039 (2001), 52-54

Table 1. No. of mutants in plants regenerated from leaf cultures irradiated by $^{12}\text{C}^{5+}$ ion beams

Dose (Gy)	No. lines tested	Mutants in flower color and/or shape (No.)	Mutation (%) in flower
5	263	Round petals (2), Light Pink (1),	1.1
10	284	Pink (1), Dark Pink (1), Light Pink (2), Salmon (2), Red (1), Striped type; pink and white (2), <i>Dianthus</i> type petals (2)	3.9
15	251	Pink (2), Pink / Round petals (1), Yellow(1) Red (1), Red / Round petals (1), Complex type; pink and white (2)	3.6
30	52	Striped type; pink and white (1), Cream (1)	3.8
Total	850	Flower color and shape mutants (24)	2.8

Table 2. No. of mutants in plants regenerated from leaf cultures irradiated by gamma rays

Dose (Gy)	No. lines tested	Mutants in flower color and/or shape (No.)	Mutation (%) in flower
30	350	Pink (1), Minute striped (3)	1.1
50	426	Pink (2), Red (1), Minute striped (4), Round petals(2)	2.1
70	264	Pink (1), Light pink (2), Minute striped (7)	3.8
100	110	Red (1), Minute striped (2)	2.7
Total	1150	Flower color and shape mutants (26)	2.3

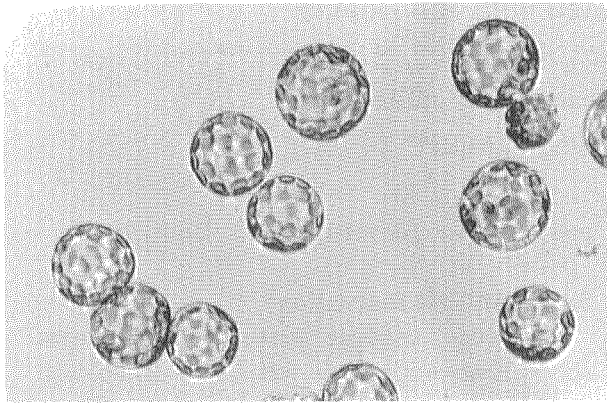


Fig.1 Mesophyll protoplasts of carnation.

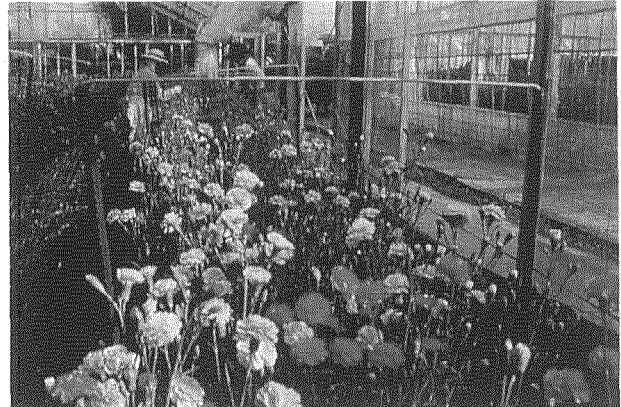


Fig.2 Flowering of the mutants by ion beam breeding.

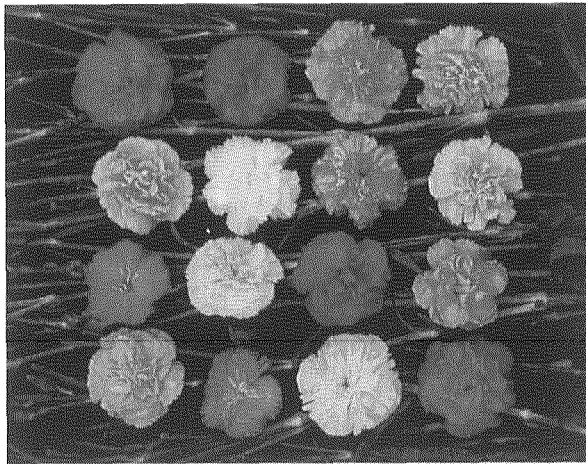


Fig.3 "Vital Ion series" by ion beam breeding.

1 L-R: Vital (cherry,serrate), Red, Dark pink, Salmon
 2 L-R: Dark bi, Yellow, Striped, Light bi
 3 L-R: Dianthus, Light pink, Round red, Round Pink
 4 L-R: Pink, Dianthus, Light Dianthus, Round

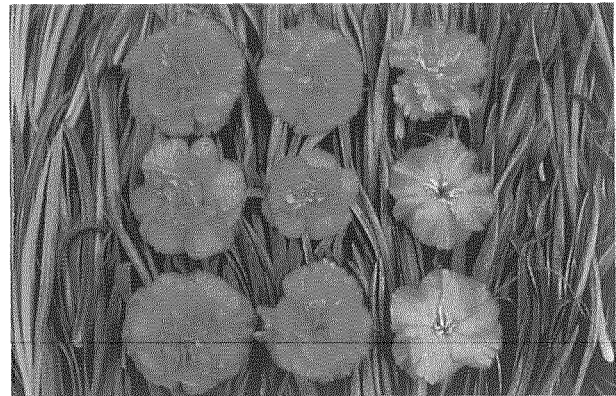


Fig.4 Flower shape mutants by ion beam breeding.

1 L-R: Vital, Less petals, Dianthus
 2 L-R: Round petals, Small flower, Dianthus
 3 L-R: Round petals, Less petals, Dianthus
 From the ABC model of whorl formation and floral organ identity, group B genes might be mutated in a series of Dianthus type mutants.



Fig.5 Commercialized varieties of "Vital Ion series" developed by ion beam breeding.



Fig.6 Rose type mutant developed by ion beam breeding: Most of the mutants retained superior characteristics of the parent variety Vital.

2.7 Mutation Generation in Chrysanthemum Plants Regenerated from Floral Organ Cultures Irradiated with Ion Beams

M.Okamura*, N.Yasuno*, M.Takano*, A.Tanaka**, N.Shikazono** and Y.Hase**

Plant Laboratory, Agribio business company, Kirin Brewery Co., Ltd.*

Department of Ion-Beam-Applied Biology, JAERI**

1. Introduction

Most mutagens used for mutation breeding of crops in the world are gamma rays and X-rays. Ion beams are expected to be utilized widely as new mutagens, because they have much higher linear energy transfer (LET) and relative biological effectiveness (RBE) than those of gamma rays and X-rays¹⁾. By ion beam irradiation, specific flower color mutants were obtained in chrysanthemum²⁾. By the combined method of ion beam irradiation with in vitro leaf culture, we succeeded in the development of new carnation varieties "Vital Ion series" in a short period of time³⁾.

In this study, we investigate the efficiency of mutation generation by a combined method of ion beam irradiation with floral organ cultures in spray chrysanthemum, and characterize the feature of mutation breeding using ion beam irradiation.

2. Materials and Methods

Spray chrysanthemum variety, 'Grand pink' (pink flower), was used for the experiment. The disk floret segments were placed in petri dish containing Murashige and Skoog medium supplemented with 0.1mg/l NAA and 0.5mg/l BA, 30g/l sucrose and 7g/l agar (MSNB medium). The samples covered with Kapton film were irradiated with 320 MeV carbon ($^{12}\text{C}^{6+}$) ion beams from the TIARA AVF cyclotron (JAERI, Takasaki). After irradiation, the disk floret segments were transferred onto fresh MSNB medium and cultured in the growth room. The frequency of adventitious shoot regeneration was examined 1.5 months after irradiation. The regenerated plants were acclimatized in the greenhouse and their flower color and shape were investigated. The regeneration frequency of adventitious shoots from the disk floret cultures irradiated with X-rays was examined and their flower color

and shape were investigated as comparison.

3. Results and Discussion

The dose response curve of adventitious shoot regeneration by ion beam irradiation was shown in Fig.1A, and that by X-ray irradiation in Fig.1B. In $^{12}\text{C}^{6+}$ ion beams, the regeneration frequency decreased at the dosage of 7Gy and the median regeneration dose (RD50) was estimated at 6Gy. In X-rays, RD50 was around 30Gy. The RBE of $^{12}\text{C}^{6+}$ ion beams relative to X-rays was estimated to be about 5.

The mutants of flower color and shape in plants regenerated from disk florets irradiated by $^{12}\text{C}^{6+}$ ion beams were shown in Table 1. The mutation rates are 6.5 % and 7.3 % in $^{12}\text{C}^{6+}$ ion beams and X-rays, respectively. Flower color mutants such as dark pink, orange, salmon and flower shape mutants such as round petals were obtained by X-ray irradiation, whereas those by $^{12}\text{C}^{6+}$ ion beam irradiation contained light pink, dark pink, dark orange, orange, salmon, pink and pearl striped type color mutants (Fig. 2) and flower shape mutants such as cup shaped (Fig. 3), and small types.

In this study using spray chrysanthemum, new mutants in flower color and in flower shape such as striped type and cup shaped type have been obtained in carbon ion beam irradiation. The results were correspond with the report in chrysanthemum²⁾ and carnation³⁾ in that the color spectrum of the ion beam induced mutants was wider than that of electron beam induced mutants and the specific mutants such as striped color type and new flower shapes were obtained. These results show that ion beams have different effect from that of electron beams on mutation generation of crops and have great impact on plant seed and seedling business.

References

- 1) A. Tanaka et. al., Int. J. Radiat. Biol 72 (1997), 121-127
- 2) S. Nagatomi, et. al., JAERI-Review 97-015 (1998), 50-52
- 3) M. Okamura et. al., JAERI-Review 2001-039 (2001), 52-54

Table 1. No. of mutants in plants regenerated from disk florets irradiated by $^{12}\text{C}^{6+}$ ion beams

Dose (Gy)	No. lines tested	Mutants in flower color and/or shape (No.)	Mutation rate (%)
0	50	Earlier flowering (1), Light pink (1),	4.0
1	40	Dark pink (1), Light pink (1)	5.0
3	92	Dark pink (3), Light pink (2), Pink and pearl striped (2), Dark orange (2), Salmon (1), Cup shaped (1)	11.9
5	86	Light pink (2), Orange (1), Acute petals (1)	4.7
7	22	Dark pink, small (1)	4.5
10	4		0
Total	294	Color, shape mutants (19)	6.5

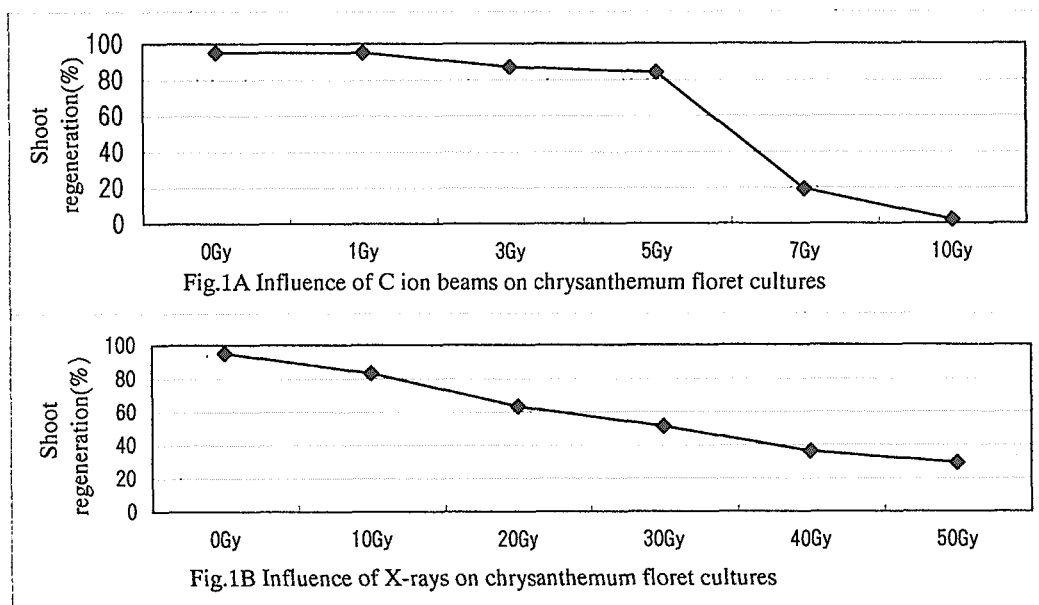


Fig. 2 Mutants of cv. "Grand pink" (upper left) obtained by $^{12}\text{C}^{6+}$ ion beam irradiation: dark pink, dark orange, pink and pearl-striped type etc.

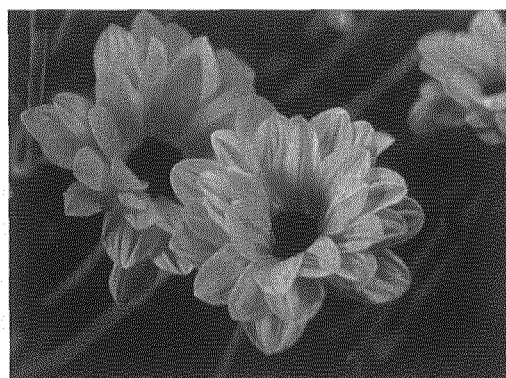


Fig. 3 Development of flower shape mutant: Cup shaped flowers obtained by $^{12}\text{C}^{6+}$ ion beam irradiation.

2.8 Effects of Ion Beam Irradiation on Chrysanthemum Leaf Discs and Sweetpotato Callus

K. Ueno*, S. Nagayoshi*, K. Shimonishi*, Y. Hase**, N. Shikazono** and A. Tanaka**

Kagoshima Biotechnology Institute*, Department of Ion-Beam-Applied Biology, JAERI**

1. Introduction

Chrysanthemums have some agronomical traits to be improved such as reducing axillary buds to save farmer's labor and lower temperature flowering to save the cost of heating. Sweetpotato is facing serious economic situations caused by increasing imports of cheap starch, which require new type variety of different starch composition such as high amylose content that could be used for degradable plastics.

New type plant mutants such as UV-resistant *Arabidopsis* and chrysanthemum with novel flower colors have been obtained using ion beams as a mutagen^{1), 2)}. The objectives of our research are to develop effective method for mutation of these crops using ion beams and to obtain desirable variants. In this paper, we describe effects of ion beam irradiation on cultures of chrysanthemum and sweetpotato.

2. Materials and Methods

2.1 Plant materials

Chrysanthemum (cv. *Jimba* and *Sanyo-ohgon*) leaves were cut into appropriately 4 mm × 2 mm disc and cultured on MS medium with 5 mg/l IAA and 1 mg/l BA prior to 3-6 days of irradiation, followed by culture on MS medium with 0.01 mg/l NAA and 0.05 mg/l BA for adventitious shoot development.

Embryogenic callus of sweetpotato (cv. *Shirosatsuma*) was subcultured on MS medium

with 0.05 mg/l 2,4-D. Callus was prepared around ϕ 1-2 mm in size prior to irradiation. Somatic embryos were induced using 4 mg/l ABA and 1 mg/l GA₃, followed by transfer to MS hormone-free medium for plantlet development.

2.2 Ion beam irradiation

Leaf discs and callus were irradiated with 50 MeV or 100 MeV helium ions and 220 MeV or 320 MeV carbon ions, accelerated by AVF cyclotron at JAERI at doses of 0.5-10 Gy for chrysanthemum and 20-300 Gy for sweetpotato.

3. Results and discussions

3.1 Chrysanthemum

In 220MeV $^{12}\text{C}^{5+}$ and 320MeV $^{12}\text{C}^{6+}$ ion beams, regeneration frequency decreased rapidly with increasing dose and the 90% re-generation dose (RD90) was estimated at 2 Gy and 3 to 4 Gy, respectively. In 100MeV $^4\text{He}^{2+}$ ion beams, regeneration frequency also decreased with increasing dose and the RD90 was estimated at 5 Gy³⁾. Therefore, specimens were irradiated at nearly RD90. In this study, more than 10,000 regenerated plants were obtained and cultured in three different cropping systems; for selection fewer axillary flower buds or lower temperature flowering line. From the screening of 10,468 and 1,086 M1 plants derived from the ion-beam and X-ray irradiated leaf discs, respectively, more than 40 visible mutants were selected (Table 1).

Table 1. The number of tested and selected plants in three different cropping systems, which regenerated from leaf cultures irradiated by ion beam or X-ray.

Cultivar	Radiation	Energy MeV	Dose Gy	Flowering period, items of selection, and the number of tested and (selected) plants.			
				Dec. & Apr. * (B), (F) **	March (B)**	April (B+F)**	Total
Jimba	He	50	1.3	44 (1)***			44 (1)
		100	1.10	2,032 (2)			2,032 (2)
	C	220	1.5	39 ()	1,801 (10)	1,793 (14)	3,633 (24)
		320	0.5-10	351 ()	1,091 (5)	1,358 (2)	2,800 (7)
	X-ray		5	223 ()	341 (1)	522 (2)	1,086 (3)
Snayo-ohgon	He	100	1-10	632 ()	243 (1)		875 (1)
	C	220	1.5		639 (5)		639 (5)
		320	0.5-10		445 (4)		445 (4)
		Total			3,321 (3)	4,560 (26)	3,673 (18)

*: The first flowering was December and second sprouting shoots were flowering on April.

**: Selected by a few axillary buds is (B), and selected by early flowering is (F).

***: () = No. of selected plants.

In the original cv. "*Sanyo-ohgon*", the number of axillary flower buds is almost more than 20. However, the number of axillary buds of the mutants was less than 9, and these were obtained from leaf cultures irradiated with 320MeV $^{12}\text{C}^{6+}$ ion beams at 3 to 5 Gy. The mutation rates of a few axillary buds were 6 % and 20 % in $^{12}\text{C}^{6+}$ ion beams at 3 and 5 Gy, respectively (Fig. 1). Furthermore, the mutants such as the number of axillary buds were less than 5, were obtained by $^{12}\text{C}^{6+}$ ion beams irradiation of 5 Gy. The mutation rates were 15 % (Fig. 1). Among them, the plants were selected which have few axillary bud, but the other floral and vegetative organs are not affected (Fig. 2-A).

In a similar way, we also obtained the few axillary bud mutants from cv. "*Jimba*" irradiated with 320MeV $^{12}\text{C}^{6+}$ at 3 Gy. Among them, we obtained one mutant, which has few axillary buds, normal flowers and normal vegetative organs. The axillary buds from basal to middle parts of this mutant were aborted and the meristem tissues were perfectly absent (Fig. 2-B). In this mutant, the mutation rate is 0.01 % (1/9,595) among the plants regenerated from leaf cultures irradiated with ion beam or X-ray.

Under low temperature, flowering period of "*Jimba*" is greatly delayed. Thus, in winter season, this cultivar is forced to culture under

high temperature at 15 to 20 °C. Therefore, we tried to select early flowering type to behave safely even under low temperature of 10 to 12 °C.

In 220MeV $^{12}\text{C}^{5+}$ ion beams, early flowering type (until 9 weeks flowering after lighting stop) frequency gradually increased with increasing dose, and late flowering type (more than 14 weeks) frequency also increased (Fig. 3). A lot of mutants with different flowering period were obtained by ion beam irradiation. In X-ray, we also obtained early flowering type and similar frequency of this mutation (Fig. 3).

Now, we are going to prepare for selection of mutants which have both few axillary buds and low temperature flowering trait.

3.2 Sweetpotato

In 100MeV $^4\text{He}^{2+}$ ion beams, regeneration frequency decreased with increasing dose and the RD50 was estimated at 100 Gy. Irradiation by 320 MeV $^{12}\text{C}^{6+}$ ions suppressed regeneration at 80 Gy or higher dose (Table 2).

We obtained more than 900 regenerated plants, which were 675 and 230 plants in $^4\text{He}^{2+}$ and $^{12}\text{C}^{6+}$ ion beams irradiated, respectively. These regenerated plants have been acclimated. After nursery management, they will be transplanted into field. When harvested the investigation into effects of ion beam irradiation on different starch composition, particularly on high amylose content, will be conducted.

References

- 1) A. Tanaka et al., TIARA Ann. Rep. 1995 (1996) 32-34.
- 2) S. Nagatomi et al., TIARA Ann. Rep. 1997, JAERI-Review 98-016 (1998) 41-43.
- 3) K. Ueno et al., Ikushugaku Kenkyu 3 (2001) (Suppl. 2): 62.

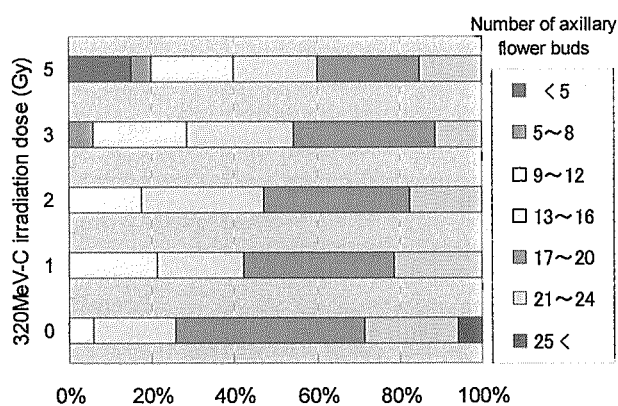


Fig. 1 Percentage of variants on the number of axillary flower buds of "Sanyo-ohgon".

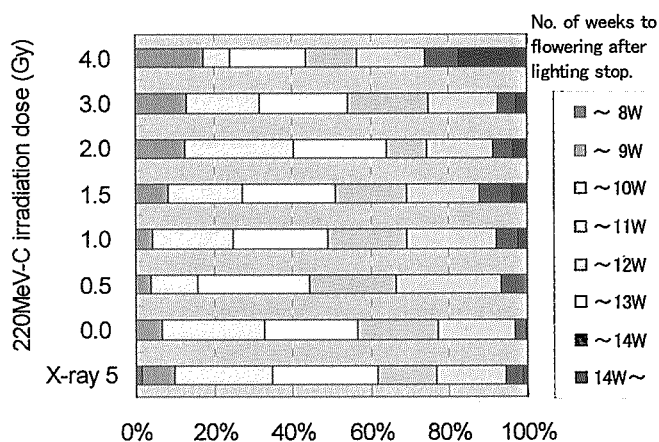


Fig. 3 Percentage of variants on the number of weeks to flowering after lighting stop of "Jimba".

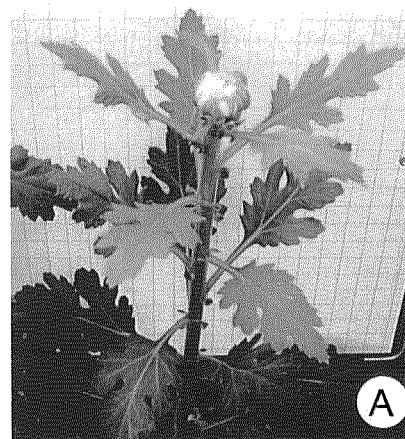


Fig. 2 A few axillary flower bud mutants of chrysanthemum.

A: "Sanyo-ohgon" and B: "Jimba".

Table 2. Effect of ion beam irradiation on regeneration from embryogenic callus of sweetpotato.

100 MeV He ions					320 MeV C ions			
Dose	No. of irradiated petri dish	Somatic embryo formation	No. of regenerated shoot	B/A	Dose	No. of irradiated petri dish	No. of regenerated shoot	B/A
Gy	(A)	%	(B)		Gy	(A)	(B)	
0	4	91.0	460	115	0	1	39	39
25-50	6	71.0	200	33	20-25	3	61	20
75-100	8	58.5	422	53	40-50	4	146	37
150-200	10	8.5	53	5	80-100	2	19	10
250-300	4	0.5	0	0	250-300	2	4	2

2.9 RAPD Analysis of Xanta and Waxy Mutants Induced by Ion Beam Irradiation to Hinoki Cypress(*Chamaecyparis obtuse*)

K. Ishii*, Y. Yamada*, Y. Hase**, N. Shikazono**, and A. Tanaka**

Department of Molecular and Cell Biology, Forestry and Forest Products Research Institute*, Department of Radiation Research for Environment and Resources, JAERI**

1. Introduction

Hinoki cypress (*Chamaecyparis obtusa* Sieb. et Zucc.) covers 24 % of the plantation area in Japan and is the most important endemic forest conifer. It produces the highest quality wood and can be grown throughout Japan, excluding Hokkaido and the Ryukyu Island. In forest tree species, many mutants were obtained by Gamma-rays radiation breeding. In Hinoki cypress, a juvenile leaf-form mutant was reported¹⁾.

Ion beam is expected to increase the mutation frequency and wide spectrum, since it has a high LET (linear energy transfer). The combination of ion beams irradiation and tissue culture was sometimes beneficial for high frequent mutation induction²⁾³⁾⁴⁾. In the previous report, we have obtained the xanta and wax rich mutants by ion beam irradiation⁵⁾. However, those mutants were identified using the morphological characteristics. To clarify the genetic background for such mutants, RAPD analysis is useful. There are many reports of detecting genetic aberration of plants by RAPD analysis⁶⁾⁷⁾⁸⁾.

In this study, we conducted RAPD analysis of mutants obtained by irradiation of the shoot primordia of Hinoki cypress with $^4\text{He}^{2+}$ and $^{12}\text{C}^{5+}$ heavy ion beams.

2. Experimental procedure

Shoot primordia of Hinoki cypress was used for the experiments. They are cultured on CD medium⁹⁾¹⁰⁾ supplemented with 2.25 mg/l 6-benzylaminopurine and 0.005 mg/l naphthalene acetic acid (NAA). Fresh shoot primordia were subcultured on the same medium in petri dish (35 x 10 mm) which was covered with Kapton film. They were irradiated with 50 MeV $^4\text{He}^{2+}$ or 220 MeV $^{12}\text{C}^{5+}$ ion beam from AVF cyclotron in JAERI. After irradiation the shoot primordia were subcultured to the new CD media containing 0.005 mg/l NAA for shoot differentiation.

Plant genomic DNA was extracted from leaf tissue (200 mg) using a GenomicPrep Cells and Tissue DNA Isolation Kit (Pharmacia Biotech) according to the instructions of the manufacturer. PCR analysis was done according to following condition. Ten ng template DNA and 0.25 μM of each primer were mixed with 2 μl of 10 x Stoffel buffer (containing 100 mM KCl, 100 mM Tris-HCl, pH8.3), 3 mM MgCl_2 , 0.2 mM of a dNTP mixture (equimolar dATP, dCTP, dGTP and dTTP) and 1 unit of Ampli Taq DNA polymerase (Parkin-Elmer) in a total volume of 20 μl . Fifty cycles of PCR were performed in a programmed temperature control system

(Takara, PCR Thermal Cycler MP TP3000). A single cycle consisted of the following steps; denaturation at 94 °C for 10 sec, annealing at 38.5 °C for 30 sec, and DNA synthesis at 72 °C for 1 min. Amplified DNA was analyzed by EtBr staining after 2 % agarose gel electrophoresis at 50 V.

3. Results and Discussion

We observed albino, xanta and wax rich type mutation shoot regeneration from these irradiated shoot primordia.

Xanta, waxy and control type of regenerated Hinoki cypress in vitro were checked for their DNA level difference using RAPD analysis. Among 81 primers used, 23 primers produced the 68 bands. Among them stable 44 bands produced by 15 primers were compared between mutants and control plant. One example of the experiment is shown in the Figure 1. So far, there is no variation among the RAPD analysis band patterns of those mutants. Bigger test size may detect the gene variation specific for mutants, although we expected the less DNA level mutation in this experiment.

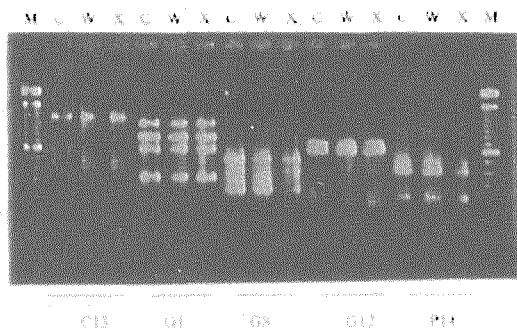


Fig. 1 PCR analysis of control and mutants of Hinoki cypress. C: control, W: Waxy mutant, X: Xanta mutant M: Marker DNA

4. Summary

Combination of ion beam irradiation and tissue culture was effective to induce morphological mutation of Hinoki cypress. There is no variation among the RAPD analysis band patterns of those mutants (xanta and wax rich type) and control.

References

- 1)T. Kondo, Forest Tree Breeding 167(1993)12-15.
- 2)S. Nagatomi, A. Tanaka, A. Kato, H. Watanabe and S. Tano, TIARA Annual Report 5(1996)50-52.
- 3)S. Nagatomi, A. Tanaka, H. Watanabe and S. Tano, TIARA Annual Report 6(1997) 48-50.
- 4)T. Nakahara, K.Hirashima, M. Koga, A. Tanaka, N. Shikazono and H. Watanabe, TIARA Annual Report 1998(1999)28-29.
- 5)K.Ishii, Y.Hase, N. Shikazono and A.Tanaka, TIARA Annual Report 2000(2001)55-56.
- 6)Keil,M. and Griffin,A.R.,Theor. Appl. Genet.,89 (1994) 442-450.
- 7)Mailer,R.J. et al.,Theor. Appl. Genet., 87(1994) 697-704.
- 8)Shnell,R.J. et al.,Theor. Appl Genet, 90(1995)296-274.
- 9)R.A. Campbell and D.J. Durzan, Can J. Bot. 53(1975)1652-1657.
- 10)K. Ishii, Plant Cell Tissue and Organ Culture 7(1986)247-255.

2.10 Induction of Mutation in Garlic (*Allium Sativum* L.) By Ion Beam Irradiation

T.Tashiro*, Y. Yamamoto*, A.Tanaka**, N.Shikazono** and Y.Hase**

University Farm, Faculty of Bioresearch, Mie University*

Department of Ion-Beam-Applied Biology**

1. Introduction

Recently there is a great demand for garlic because garlic is one of the remarkable health foods. Garlic belongs to a group of the *Allium* family. Since garlic is sexually sterile and propagated by bulbs, the positive plant breeding is difficult. Therefore, the consumer and the producer could not satisfy the breeding in garlic. We established a novel system of practical micropropagation of garlic, which effectively produced bulblets in vitro (Fig.1), because it is a wise method to proliferate, to select, and to plant in field¹⁾.

Ion beam is expected to increase the mutation frequency and wide spectrum, since it has higher LET (linear energy transfer)²⁾. A combined method of ion beams irradiation with tissue culture was beneficial for high frequent mutation. We supposed that ion beam induced specific mutation not only morphological character but also chemical composition for garlic.

The purpose of this study is to investigate the effects of ion beam on the mutant of volatile sulfur compounds of garlic. In this paper, we report the effects of ion beam on callus proliferation and shoot regeneration from the irradiated callus induced from basal plate of garlic bulb, and bulblet induction from explants of basal plate bulb.

2. Materials and Methods

Garlic cultivars, 'Fukuchi-white' treated sterilely were used for the experiments. One of irradiated materials was thin sections of bulb basal plates. Another one was compact and granular callus like embryogenic callus.

2.1 Basal plate

Multiple shoots are induced directly from basal plates in very short culture period, but it is difficult to obtain many regenerated plantlets. Basal plate was cut off 1~1.5mm thickness as ion beam could irradiate through them perfectly and trimmed 5x5mm in length, and then divided into 4 equal segments. 8-12 segments were placed on a 30mm diameter plastic petri dish containing LS medium supplemented with 30g/l sucrose and 3g/l gelrite for shoot differentiation³⁾. The dishes were covered with Kapton film, and then irradiated with 320 MeV $^{12}\text{C}^{6+}$ ion beams from the TIARA AVF cyclotron in JAERI (Fig.2). Irradiation dosage ranged from 0Gy to 10Gy at 9 levels in carbon ion beam. After irradiations the both samples were transferred to the fresh medium for shoot differentiation. Fresh shoots were subcultured on medium for bulblet formation.

2.2 Callus

It takes over four months to obtain bulblets, but the regenerated plantlets can be obtained enough numbers to select mutants. Callus in liquid-shaking culture

were placed on 1mm thickness in 30mm diameter plastic petri dish containing MS medium supplemented with plant growth regulator (2,4-dichlorophenoxy acetic acid). The dishes were covered with Kapton film, and then irradiated with 50 MeV $^4\text{He}^{2+}$ and 320 MeV $^{12}\text{C}^{6+}$ ion beams same as basal plates(Fig.2). Irradiation dosage ranged from 0Gy to 10Gy at 7 levels in helium ion beam and from 0Gy to 1Gy at 6 levels in carbon ion beam. After irradiations the both samples were transferred to the medium for shoot differentiation after one month. Fresh shoots were subcultured on medium for bulblet formation.

The experiments were performed under 3000 lux(day /night of 16/8hrs) at 25°C. Proliferation rate of callus and formation rate of callus colony that had the regenerated ability to obtain shoot, and survival rate of basal plate segment and bulblet formation rate from basal plate segment were investigated.

3. Results and Discussions

Basal plates: In carbon ion beams, the survival rate of basal plate segments gradually decreased with increasing dosage and the median lethal dose (LD_{50}) was estimated around 2Gy. However, LD_{50} in bulblet formation rate was estimated around 1Gy. These results suggested that carbon ion beams have penetrated through segments and have affected to the plantlet regenerations(Fig.3).

Callus: In helium ion beams, the callus proliferation rate on 39th days after radiation drastically decreased with increasing dosage and almost suppressed

at higher than 2Gy. The callus colony formation rate on 144th days after radiation also decreased with increasing dosage and LD_{50} was estimated around 0.5Gy. These results suggested that helium ion beams have affected to the cell differentiations. In carbon ion beams, the relation between irradiation dose and the callus proliferation rate on 35th days after radiation was not apparent. The callus colony formation rate on 140th days after radiation decreased gradually with increasing dosage(Fig.4).

The regenerated bulblets were placed on soil for sprouting and now they are well grown in experimental field(Fig.5-6). They will be harvested in June 2002 and estimated agricultural traits in details.

References

- 1)Y.Yamamoto, T.Tashiro, International Plant Propagators' Society 7:17-18(2000)
- 2)A.Tanaka, N.Shikazono, Y.Yokota, H.Watanabe and S.Tano, Int. J. Radiat. Biol. 72:121-127(1997).
- 3)M.Maybe, S.Sumii, Plant Cell Reports 17:773-779(1998)



Fig.1 Garlic bulblets regenerated from *in vitro* culture.

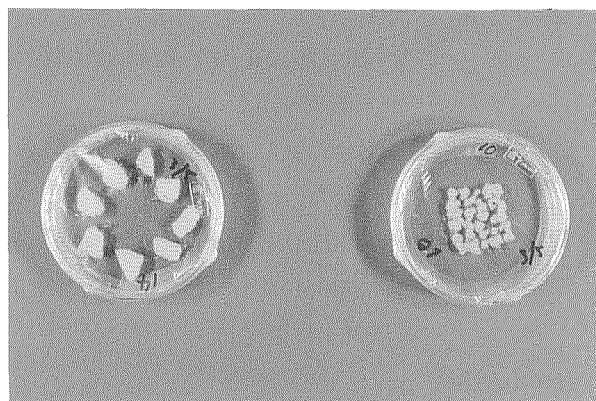


Fig.2 Petri dish covered with Kapton film. Basal plates of garlic bulb (left), Callus derived from basal plate of garlic bulb (right).

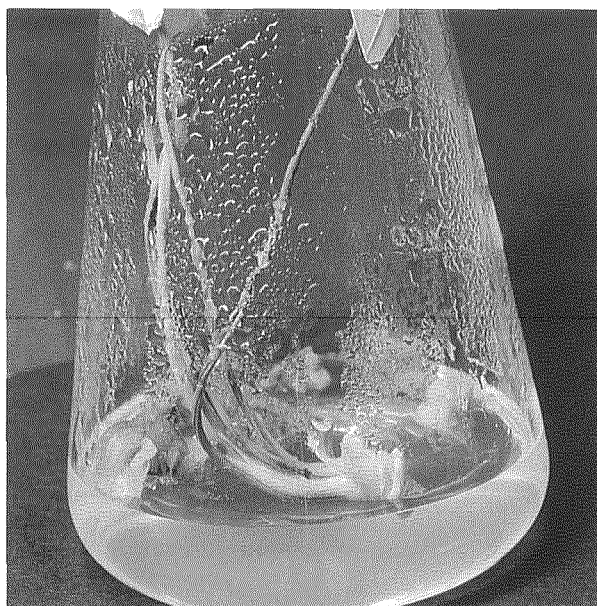


Fig.3 Shoots induced by basal plate irradiated with ion beams.

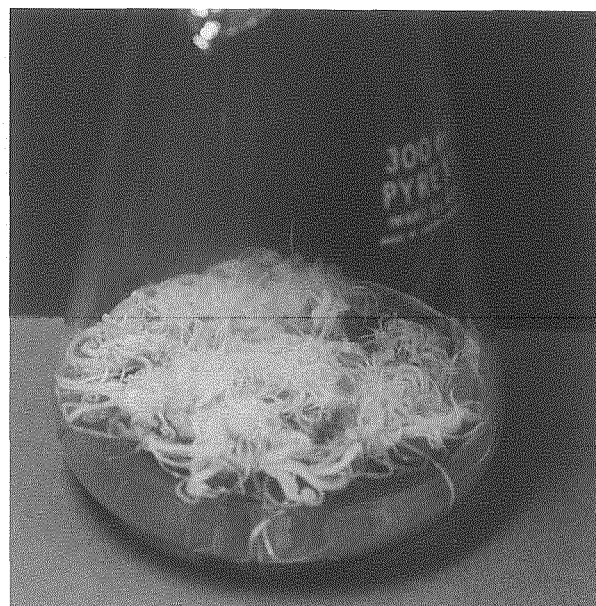


Fig.4 Multiple shoots regenerated from callus irradiated with ion beams.

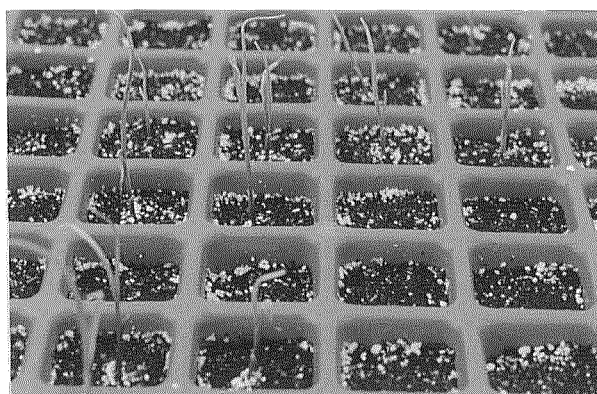


Fig. 5 Young garlic seedlings derived from bulblets.



Fig.6 Garlic plants regenerated from basal plate callus irradiated with ion beams.

2.11 Characters of Tomato cv. First Mutant with Short Internode Induced by Irradiation of $^{12}\text{C}^{5+}$ Ion Beam to the Seeds

M. Masuda*, K. Murakami*, S. G. Agong*, T. Yuasa*, A. Tanaka** and Y. Hase**

Department of Applied Plant Science, Faculty of Agriculture, Okayama University*

Department of Ion-Beam-Applied Biology, JAERI**

1. Introduction

With the increasing demand and the changing human taste preferences, there is a continuous drive to generate new tomato cultivars for the modern production and consumer purposes. Ion beam, a recently innovated technique has been shown to produce a new type of mutant in *Arabidopsis thaliana*¹⁾. Since biological effects of ion beam is different from that of gamma-rays, we expect that ion beam irradiation will be new technique for obtaining novel mutants. Masuda et al. (2001) reported that 50Gy of $^{12}\text{C}^{5+}$ and 150Gy of $^4\text{He}^{2+}$ were the optimum dosages for irradiating tomato seeds with the possibility of generating tomato mutants without causing excessive injury to the embryo²⁾. Short internode is useful character in tomato, especially in protected cultivation. In this paper, we report that characters of tomato cv. First mutant with short internode induced by irradiation of $^{12}\text{C}^{5+}$ ion beam to the seeds.

2. Experimental procedure

2.1 Plant material

A mutant with short internode was induced from cv. First tomato irradiated with 50 Gy of $^{12}\text{C}^{5+}$ ion beam (220 MeV) to their seeds²⁾. Material seeds (M_3) were derived from self-pollination of the M_2 plant.

2.2 Morphological character of mutant

Seeds of mutant and original cv. First were sown in vermiculite on 27 March. Shoot length and number of leaves unfolded were measured every weeks. Morphological characters were recorded 11 weeks after sowing.

2.2 Effect of GA_3 treatment on shoot growth

Mutant and original cv. First plants at 3rd leaf-stage were used. GA_3 at the concentration of $100 \text{ mg}\cdot\text{L}^{-1}$ was applied with a sprayer. Second application were made 10 days after 1st application. Shoot length was measured every 5 days.

2.3 Shoot growth of F_1 plant

F_1 plants were obtained from crossing (mutant (M_2) \times original cv. First). Seeds of mutant, F_1 and original cv. First were sown in vermiculite on 17 April. Shoot length was measured every 5 days.

3. Results and discussion

3.1 Morphological character of mutant

Mutant plant grew vigorously, but its shoot length was about 50 % of original cv. First (Table 1). Leaf number and size of mutant plants (M_3) were almost similar to that of original cv. First. Internode length (stem length / leaf number) was also about 50 % of original cv. First.

Table 1. Morphological characters in a tomato mutant.

Line	Shoot length ^z (cm)	Longest leaf (stalk and blade) (cm)	No. of leaves unfolded	Internode length ^y (cm)	No. of flowers in inflorescence			Length of peduncle (cm) (Distance to 1st fruit)		
					1st	2nd	3rd	1st	2nd	3rd
First	85.7±4.4	35.3±3.6	15.2±0.0	5.7±0.3	9.7±0.2	9.3±0.4	10.5±0.1	5.8±0.4	5.2±0.7	7.0±2.2
Mutant	45.9±4.7	39.2±3.8	16.3±0.1	2.8±0.3	18.3±0.5	15.0±0.4	13.8±0.6	2.1±0.5	3.5±1.0	4.4±0.9

Plants were measured 11 weeks after sowing. Values indicate the mean ±SD.

^zShoot length was measured from cotyledonary node to apical bud.

^yStem length / Leaf number

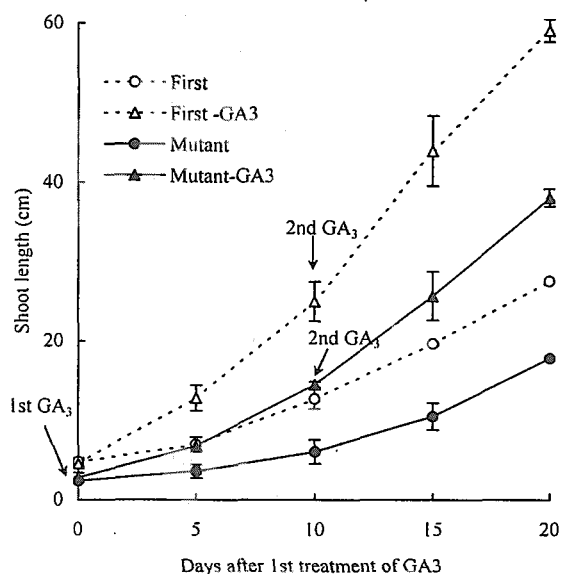


Fig. 1. Effect of GA₃ treatment on shoot growth in original 'First' and a mutant with short internode.

Arrows indicate the application of 100mg/l GA₃.
Vertical bars indicate standard deviation.

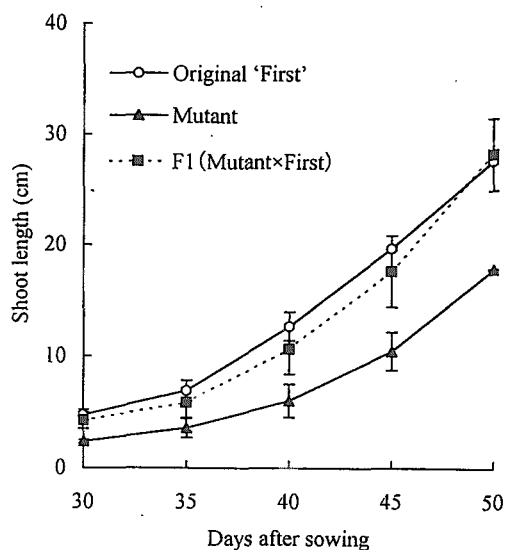


Fig. 2. Shoot growth of F₁ plant obtained from crossing original 'First' and a mutant with short internode.

Seeds were sown on 17 Apr.

Shoot length was measured from cotyledonary node to apical bud.

Vertical bars indicate standard deviation.

Mutant had a unique feature in the morphology of inflorescence. This plant formed many flowers and its peduncle was shorter than that of original cv. First (Table 1).

3.2 Effect of GA₃ treatment on shoot growth

GA₃ was effective on the stem elongation in similar manner in both original cv. First and mutant (Fig. 1). Shoot was elongated with application of GA₃, which was longer than that of untreated original cv. First.

3.3 Shoot growth of F₁ plant

Shoot length of F₁ plants was not different from that of original cv. First (Fig. 2). This result suggested that a short internode character was involved in a few recessive gene control.

3.4 Conclusions

This mutant plant grew vigorously and its leaf size was similar to original cv. First, but the internode length decreased about 50 % of original cv. First. Further studies are needed to clarify the inheritance of characters and gene application to other cultivars.

References

- 1) A. Tanaka, N. Shikazono, Y. Yokota, H. Watanabe and S. Tano. Int. J. Radiat. Biol. 72:121-127 (1997).
- 2) M. Masuda, S. G. Agong, A. Tanaka, N. Shikazono and Y. Hase. JAERI-Review 39:42-44 (2001).

2.12 Mutation Breeding of Rice, Eggplant and Gloriosa by Ion Beam

Irradiation

M. Mizobuchi*, M. Okada*, M. Matsumoto*, A. Iwasaki*, A. Tanaka**, Y. Hase**

Kochi Prefectural Agriculture Research Center*, Department of Radiation Research for Environment and Resources, JAERI**

1. Introduction

In Kochi Prefecture, we are carrying out mutation breeding of rice, eggplant and gloriosa. While we have used γ -rays and MNU as mutagens, we attempt to use ion beams in this study. Because the linear energy transfer and relative biological effectiveness of ion beams are extremely higher than those of γ -rays. Thus, seeds of rice, eggplant, and gloriosa were irradiated with ion beams and several biological effects were examined. Moreover, we selected individuals that have excellent mutant characters. We used helium(He) and carbon(C) ions that were accelerated by using the AVF cyclotron in Takasaki, JAERI.

2. Materials and Methods

In rice, dry seeds of varieties 'Tosapika' and 'Koshihikari' were irradiated to investigate their germination rates and survival rates. The seeds of 'Tosapika' with various storage periods and water contents were used to investigate the effects of ion beams to those seeds. Then we grew M_2 generation plants in the field and determined the adequate irradiation dosages on the basis of the amylose contents variance of their seeds.

In eggplant, we irradiated 220MeV C ions to seeds of variety 'Waseshinnkuro' and grew them. Then we cultured their anthers to investigate the correlation of the irradiation with regeneration rates of plantlets from anthers.

In gloriosa, seeds of 10 cultivars were

irradiated with 50Gy of 100MeV He, 5~40Gy of 220MeV C or 5Gy of 320MeV C to investigate the germination rates. For the S_1 population of 'Misato Pink' raised from the seeds irradiated with 220MeV C ion beam, their morphological characterizations were recorded.

3. Results and Discussions

In rice, the storage periods did not influence the survival rates of irradiated M_1 seeds. The less water content the seeds had, the lower survival rate the irradiated seeds showed (Fig.1). In 'Tosapika', the plants that had low amylose content seeds could not be obtained by the irradiations of 50MeV He and 100MeV He. By the irradiation of 220MeV C, the plants that had low amylose content seeds with suitable growth traits and brown rice qualities were obtained. The adequate irradiation dosages were thought to be about 20Gy because of the large standard deviation of amylose content (Table 1). In 'Koshihikari', though the plants that had low amylose content seeds were not obtained by the irradiations of 220MeV C, these were obtained by the irradiations of 50MeV He and 100MeV He. The adequate irradiation dosages were thought to be about 100Gy of 50MeV He and about 175 Gy of 100MeV He.

In eggplant, the plantlets were regenerated from inside of anthers via embryoids. The higher dosage the irradiation had, the lower the regeneration rate showed. More than 50Gy, there were few regenerated plants obtained. There was

one regenerated plant obtained from the 60Gy-irradiated plant, but it had no chlorophyll and could not be acclimatized (Table 2). Less than 50Gy, the regenerated plants grew well and could be acclimatized. From these results, 30~40Gy were thought to be the effective dosages to obtain regenerated plants.

The germination rates of irradiated gloriosa seeds varied much by the cultivars. The germination rates of the seeds irradiated with 80Gy of 100MeV He were 16~73%. Those with 5~10Gy of 220MeV or 320MeV C were 6~83%. The survival rates were almost same as the germination rates.

The small tubers, those were less than 6cm in length, were harvested to culture the seedlings for one growing season. Some plants of the S1 population of 'Misato Pink' from the seeds irradiated with 220MeV C were flowered. No mutation for petal color was observed (Table 3). One plant showed a chlorophyll mutation on the leaves.

4. Reference

- 1) A. Tanaka et al., TIARA Ann Rep., 1998,p39
- 2) H. Yamaguchi et al., TIARA Ann Rep., 1998,p42

Table 1 The amylose content of the M₂ generation of 'Tosapika'

Ion exposure dose	NO. of analyses	Amylose content (%)		Ion exposure dose	NO. of analyses	Amylose content (%)	
	107	mean	16.27		21	mean	16.92
¹² C ⁵ +220MeV		standard deviation	0.83	⁴ He ² +50MeV		standard deviation	0.34
10 G y		Minimum value	13.73	25 G y		Minimum value	16.08
		Maximum value	18.88			Maximum value	17.43
	64	mean	16.21		24	mean	16.96
¹² C ⁵ +220MeV		standard deviation	1.23	⁴ He ² +50MeV		standard deviation	0.26
20 G y		Minimum value	11.83	50 G y		Minimum value	16.28
		Maximum value	17.74			Maximum value	17.38
	29	mean	17.13		43	mean	17.60
¹² C ⁵ +220MeV		standard deviation	0.36	⁴ He ² +50MeV		standard deviation	0.28
30 G y		Minimum value	16.53	100 G y		Minimum value	16.76
		Maximum value	17.78			Maximum value	18.20
	45	mean	17.02		10	mean	16.85
⁴ He ² +100MeV		standard deviation	0.51	⁴ He ² +50MeV		standard deviation	0.38
25 G y		Minimum value	15.68	125 G y		Minimum value	16.22
		Maximum value	18.04			Maximum value	17.34
	47	mean	17.10		8	mean	16.95
⁴ He ² +100MeV		standard deviation	0.31	⁴ He ² +50MeV		standard deviation	0.19
50 G y		Minimum value	16.38	150 G y		Minimum value	16.62
		Maximum value	17.67			Maximum value	17.19
	25	mean	17.40		35	mean	17.16
⁴ He ² +100MeV		standard deviation	0.47	⁴ He ² +50MeV		standard deviation	0.48
100 G y		Minimum value	16.47	175 G y		Minimum value	15.62
		Maximum value	18.31			Maximum value	17.95
	4	mean	17.21		4	mean	16.69
⁴ He ² +100MeV		standard deviation	0.31	⁴ He ² +50MeV		standard deviation	0.17
125 G y		Minimum value	16.93	200 G y		Minimum value	16.49
		Maximum value	17.65			Maximum value	16.83
	13	mean	17.14		50	mean	16.62
⁴ He ² +100MeV		standard deviation	0.40	Tosapika		standard deviation	0.40
150 G y		Minimum value	16.52	Without management		Minimum value	15.65
		Maximum value	18.03			Maximum value	17.43
	4	mean	17.18				
⁴ He ² +100MeV		standard deviation	0.16				
175 G y		Minimum value	16.99				
		Maximum value	17.33				

1)irradiation in 2000

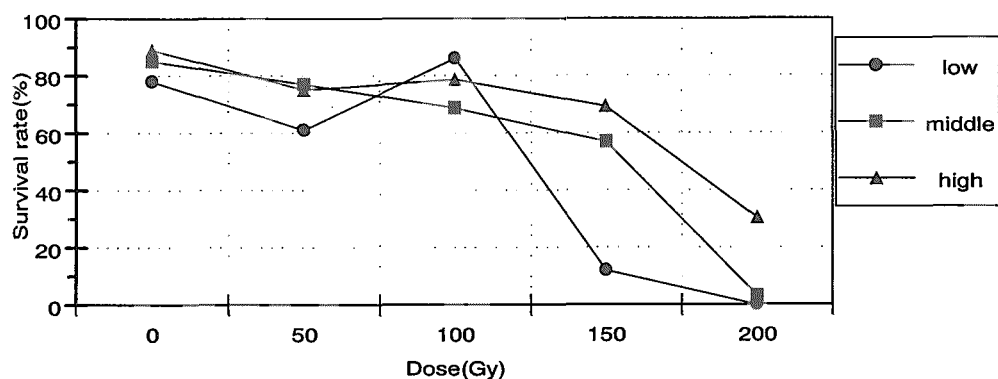


Fig.1 Survival rate of 'Tosapika' in Helium(50MeV) irradiation

watercontent of the brown rice. low:11.2%, middle:12.8%, high:13.8%.

Table 2 Anther culture of the eggplants irradiated with 220MeV C

Dose (Gy)	No. of flower buds cultured	No. of flower buds regenerated	regeneration rate (%)
0	86	24	27.9
30	98	21	21.4
40	107	20	18.7
50	103	5	4.9
60	20	1	5.0

Table3 Petal color and morphological mutations of the gloriosa plants from the seeds irradiated with ion beam(*MP(s)* S_i population of 'Misato-Pink', *SP* strong pink, *BR* bright red, *DP* deep pink, *VR* vivid red, *YP* yellowish pink, *BYR* bright yellowish red, *DYP* deep yellowish pink, *SYP* strong yellowish pink, *BRO* bright reddish orange, *BO* bright orange, *VYR* vivid yellowish red, *VY* vivid yellow, *BGY* bright greenish yellow, *CM* chlorophyll mutation)

Ion, Energy	Genotype	Dose (Gy)	Irradiation side of seed	Petal color				showing mutants (plants)
C 220MeV	MP(s)	40	ventral	DP	DP			CM(1)
		80	ventral	SP	SP	DP	BR	(0)
			dorsal	VR	SP			(0)
		160	ventral	SP	SP	SP	SP	(0)
				BR	BR	DP	BR	
				YP	YP			
			dorsal	SP	SP	BR	BR	(0)
(Control)	MP(s)	0	-	SP	SP	DP	BR	(0)
				BYR	VYR	DYP	SYP	
				BRO	BO	VY	BGY	

2.13 Regeneration of variegated plants from ion-beam irradiated explants of *Ficus stipulata* Thunb.

M. Takahashi*, S. Kohama*, K. Kondo*, M. Hakata*, Y. Hase**, N. Shikazono**, A. Tanaka**, and H. Morikawa****

Department of Mathematical and Life Sciences, Graduate School of Science, Hiroshima University, Higashi-Hiroshima, Japan*, Department of Radiation Research for Environment and Resources, JAERI, Takasaki, Japan**, Core Research for Evolutional Science and Technology (CREST), Japan Science and Technology Corporation (JST)***

Abstract

Young 1-mm-long apical shoots *Ficus stipulata* Thunb. were irradiated with $^{12}\text{C}^{5+}$ (220 MeV), $^{12}\text{C}^{6+}$ (220 MeV) and $^4\text{He}^{2+}$ (50 MeV) ion beams from the AVF cyclotron (JAERI). The frequency of regeneration of plants from the irradiated shoots and phenotypic variations were studied. A distinct suppression was observed at 20, 40 and 40 Gray (Gy) with $^{12}\text{C}^{5+}$, $^{12}\text{C}^{6+}$ and $^4\text{He}^{2+}$, respectively. Some of regenerated shoots from the irradiated explants had variegated leaves. At most 15%, 20% and 21% of the plants regenerated from explants irradiated with $^{12}\text{C}^{5+}$, $^{12}\text{C}^{6+}$ and $^4\text{He}^{2+}$, respectively, had variegated leaves. These results indicate that the ion beam irradiation provides a pivotal method to induce mutation in the genome of *Ficus stipulata*.

Introduction

Ficus stipulata Thunb. (= *Ficus thunbergii*), "Hime-itabi" is an evergreen, climber that belongs to Moraceae, the mulberry family. This tree will be useful to cover highway corridors and vertical surfaces of building to decontaminate various pollutants, including nitrogen dioxide derived from vehicles, in urban areas. Plants take up NO_2 ¹⁾ and assimilate its nitrogen through a primary nitrate assimilation pathway²⁾. We discovered that among naturally

occurring 217 taxa of the higher plants, there is more than 600-fold variation in the ability to assimilate NO_2 ³⁾. We also reported that the overexpression of a chimeric nitrite reductase (NiR) gene resulted in a 1.4-fold increase in the capability to assimilate NO_2 than that of wild-type⁴⁾. Conceivably, the irradiation of plants with ion beams may cause modification of the plant genome^{5), 6), 7), 8), 9)}. With an eventual aim to produce novel *Ficus stipulata* plants that have high capability to assimilate atmospheric nitrogen dioxide, we have been studying the conditions for irradiation with ion beams¹⁰⁾.

Materials and methods

Aseptically grown *Ficus* plants were cultured in tubes containing fluorialite with MS¹¹⁾ medium, supplemented with 2% sucrose and 100 $\mu\text{g/l}$ indole-3-butyric acid (IBA). Plants were cultured for up to two months at 25°C in the light (30 to 40 $\mu\text{mol/s/m}^2$). About 4-mm-long explants with apical shoots (cut longitudinally in the middle) and 1-mm-long shoots bearing nodes were cut with a surgical blade, and placed in petri dishes with shoot formation medium, which was consisted of woody plant medium (WPM)¹²⁾ supplemented with 2% sucrose, 0.3% Gellan Gum, 1.78 μM benzyl adenine (BA) and 46.7 nM thidiazuron (TDZ), pH 5.8. Eighteen to 20 explants were placed on each petri dish. Two days after preparation, the samples were

irradiated with $^{12}\text{C}^{5+}$ (220 MeV), $^{12}\text{C}^{6+}$ (320 MeV) and $^4\text{He}^{2+}$ (50 MeV) ion beams, with an irradiation dose average ranging from 10 to 200 Gray (Gy), by the AVF cyclotron at Japan Atomic Research Institute (JAERI, Takasaki). During irradiation, the lid was removed and the petri dish was covered with a thin film to avoid the energy loss of the ion beam¹³⁾. After irradiation, the explants were transferred to fresh shoot formation media, and cultured for up to three months. When regenerated shoots became about 1 cm long, they were transferred into glass tubes, and the culture was continued.

Results and Discussion

As reported previously¹⁰⁾, the frequency of regeneration of plants from irradiated explants changed as a dosage-dependent manner in the range of 10 to 200 Gy. Regenerated shoots were classified, depending on the length, into three groups; H (more than 1 cm long), M (between 0.5 to 1 cm) and S (less than 0.5 cm). Along the increase in the energy with $^{12}\text{C}^{5+}$, the frequency of H- and M-type shoots was decreased and that of the S-type increased. At more than 20 Gy, about one-fourth of the regenerated shoots was the S-type. At the same time, the frequency of the appearance of plants with variegated leaves was increased, at most 15% of regenerated plants had variegated leaves (Fig. 1). Similar results were obtained with $^{12}\text{C}^{6+}$ and $^4\text{He}^{2+}$; a distinct suppression was observed at 40 Gy with $^{12}\text{C}^{6+}$ and 40 Gy with $^4\text{He}^{2+}$, and at most 20% ($^{12}\text{C}^{6+}$) and 21% ($^4\text{He}^{2+}$) of the regenerated plants had variegated leaves. These variegated plants showed slow growth and less aerial roots. Taken together, the present data strongly suggest that ion beam irradiation is a pivotal method to induce mutations in the genome of *Ficcus stipulate*. We are currently studying the capability of these mutated *Ficcus stipulate* plants to assimilate atmospheric nitrogen dioxide.

References

- 1) A.C. Hill. J. Air Pollut. Contr. Ass. 21 (1971) 341-346.
- 2) T. Yoneyama, H. Sasakawa. Plant and Cell Physiol. 20 (1979) 263-266.
- 3) H. Morikawa, A. Higaki, M. Nohno, M. Takahashi, M. Kamada, M. Nakata, G. Toyohara, Y. Okamura, K. Matsui, S. Kitani, K. Fujita, K. Irifune, N. Goshima. plant taxa. Plant, Cell Environ. 21 (1998) 180-190.
- 4) M. Takahashi, Y. Sasaki, S. Ida, H. Morikawa. Plant Physiol. 126 (2001) 731-741.
- 5) A. Tanaka, S. Tano, T. Chantes, Y. Yokota, N. Shikazono, H. Watanabe. Genes Genet. Syst. 72 (1997) 141 - 148.
- 6) A. Tanaka, N. Shikazono, Y. Yokota, H. Watanabe, S. Tano. Int. J. Rad. Biol. 1 (1997) 121 - 127.
- 7) A. Tanaka, H. Watanabe, T. Shimizu, M. Inoue, M. Kikuchi, Y. Kobayashi, S. Tano. Research B. 129 (1998) 42 - 48.
- 8) N. Shikazono, Y. Yokota, A. Tanaka, H. Watanabe, S. Tano. Genes Genet. Syst. 73 (1998) 173 - 179.
- 9) Y. Hase, K. Shimono, M. Inoue, A. Tanaka, H. Watanabe. Radiat. Environ. Biophys. 38 (1999) 111 - 115.
- 10) M. Takahashi, S. Kohama, M. Hakata, Y. Hase, N. Shikazono, A. Tanaka, and H. Morikawa. Annual Reports of TIARA, 39 (2001) 62-63.
- 11) T. Musashighe, F. Skoog. Physiol. Plant. 15 (1962) 473 - 489.
- 12) G. Lloyd, B. McCown. Combined proceedings of the international plant propagators society. 30 (1980) 421 - 427.
- 13) A. Tanaka, H. Watanabe, T. Shimizu, M. Inoue, M. Kikuchi, Y. Kobayashi, S. Tano. Nucl. Instr. And Meth. B 129 (1997) 42-48.

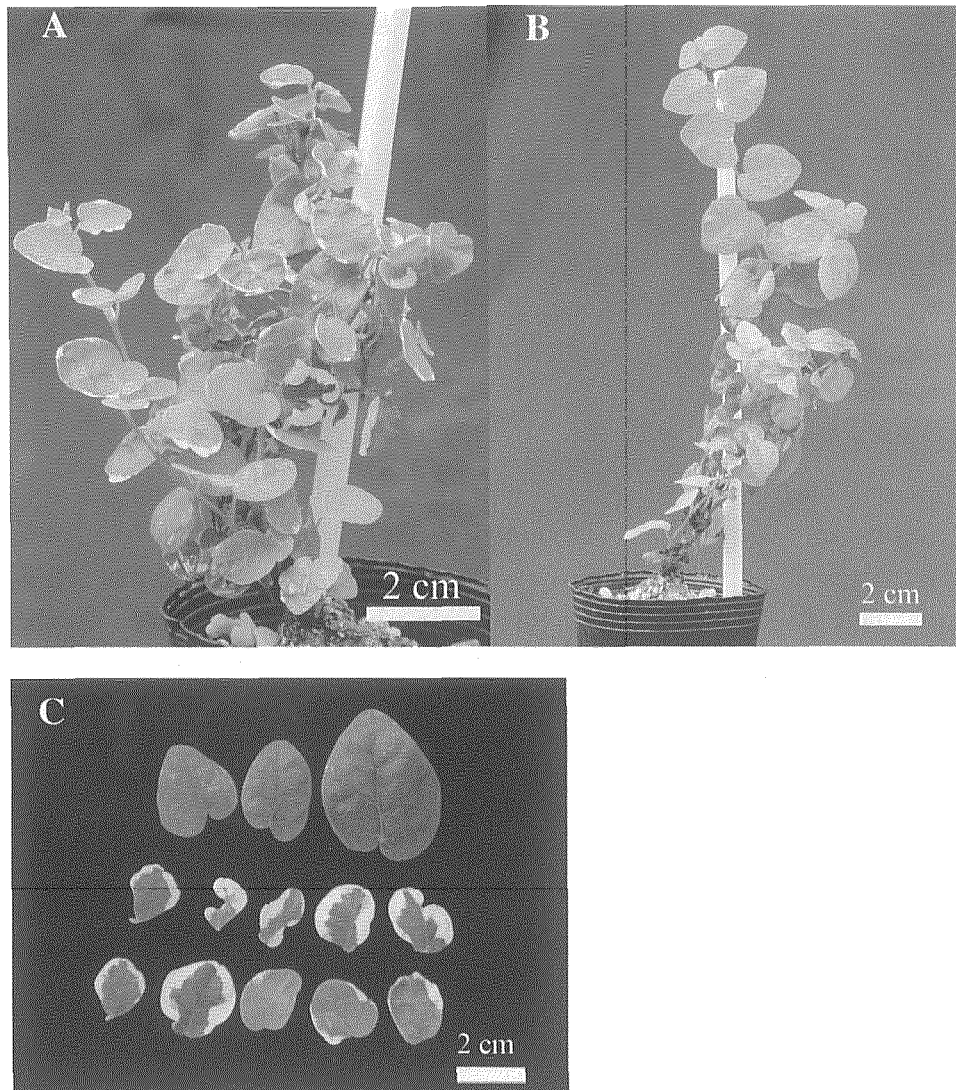


Figure 1. Typical *Ficus stipulate* plants with variegated leaves regenerated from apical shoots irradiated with $^{12}\text{C}^{5+}$ at 30 Gy (A) and their leaves (C). Plants regenerated from nonirradiated apical shoots (B).

2.14 Effect of ion beam irradiation on the growth of netted melon (*Cucumis melo* L.)

M. Taneishi*, H. katai*, H. Yamada*, H. Otsuka*,
Y. Hase**, N. Shikazono** and A. Tanaka**

Shizuoka Agricultural Experiment Station*

Department of Ion-Beams-Applied Biology, JAERI**

1. Introduction

Netted melon (*Cucumis melo* L.) is cultivated as an important fruit in Shizuoka prefecture.

Because ion beams have higher LET (Linear Energy Transfer) and deposit their energies quite locally, it is considered to be an efficient mutagenic agent applicable to mutation breeding of melon.

The aim of this study is to develop high fruit-thickening ability lines under low-temperature by the irradiation of ion beams to melon seeds. We started the mutation breeding of melon in 2000, and melon seeds were irradiated with several doses of carbon ion beam¹⁾.

Ezura et al. developed high fruit-thickening ability lines by selection of low-temperature germinabilities in melon²⁾. In order to breed the high fruit-thickening ability line, we also investigated the selection method of low-temperature germinabilities in netted melon.

In this paper, we report the results of fruit set rate of M1 plants and the selection method of low-temperature germination in netted melon.

2. Materials and Methods

Melon cultivar 'Earls Favorite Kenon Fuyu2' was used in this study.

The melon seeds which were irradiated with 220 MeV carbon ion beam (20Gy to 70Gy) at the TIARA AVF cyclotron in JAERI was grown in a greenhouse, and the M2 seeds were obtained.

Germinating rate of non-irradiated seeds at 11, 13, 15, and 18°C was recorded every 5 days for 20 days. A seed was considered to be germinated when the crevice was made between its radicle and cotyledon.

Secondly, number of germinated seeds at 15°C was recorded daily for 13 days.

3. Results and Discussion

The number of fertile plants that could yield M2 seeds was shown in Table 1, and it was decreased with increase of dose of ion beams. The main reason of reduced fertility was a problem in a bisexual flower setting, and partially the decrease of pollen germinabilities.

The period of germination became longer as the incubation temperature became lower (Fig.1).

After 5 days incubation, all seeds were germinated at 18°C, but no seed was germinated at lower than 15°C.

At 15°C, the average of germination

period was 7.2 days, and no seed was germinated before 4 days (Fig.2).

From these results, we considered the selection method for M2 seeds was at 15°C for 3 days to develop the high fruit-thickening lines under low-temperature.

4. Reference

- 1) K. Katai et al. TIARA Ann. Rep., 2.5, 40-41(2000)
- 2) H. Ezura Bulletin of the Plant Biotechnology institute Ibaraki Agriculture Center. No 1:1-66(1995)

Table.1 Effect of C ion beam on the number of plants and the fertility

Dose (Gy)	Number of M1plants tested	Number of fertile plants (%)
20	291	291 (100)
40	470	414 (88.1)
50	135	111 (82.2)
60	21	15 (71.4)
70	7	4 (57.1)
0	8	8 (100)

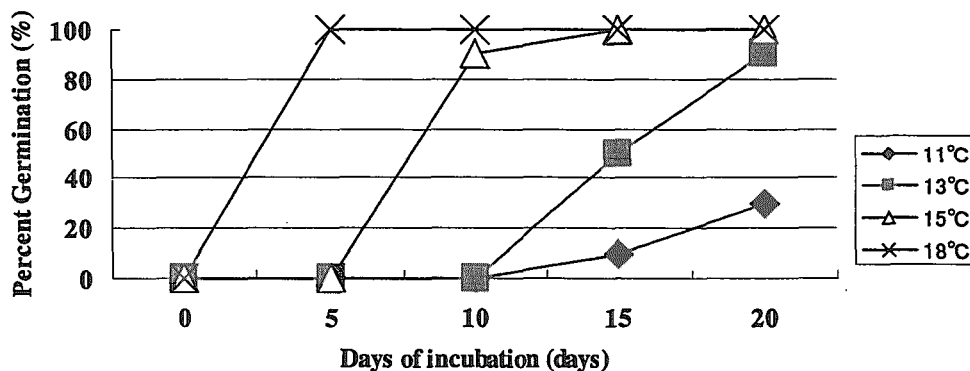


Fig.1 Percent Germination at several temperature for decoated seeds of 'Earls Favorite Kenon Fuyu2' (n = 10)

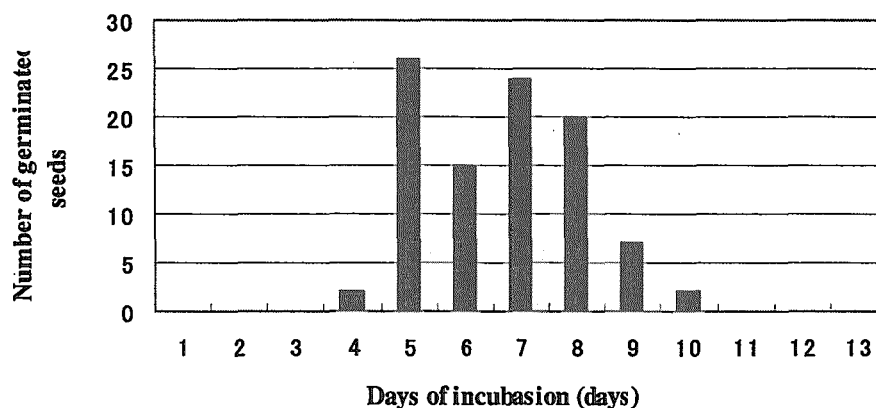


Fig.2 Number of germinated seeds at 15°C for decoated seeds of 'Earls Favorite Kenon Fuyu2' (n = 200)

2.15 Mutation Induction with Ion Beam Irradiation in *Solanum* Plants

N. Matsuzoe*, T. Umeda*, Y. Hase** and A. Tanaka**

Faculty of Environmental and Symbiotic Sciences, Prefectural University of Kumamoto*, Department of Radiation Research for Environment and Resource, JAERI**

Introduction

Solanum toxicarium can be used for the rootstock of the tomato, because *S. toxicarium* has highly resistance to the soil-born disease^{1,2)}. However, *Solanum toxicarium* is not used for the rootstock easily because of its sharp prickles. So, we have decided to try to obtain the individual of *S. toxicarium* without prickles by using the ion beam irradiation. In this research, we examined the effect of the ion beam irradiation on germination and survival rates of *Solanum* plants.

Materials and Methods

In this experiment, *Solanum melongena* (cvs. 'Kitta', 'Black-beauty' and 'Kumamotonaga') and *S. toxicarium* were used. These seeds were irradiated with ion beam (220 MeV $^{12}\text{C}^{5+}$) at various doses (25, 50 and 75 Gy) to find out the adequate doses of the ion beams to *Solanum* plants. After the irradiation, seeds of 'Kitta', those of 'Black-beauty' and those of 'Kumamotonaga' were germinated in the petri dish in incubator at the 12h/12h 23/28°C cycle, then the germinated seed were transferred in soil in greenhouse. Then, survival rates of the seedlings were investigated. On the other hand, after the irradiation, seeds of *S. toxicarium* were surface-sterilized with 70% ethanol and 1% sodium hypochlorite solution and washed three times in sterile water. They were put

to grow in MS medium with 6% sucrose and 0.8% agar in incubator at the 12h/12h 23/28°C cycle. Then, survival rates and morphological change of the seedlings were investigated.

Results and Discussion

The influence of the ion beam irradiation on germination and survival rates are shown in Fig. 1 and Fig. 2. The germination rate were about 100% with 0 Gy, about 90% with 25, 50 and 75 Gy. The survival rates were 20% or less in all cultivars with 75 Gy, about 30% in 'Kitta' with 50 Gy, about 80% in 'Black beauty' and 'Kumamotonaga' with 50 Gy and 90% or more in all cultivars with 25 Gy at the final stage. In *Solanum toxicarium*, the germination rates were 60% with 0 Gy, about 40% with 25, 50, and 30% with 75 Gy (Fig. 3). After germination, many individuals showed abnormal growth, such as non-germination, non-rooting, loss of growing point, undevelopment of cotyledon (Fig. 4). This result suggests that the best dose to obtain mutant of *S. toxicarium* is about 25 Gy with ion beam irradiation (220 MeV $^{12}\text{C}^{5+}$).

References

- ¹⁾N. Matsuzoe, H. Okubo and K. Fujieda, J. Japan. Soc. Hort. Sci. 61, 865-872 (1993)
- ²⁾M. Ali, N. Matsuzoe, H. Okubo and K. Fujieda, J. Japan. Soc. Hort. Sci. 60, 921-926 (1992)

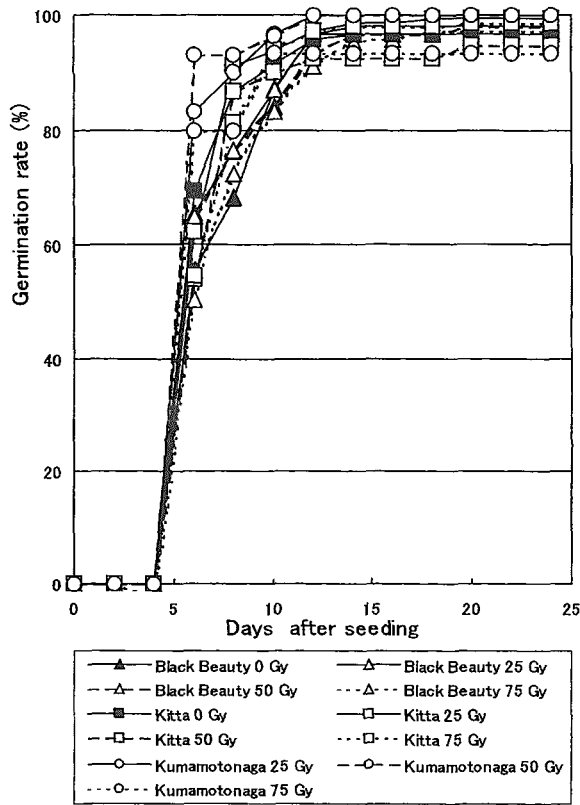


Fig. 1 Effect of carbon ion beam on the germination of *Solanum melongena*

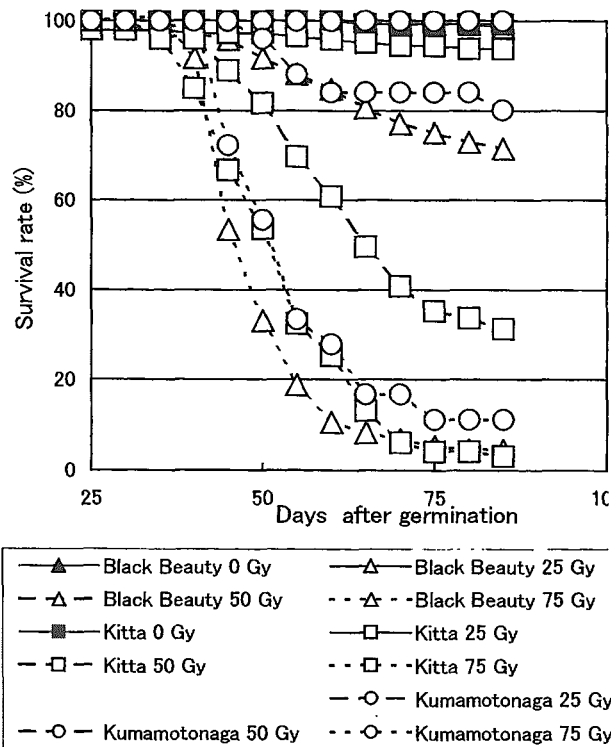


Fig. 2 Effect of carbon ion beam on the survival rate of *Solanum melongena*

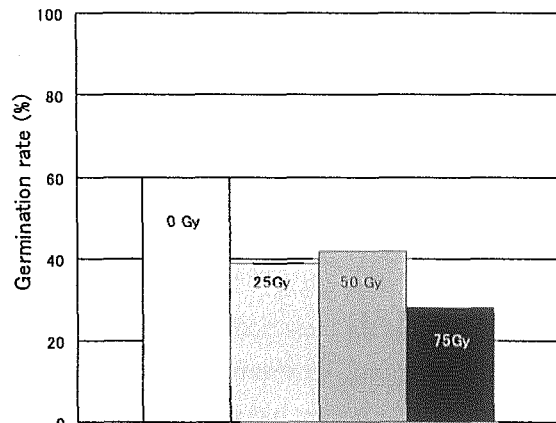
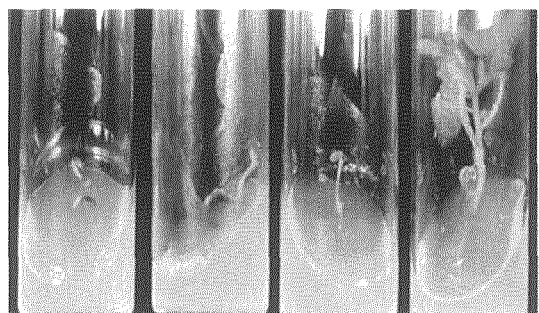
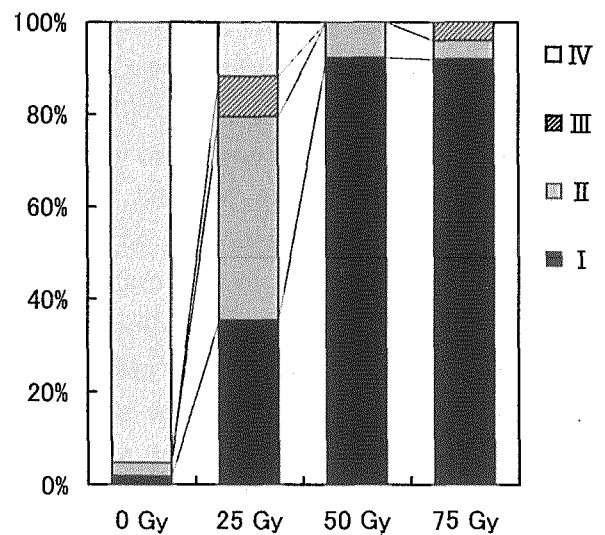


Fig. 3 Effect of carbon ion beam on the germination of *S. toxicarium*



I II III IV

Fig. 4 Effect of carbon ion beam on germination and growth of *S. toxicarium*

Data recorded 60 days after germination

2.16 Instability of Rice Chlorophyll Mutants Induced at M1 by Carbon Ion Beam Irradiation Is Inherited

M. Maekawa*, Y. Hase**, N. Shikazono** and A. Tanaka**

Research Institute for Bioresources, Okayama University*,

Department of Ion-Beam-Applied Biology, JAERI**

1. Introduction

A DNA transposable element (TE) is very useful for gene-tagging in several plant species and maize *Ac/Ds* or *En/Spm* has been utilized for gene-tagging in heterologous plants^{1),2)}. However, inactivation of TE has occurred frequently in heterologous plants through generations²⁾. Since so far, any class II type active TEs have not been discovered in rice, *Ac/Ds* system in maize was introduced into rice and was tried to be applied for gene-tagging in rice³⁾. If an endogenous active TE were discovered in rice, it could be used easily as a powerful tool for gene-tagging in open environments. As *En/Spm* was discovered in a population of maize exposed to atomic bomb at Bikini⁴⁾ and inactive *Mu* in maize was reactivated by gamma-ray irradiation⁵⁾, it is possible that an active TE may be induced in mutagenized rice. As ion beams are a type of high linear energy transfer (LET) radiation and can deposit high energy on a target compared to low LET radiations such as gamma rays, the novel mutants or large DNA rearrangements are expected to be induced by ion beam irradiation^{6),7)}. So, it is expected that inactive transposon may be reactivated by ion beam irradiation in rice. Maekawa⁸⁾ found a variegated yellow leaf (yl-v) mutant in F2 of a cross between distantly related rice varieties. Through the genetic analysis, the yellow leaf character was controlled by a nuclear recessive gene. This mutant was also found to segregate stable yellow leaf (yl-stb) plants and revertants⁹⁾. This results suggested that the variegation of the yellow leaf mutant might be caused by a class

II autonomous element and the stable phenotype was strongly suggested to be caused by defective type of the element. Although a near isogenic line (NIL) for stable yellow leaf with T-65 genetic background was bred, this line did not show any variegations through generations. So, if variegation could be induced by mutation in this NIL and the variegation could be inherited together with segregation of revertants, it was strongly suggested that a cryptic inactive element was restored. Maekawa et al.¹⁰⁾ obtained one variegated yl plant induced at M1 by carbon ion beam irradiation. Thus, this study aims to confirm the inheritance of somatic instability at M1 in this stable yellow leaf mutant line with ion beams

2. Experimental procedure

Progeny tests derived from a variegated mutant of yl-stb plants induced at M1 by carbon-ion beam from an AVF cyclotron of JAERI, Takasaki, Japan were conducted by panicle-row lines method. After three weeks from seeding, presence/absence of variegations were observed because yl mutants start withering from this time. Spikelet fertility was scored as percentage of fertile spikelets to total spikelets.

3. Results and Discussion

Out of 992 M1 plants survived after carbon ion beam irradiation, one variegated plant was obtained¹⁰⁾. The variegated yl plant at M1 bore 9 panicles. The frequencies of clear variegation were examined in panicle-row lines at M2. Spikelet fertilities in 9 panicles were low, varying

from 0 % to 41.7 %. Most of panicle-row lines, no.2 to 6 and no.9, segregated variegated and stable *yl* plants (Table.1). In no.5 line, 2 revertants were segregated. Totally, the ratio of variegated to stable *yl* plants was good fitness to 3:1. Through progeny test derived from *yl-v* plants at M2, it was found that some of variegated *yl* plants at M2 (Pan.2;*yl-v*-10, Pan.5;*yl-v*-1, Pan.6;*yl-v*-1, Pan.8;*yl-v*-2, Pan.9;*yl-v*-3 and 4) were fixed as given in Table 2. Furthermore, one of two revertants generated at M2 was fixed at M3 (Table 2). These results strongly suggested that gene conversion of recessive to dominant at germ line as well as somatic line might be induced by carbon ion beam irradiation. In addition, no.2 and 5 lines segregated albino plants at M2 (Table 1) and another albino plants were segregated at M3 (Table 2).

Table.1 Segregation of *yl* phenotype in M2 plants derived from the variegated *yl* plants generated at carbon ion-irradiated M1 plants

Panicle no.	Spik. fert.(%) of M1 plant	<i>yl</i> phenotype				Total
		Normal	Variegated	Stable	Albino	
1	0.0	0	0	0	0	0
2	41.7	0	12	3	2	17
3	7.7	0	1	1	0	2
4	9.8	0	1	2	0	3
5	17.0	2	3	1	1	7
6	9.1	0	3	2	0	5
7	3.3	0	1	0	0	1
8	3.9	0	2	0	0	2
9	16.2	0	4	1	0	5
Total		2	27	10	3	42

We found that clear variegation in stable *yl* plants was somatically induced by carbon ion beam irradiation at M1 generation and induced variegation was heritable. This results suggested that clear variegation induced by carbon ion beam irradiation at M1 plants was caused by germinal conversion of *yl* to *Yl*. This result could be explained by the possibility that *yl*

phenotype is caused by non-autonomous TE inserted into *Yl* gene and inactive autonomous TE which is located at another locus or chromosome. Through change of inactive into active state of autonomous TE, non-autonomous TE in *yl* gene is excised from *yl* gene by active autonomous TE. The latter two explanations are based on the hypothesis that *yl* phenotype is caused by TE. Actually, revertants were obtained at M2 and one of the revertants was fixed (Table 2). This result indicated that gene conversion of *yl* into *Yl* occurred in germ lines, suggesting that *yl* phenotype is caused by TE. However, whether the TE inserted into *yl* gene is autonomous or non-autonomous still remains unknown. However, as shown in Tables 1 and 2, stable *yl* plants were segregated in the progenies of variegated plants. This result is consistent with the observations that variegated plants generated in F2 of the cross between distantly related varieties segregated stable plants⁹⁾. From these results, it is plausible that stable phenotype is caused by a non-autonomous TE. Consequently, induced variegation is presumed to be caused by a cryptic and silent autonomous TE.

What is the mechanism for change of inactive into active state of TE by ion beam irradiation? Chomet et al.¹¹⁾ and Kunze et al.¹²⁾ demonstrated that hypermethylation of Ac was associated to the inactivation of Ac. Furthermore, hypomethylated state occurred in *ddm1* mutant of *Arabidopsis* provoked activity of cryptic endogenous TEs¹³⁾. These suggested that mutagen treatment might induce epigenetic modification of DNA. On the other hand, Walbot⁵⁾ speculated that chromosome breakage by gamma ray irradiation and following DNA repair could make methylation level hypomodified transiently. Removal of DNA modification might be needed to induce activation of autonomous TE. Ion beam irradiation was

found to induce large structural change of chromosome⁷⁾. Thus, transient hypomethylation state could be brought by chromosome breakages induced by ion beam irradiation and following DNA repair and this state could make inactive autonomous TE active. As shown Table 2, low fertile M1 plants segregated high fertile pedigrees with a frequency of 44%, indicating that the frequency of high fertile plants is in good agreement with 50% for segregation frequency of reciprocal translocation. Although any check for chromosome association in M1 plants are not conducted, chromosome breakages might occurred in M1 plants by ion beam irradiation. "genomic stress" McClintock¹⁴⁾ addressed, such as chromosome breakages, deletion or translocation possibly reactivates a cryptic silent TE²⁾. Stable *yl* phenotype is useful for monitoring induction of variegation by mutagen treatments.

It is very important to reveal the genomic sequence for *yl* gene in order to prove that the variegation induced by ion beam irradiation might be caused by reactivation of cryptic TE and utilize an active TE in functional genomics of rice.

References

- 1) V. Sundaresan, V., Trends in Plant Science 1 (1996) 184-190.
- 2) R. Kunze, H. Saedler and W.E. Lonnig, Advances in Botanical Research 27 (1997) 331-470
- 3) T. Izawa, T. Ohnishi, T. Nakano, N. Ishida, H. Enoki, H. Hashimoto, K. Itoh, C. Wu, C. Miyazaki, T. Endo, S. Iida and K. Shimamoto, Plant Molecular Biology 35 (1997) 219-229.
- 4) P. A. Peterson, Genetics 38 (1953) 682-683.
- 5) V. Walbot, Molecular and General Genetics 212 (1988) 259-264.
- 6) A. Tanaka, Gamma Field Symposia 38 (1999) 19-28.
- 7) N. Shikazono, A. Tanaka, H. Watanabe and S. Tano, Genetics 157 (2001) 379-387.
- 8) M. Maekawa, In Modification of Gene Expression and Non-Mendelian Inheritance, Oono, K. and F. Takaiwa (eds.), Natl. Inst. Agr. Res., (1995) p. 379-388.
- 9) M. Maekawa, K. Rikiishi, T. Matsuura and K. Noda, Japan Journal of Breeding 46 (Suppl. 2) (1996) 107.(in Japanese)
- 10) M. Maekawa, A. Tanaka, N. Shikazono and Y. Hase, JAERI-Review 2001-039 (2001) 64-66.
- 11) P. S. Chomet S. Wessler and S. L. Dellaporta, EMBO Journal 6 (1987) 295-302.
- 12) R. Kunze, P. Starlinger and D. Schwartz, Molecular and General Genetics 214 (1988) 325-327.
- 13) A. Miura, S. Yonebayashi, K. Watanabe, T. Toyama, H. Shimada and T. Kakutani, Nature 411 (2001) 212-214.
- 14) B. McClintock, Science 226 (1984) 792-801.

Table 2. Segregation of *yl* phenotype in M3 plants derived from a variegated *yl* plant and normal plant generated at M2

M3 line	Spik. fert.(%) of M2 plant	<i>yl</i> phenotype				Total
		Normal	Variegated	Stable	Albino	
Pan.2; <i>yl-v</i> -1	7.0	0	5	3	1	9
-2	15.3	0	10	7		17
-3	8.1	0	5	1	1	7
-4	82.5	0	25	6		31
-5	93.8	0	44	15		59
-6	20.2	0	14	2		16
-7	92.0	0	43	24		67
-8	88.9	0	32	13		45
-9	95.4	0	25	9		34
-10	41.2	0	25	0		25
-11	52.3	0	16	4		20
-12	73.7	0	29	9		38
Pan.3; <i>yl-v</i>	97.1	0	30	15		45
Pan.4; <i>yl-v</i>	67.9	0	42	16	1	59
Pan.5; <i>yl-v</i> -1	34.3	0	22	0		22
-2	85.7	0	46	23		69
-3	94.9	0	43	12		55
Pan.5; <i>G</i> -1	65.7	41	11	4		56
-2	82.3	59	0	0		59
Pan.6; <i>yl-v</i> -1	95.5	0	82	0		82
-2	5.1	2	1	1		4
-3	20.3	0	7	4		11
Pan.7; <i>yl-v</i>	28.6	0	17	2	2	21
Pan.8; <i>yl-v</i> -1	25.8	0	16	6	2	24
-2	40.7	0	25	0		25
Pan.9; <i>yl-v</i> -1	74.6	0	26	14	3	43
-2	35.4	0	15	9		24
-3	51.9	0	24	0		24
-4	29.9	0	19	0		19

Note; Spikelet fertility of M2 plant underlined shows high fertility.

2.17 Studies on Flower Color and Morphological Mutations from In Vitro Chrysanthemum Explants Irradiated with Ion Beams

T.Sato*, H.Naganoma*, Y.Hase** and A.Tanaka**

Department of Vegetables and Flowers, Akita prefecture Agricultural experiment station.* Department of Radiation Research for Environment and Resources, JAERI**

1. Introduction

Chrysanthemum is important flower in Akita prefecture. Especially chrysanthemum cultivar "Natsuyasumi" (purplish red flower) is suited for climate of Akita prefecture. However, producer, market and consumer are demanding yellow or white color cultivar.

Ion beam is expected to be a new and efficient mutagen for plant mutation breeding. In flower color of chrysanthemum, it has been reported that mutant was frequently regenerated from in vitro explants with irradiation of ion beam¹⁾.

The final goal of this study is breeding of yellow or white flower color line with ion beam irradiation to chrysanthemum. In this paper, we report the effect of ion beam irradiation on callus induction and plant regeneration from chrysanthemum cultivar "Natsuyasumi" in vitro explants.

2. Materials and Methods

Using a chrysanthemum cultivar, "Natsuyasumi", the explants of petals on callus inducing medium were irradiated with $^{12}\text{C}^{5+}$ or $^{12}\text{C}^{6+}$ ion beam from TIARA AVF cyclotron in JAERI. The energy of $^{12}\text{C}^{5+}$ was 220MeV, and that of $^{12}\text{C}^{6+}$ was 320MeV.

After irradiation, the cultured

materials were transferred to a new medium for callus proliferation. Two weeks after, callus was transferred to plant regeneration medium.

3. Results and Discussion

In $^{12}\text{C}^{5+}$ ions, more than 5Gy of irradiation influenced callus induction (Fig.1). Median lethal dose (LD_{50}) was between 5 and 20Gy. At more than 30Gy, callus induction was not observed.

Plant regeneration was suddenly decreased by ion beam irradiation. At 5Gy plant regeneration was about 20%. At more than 20Gy, it was not observed.

Therefore, we adopted 5Gy as an adequate dose.

In $^{12}\text{C}^{6+}$ ions, the irradiation with 5Gy influenced callus induction (Fig.2). LD_{50} of callus induction was about 5Gy. At more than 20Gy, callus induction was not observed.

Plant regeneration was 10% by the irradiation of 5Gy. At more than 10Gy, plant regeneration was not observed.

Therefore, we adopted less than 5Gy as an adequate dose.

From these results, in comparison with $^{12}\text{C}^{5+}$ ions, it was thought that $^{12}\text{C}^{6+}$ ions have higher influence on callus induction and plant regeneration of chrysanthemum

cultivar "Natsuyasumi" explants.

Now, regenerated plants are growing in field nursery, and the induction of mutation are investigated.

On the other hand, white flower color mutant was obtained with 50Gy of soft X ray irradiation²⁾.

After these studies, we compare to the effects of soft X ray and ion beams on the

color of flower.

References

- 1) S.Nagatomi, A.Tanaka, A.Kato, H.Watanabe and S.Tano, TIARA Annual Report (1995) 50-52.
- 2) T.Sato, Annual of Akita prefecture Agricultural experiment station (2001) in press.

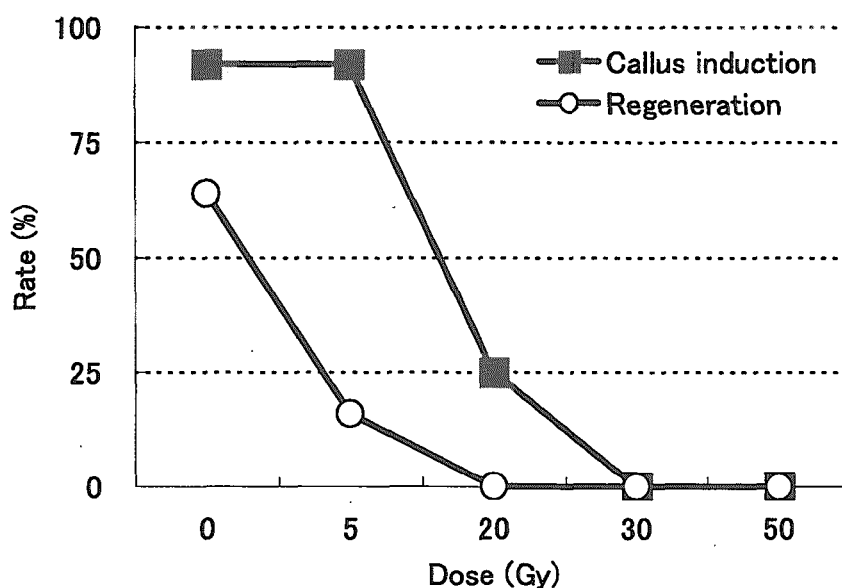


Fig.1 Effect of $^{12}\text{C}^{5+}$ ion beam on callus induction and plant regeneration.

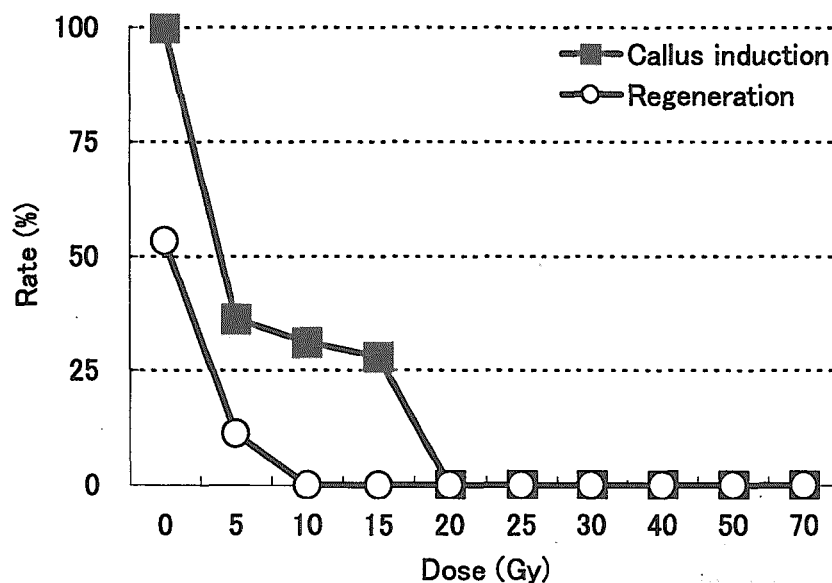


Fig.2 Effect of $^{12}\text{C}^{6+}$ ion beam on callus induction and plant regeneration.

2.18 Induction of Mutation in *Delphinium* L. by Ion-beam

Irradiation

T.Kimura^{*}, S. Tsuzuki^{*}, S. Kondo^{*}, Y. Tsuchiya^{*}, Y. Hase^{**}, A. Tanaka^{**}

Bio Research Laboratory, TOYOTA MOTOR CORPORATION^{*}

Department of Ion-Beam-Applied Biology, JAERI^{**}

1.Introduction

Ethylene is a gaseous hormone that affects many aspects of plant growth and development. Processes affected by ethylene include seed germination, stem and root elongation, flower initiation, senescence of leaves and flowers, and fruit ripening.

The ethylene insensitive mutant *etr1* was identified, and the *ETR1* gene, which encodes an ethylene receptor, was isolated and characterized¹⁾²⁾.

Delphinium L. is one of the ethylene sensitive plant, and is very weak against rubbing off flowers each other during the transportations.

Ion beams, which have a higher Linear Energy Transfer(LET), in comparison with γ and X rays. Using the ion beams, biological effects in plants have been investigated for the dry seeds of *Arabidopsis thaliana*³⁾ and *Nicotiana tabacum*⁴⁾.

We have been expecting the ion beam induce mutants of ethylene insensitive *Delphinium* L. The purpose of this study is to define the suitable irradiation condition of ion beam on the growth of M1 plants.

2.Material and Methods

Delphinium cultivars, 'Pacific Giant Summer Sky', 'Pacific Giant King Arthur' and 'Blue Mirror' were used for experiments. Dry seeds covered with Kapton films(4.5 X 4.5cm) were irradiated with 220 MeV carbon ($^{12}\text{C}^{5+}$) ion beams from the TIARA AVF cyclotron (JAERI, Takasaki), in the range of 0 to 100Gy.

After irradiation, the seeds were surface-sterilized with 2% (v/v) sodium hypochlorite and 0.05% (v/v) Tween 20, and rinsed three times in sterile water. The resultant seeds were germinated on 1/2Murashige and Skoog(MS) medium, pH5.8, containing 1.5% sucrose and 0.8% gellan gum (Gelrite, Wako Pure Chemicals) and grown at 22°C and 16 hr photo-

period.

The survival rate of 50 plants was measured 50 days after sowing. Survival seedlings were acclimatized and transferred in soil. Morphological change and the fertility rate of plants were investigated.

3.Result and Discussion

Survival rates were decreased at higher than 20Gy for all cultivars. 'Blue Mirror' was slightly more resistant than the others (Fig.1).

After transplantation to soil, the plants irradiated with more than 20Gy of ion beam could not grow. Some individuals showed dwarf phenotype and irregular shape of a leaves.

Regarding M1 plants, low fertility was observed particularly in 'Pacific Giant Summer Sky' (Fig.2).

From these results, we could adopt around 5Gy to 10Gy of ion beam as the adequate dosage for the mutagenesis of these *Delphinium* cultivars.

4.References

- 1)C. Chang, S.F. Kwok, A.B. Bleeker, E.M. Meyerowitz, Science 262(1993), 539-544
- 2)J.Q. Wilkinson, M.B. Lanahan, D.G. Clark, A.B. Bleeker, C. Chang, E.M. Meyerowitz, H.J. Klee, Nat. Biotechnol. 268(1995), 667-675
- 3)A. Tanaka, N. Shikazono, Y. Yokota, H. Watanabe, S. Tano, INT. J. RADIAT. BIOL 72(1997), 121-127
- 4)Y. Hase, K. Shimono, M. Inoue, A. Tanaka, H. Watanabe, Radiat Environ Biophys 38 (1999), 111-115

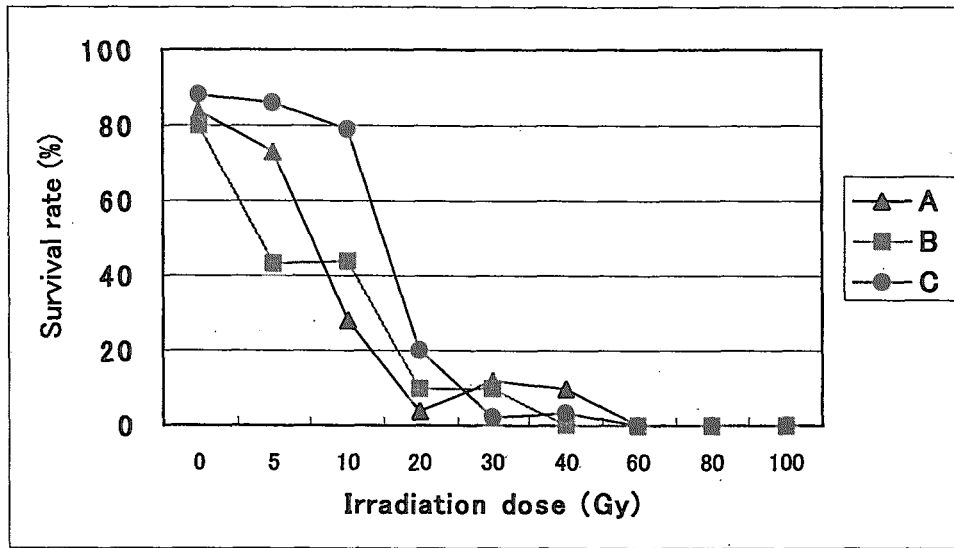


Fig.1
Survival rate of Delphinium plant in carbon(220MeV) irradiation.
A:Pacific Giant Summer Sky, B:Pacific Giant King Arthur, C:Blue Mirror.

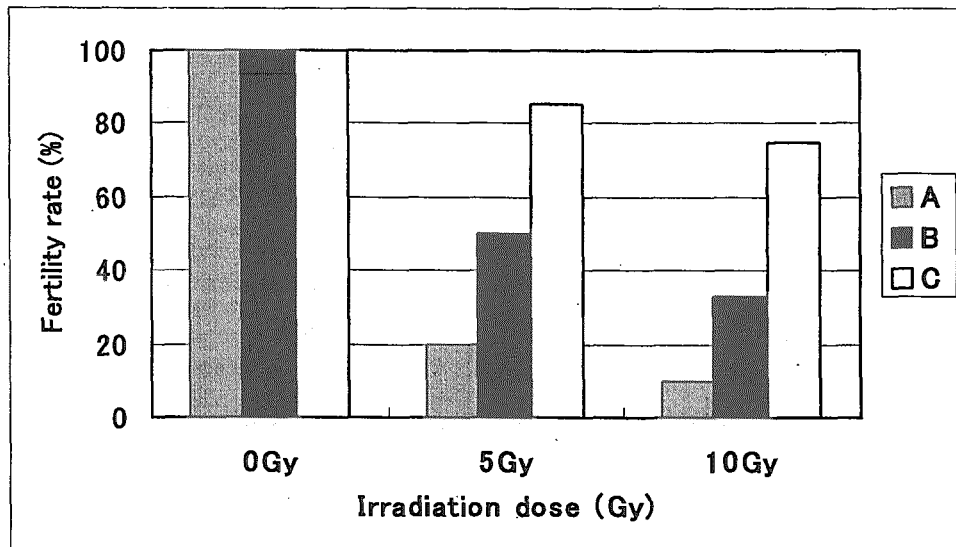


Fig.2
Fertility rate of M1 Delphinium plant in carbon(220MeV) irradiation.
A:Pacific Giant Summer Sky, B:Pacific Giant King Arthur, C:Blue Mirror.

2.19 Isolation of arabidopsis mutants defective in root hydrotropism

K. Koizumi*, G. Takata*, K. Nakaya*, N. Negishi*, Y. Sasuga*, Y. Sakata*, Y. Oono**, Y. Kobayashi***, H. Takenaga*, and S. Tanaka*

Faculty of Applied Bioscience, Tokyo University of Agriculture*, Advanced Radiation Technology Center, JAERI**, Department of Radiation Research for Environment and Resources, JAERI***

1. Introduction

The roots of terrestrial plants detect a moisture gradient around them and grow towards a soil on a higher moisture level for their life. This phenomenon termed hydrotropism was found early in the 19th century. Little attention has been paid to hydrotropism for a long time whereas gravitropism and phototropism have been studied extensively. Recently, Takahashi *et al.* showed that higher plants such as *Pisum sativum* and *Zea mays* perceive a moisture gradient in the root cap¹⁾ and seem to transduce some signals to produce differential growth in the growing zone of the root²⁾³⁾. However, molecular mechanism of hydrotropism has remained unsolved.

To elucidate the molecular mechanism responsible for root hydrotropism, molecular genetic analysis was carried out using arabidopsis which has played an important role in the latest development of plant physiology. So far, arabidopsis mutants showing aberrant root hydrotropism have not been reported.

In this study, we I) developed a new research system of detecting the positive root hydrotropism of arabidopsis, and II) attempted to isolate mutants that are defective in root hydrotropism.

2. Materials and Methods

I) Development of bioassay for hydrotropic activity

A bioassay system for hydrotropism (2 cm long, 14 cm wide and 5 cm high) is shown in Fig. 1A. About 50 seeds of *Arabidopsis thaliana* (Columbia) pretreated with a low temperature of 4°C for 5 days were sown on a filter paper at the topmost acrylic rectangular bar (Fig. 1B). The other end of the filter paper was soaked in water in a tray to supply germinating seeds with water (Fig. 1A and C). The relative humidity in the space near roots was adjusted by changing the level of water surface in the tray. The seedlings were usually grown for 4 days in 50% relative humidity at 25°C under continuous feeble light (2 $\mu\text{mol}/\text{m}^2/\text{s}$). Hydrotropic activity was expressed as a mean angle of root curvature.

II) Isolation of mutants defective in hydrotropism

The dry seeds of *A. thaliana* (Columbia) were sandwiched between kapton films and irradiated with carbon ion (220 MeV) at a dose of 100, 150, and 200 Gy at TIARA. The irradiated seeds were grown and the self-pollinated seeds (M2 seeds) harvested. After the M2 seedlings underwent the bioassay for hydrotropism, each seedling whose root failed to respond to water stimulus was grown to yield the self-pollinated seeds (M3 seeds). The M3 seeds were re-screened to select mutants.

3. Results and Discussion

I) Development of bioassay for hydrotropic activity

For the selection of mutants, we developed a new hydrotropism research system (HRS) to measure the root hydrotropism in arabidopsis (Fig. 1). The relative humidity was $55.8 \pm 1.6\%$ in a space near the roots when the seeds were placed at a distance of 3 cm from the water surface in the tray (Fig. 1B). All seedlings tested under the conditions were found to bend their roots toward the wet filter paper against gravity and the average angle of root curvature was $62.1 \pm 4.6^\circ$. On the other hand, the roots placed in 100% relative humidity grew downward by gravity and the root curvature was $4.5 \pm 5.9^\circ$. These results suggest that the roots of arabidopsis bend specifically to water stimulus and our HRS would serve as a research tool in isolating hydrotropism defective mutants.

II) Isolation of mutants defective in root hydrotropism

About 20,000 M2 seedlings from carbon ion mutagenized M1 seeds were screened using HRS. Out of 20,000 seedlings, 65 plants were found not to bend their roots toward the wet filter paper. In the M3 generation, however, all selected plants showed hydrotropism the same as the wild type.

The inadequate irradiation of arabidopsis seeds with carbon ion and genetic instability of mutagenized seeds might be involved in rare occurrence of mutants in this study.

References

- 1) H. Takahashi and T. K. Scott, *Plant Cell Environment* 16 (1993) 99-103.
- 2) M. Takano, H. Takahashi, T. Hirasawa and H. Suge, *Planta* 197 (1995) 410-413.

- 3) C. Stinemetz, H. Takahashi and H. Suge, *Plant Cell Physiology* 37 (1996) 800-805.

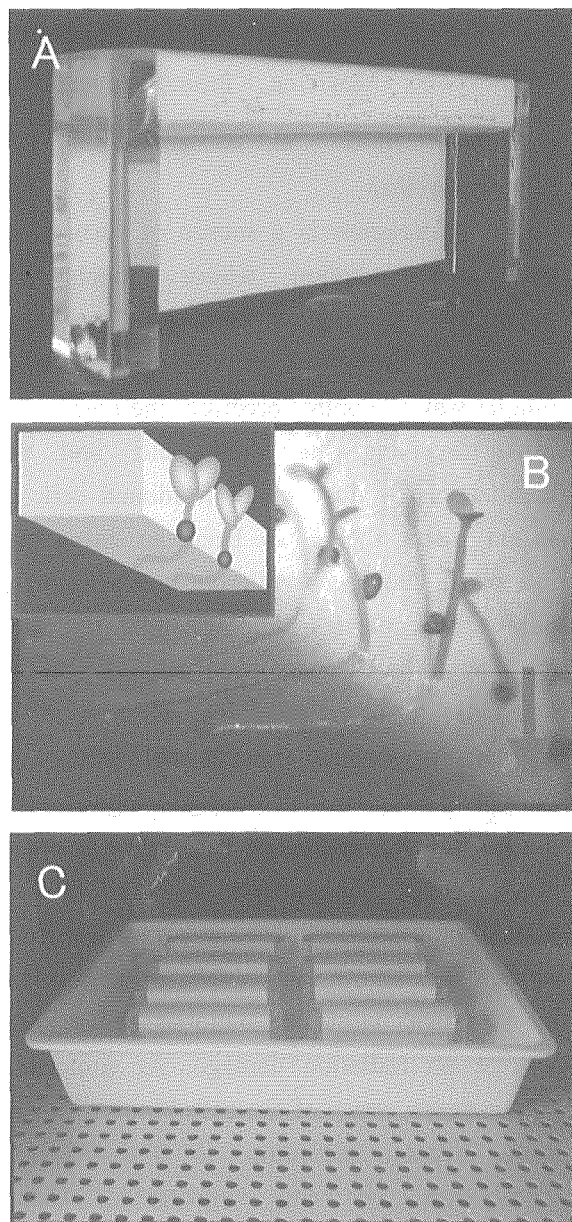


Fig. 1 Hydrotropism Research System (HRS).

(A) Overview of HRS. (B) Close-up of root bending plants at the topmost acrylic rectangular bar and its schematic drawing (inset). Arrow shows the direction of gravity. (C) Incubation in the dark chamber.

2.20 Single-hit Effects on Mammalian Cultured Cells with Heavy-ion Microbeams

Y. Kobayashi*, T. Funayama*, S. Wada**, M. Taguchi*** and H. Watanabe*

Department of Ion-Beam-Applied Biology, JAERI*, Department of Veterinary Medicine, Kitasato University**, Department of Material Development, JAERI***

1. Introduction

A microbeam is a source of focused or collimated radiation whose effects are localized to a micron-sized area of specimen. The use of heavy ion microbeams provides a unique way to control precisely the number of ions traversing individual cells and the localization of dose in an irradiated cell. In recent years there has been an increasing interest in the use of microbeams to study a number of important radiobiological processes in ways that cannot be achieved using conventional "broad-field" irradiation¹⁻³⁾.

Heavy ions can transfer their energy to biological organisms through high-density ionization and excitation of molecules and atoms along the particle trajectories. The population of cells exposed to a very low dose of high-LET heavy ions contains a few cells hit by a particle, while the majority of the cells receive no radiation damage. At somewhat higher doses, some of the cells receive two or more events according to the *Poisson* distribution of ion injections. Using microbeams, we will be able to overcome this limitation by delivering an exactly counted number of ions to each cell.

A microbeam can be used for selective irradiation of individual cells, which can be subsequently observed to ascertain what changes occur to that cell and to neighboring un-irradiated cells. The use of microbeam allows direct investigation of cell-to-cell

communications such as "bystander effects", that is, radiation effects of heavy ions transmitted from irradiated cells to neighboring un-irradiated cells.

Furthermore, a microbeam with sufficient spatial resolution will be useful for analyzing the interaction of damages produced by separate events in an irradiated cell, the dynamics of cellular repair, and the intracellular process such as *apoptosis* by means of highly localized irradiation of a part of a nucleus or cytoplasm.

Therefore, we have developed a cell irradiation system for targeting cells individually with a precise number of high-LET heavy ions⁴⁾. To elucidate radiobiological effects of exactly one particle, we tried to improve the cell irradiation system and to detect effects of single hit of 13.0 MeV/u $^{20}\text{Ne}^{7+}$ and 11.5 MeV/u $^{40}\text{Ar}^{13+}$ ion on mammalian cultured cells^{5,6)}. The irradiation procedure is shown in Figure 1.

2. Experimental procedure

The cell irradiation system has been incorporated into the high-energy heavy ion microbeam apparatus⁷⁾ which was installed under a vertical beam line of the AVF cyclotron at the TIARA of JAERI-Takasaki.

Preparation and detection of target cells

Chinese hamster ovary cells (CHO-K1) were inoculated to the cell dish, the bottom of which was made of 100 μm thick ion track

detector Harzlas TNF-1 (modified CR-39). The cell dishes were incubated for 6-12 hours to let the cells attach to the CR-39, then the cells were stained with 5 μM *CellTracker Orange* (Molecular Probe). Positional data of the individual cells were obtained by fluorescent microscopically searching at the Off-line microscope in the preparation room before irradiation. The object database created by the Off-line microscope controlling PC was shared by On-line microscope controlling PCs and the ion-beam irradiation system.

Cell targeting and irradiation

Just before irradiation, the medium was removed to make ions penetrate both the cells and the bottom of the cell dish. The cells were covered with a *Kapton* (8 μm thick polyimide) film to prevent dry-up and microbiological contamination during the exposure to air. Then the cell dish mounted on a holder was transported from the Off-line microscope to the On-line microscope in the beam room.

Using the object database, targeting and irradiation at the On-line microscope were carried out quickly. However, the mechanical positioning accuracy was not sufficient for automatic targeting of mammalian cultured cells. Therefore, the cells, once targeted according to the object database, needed to be observed at the On-line microscope, and to be re-targeted remotely from the *On-line Remote* PC console. However, it was difficult to obtain a clear image of cells with a reflected illumination system installed in the On-line microscope. To obtain a phase-contrast image of CHO-K1 cells for precise targeting, a light-guided ring-illumination device was newly attached around the newly developed sharpened microaperture, from which the collimated ions were extracted.

Then the object lens was replaced with a

plastic scintillator coupled to a photomultiplier tube (PMT) assembly mounted on the on-line microscope turret. The collimated ions were detected with the PMT assembly after passing through a target cell and the bottom of the cell dish. Energy spectra of collimated ions were measured with a multi-channel analyzer by analyzing scintillation pulses. The number of ions having traversed the sample was counted with a constant fraction discriminator coupled to a preset counter/timer. Every irradiation was terminated by the action of beam shutter, which was controlled by the preset counter/timer module or manually.

Detection of ion tracks at irradiation time

Immediately after irradiation, the cell dish was refilled with medium, and then the bottom was etched from the opposite side of the cells with alkaline-ethanol solution at 37°C for 15 minutes. After a rinse with distilled water, the bottom of the cell dish was observed microscopically for evaluation of the targeting accuracy. Almost all the ion track pits were concentrated within a collimated diameter range. The cells were then incubated at 37°C continuously to check the effect of etching treatment on the cell growth. No significant effect of the etching treatment on the cell growth was observed.

3. Effects of single hit of heavy ions

After irradiation of 13.0 MeV/u $^{20}\text{Ne}^{7+}$ and 11.5 MeV/u $^{40}\text{Ar}^{13+}$ ions, the position and the number of ion tracks penetrating the CHO-K1 cells were detected with prompt etching of CR-39 with alkaline ethanol etching solution at 37°C. The growths of the cells were observed individually up to 60 hours after irradiation. The continuous observation of the individual cell growth indicated that a single ion traversal of a cell nucleus resulted in complete growth

inhibition of the irradiated cells.

4. Conclusion

A method for irradiating individual cells with a high-LET heavy ion microbeam has been established. Detection of ion tracks provides us with accurate information about the spatial distribution of delivered ions just after irradiation time. By this method, we can observe the number of ion hits and their positions on and around the target cells at the beginning of the post-irradiation incubation of the cell samples. This method will be quite useful because the accuracy of irradiation information is important to study low dose effect, especially effects of exactly one particle. The effect of cytoplasmic irradiation and the bystander effect will soon be discussed.

References

- 1) C. R. Geard, D. J. Brenner, G. Randers-Pehrson, and S. A. Marino, *Nucl. Instr. and Meth. B54*, 411-416 (1991)
- 2) L. A. Braby, *Scanning Microscopy*, **6**, 167-175 (1992)
- 3) M. Folkard, B. Vonjnovic, K. M. Prise, A. G. Bowey, R. J. Locke, G. Schettino, and B. D. Michael, *Int. J. Radiat. Biol.* **72**, 375-385 (1997)
- 4) Y. Kobayashi, T. Funayama, M. Taguchi, S. Wada, M. Tanaka, T. Kamiya, W. Yokota, H. Watanabe and K. Yamamoto, *JAERI-Review 2001-39*, 73-75 (2001)
- 5) Y. Kobayashi, T. Funayama, M. Taguchi, S. Wada, M. Tanaka, T. Kamiya, W. Yokota, H. Watanabe and K. Yamamoto, *J. Radiat. Res.* **42**, 449 (2001)
- 6) T. Funayama, Y. Kobayashi, S. Wada, M. Tanaka, K. Yamamoto, *J. Radiat. Res.* **42**, 449 (2001)
- 7) Y. Kobayashi, H. Watanabe, M. Taguchi, S. Yamasaki and K. Kiguchi, "MICRODOSIMETRY: An Interdisciplinary Approach", Proceedings of the 12th Symposium on Microdosimetry, Oxford, 1996; pp. 343-346, The Royal Society of Chemistry, Cambridge (1997)

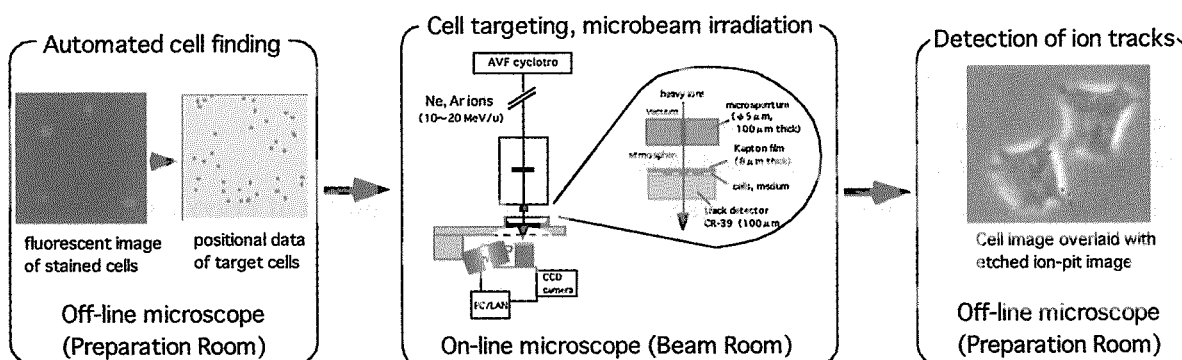


Figure 1. Procedure of the irradiation of cultured cells with a heavy-ion microbeam. Before irradiation, positional data of the individual cells obtained at the Off-line microscope in the preparation room by microscopically searching the sample dish. Using the object database, targeting and irradiation at the On-line microscope are carried out quickly. Immediately after irradiation, the cell dish is refilled with medium, and then the bottom is etched from the opposite side of the cells to detect the accurate position of ion tracks on the cells.

2.21 Regeneration of Hemopoietic Organs in the Silkworm, *Bombyx mori*, After the Selective Irradiation of 100 Gy Carbon Ions

K. Kiguchi*, E. Ling*, K. Fukamoto*, S. Xu*, K. Shirai*, R. Kanekatsu*, Y. Kobayashi**, Z.-L. Tu**, T. Funayama**, H. Watanabe**

Department of Applied Biology, Faculty of Textile Science and Technology, Shinshu University*

Department of Radiation Research for Environment and Resources, JAERI**

1. Introduction

In the previous paper, we showed that locally targeted irradiation to *Bombyx* larvae has no serious effect on the survival, but inflicts severe damage on the irradiated tissues or organs¹⁾. For example, deletion of wings can be induced in the resultant adults by irradiation to the imaginal wing discs at larval stages. We also showed that hemocyte density has significantly fallen down after the selective irradiation to the hemopoietic organs. However, the decline in the hemocyte density is later followed by drastic increase at the wandering stage²⁾.

Why does the hemocyte density rise in the larvae whose hemopoietic organs have been irradiated with heavy ion beams? Do the hemopoietic organs regenerate and release hemocytes after the irradiation? To answer the question, we have investigated the morphological changes of the hemopoietic organs by electron microscope after selectively localized irradiation with heavy ion beams to the hemopoietic organs in the silkworm, *Bombyx mori*.

2. Materials and Methods

Insects

A laboratory colony of the *pnd p^s* strain of the silkworm, *Bombyx mori*, was used for experiments. They were reared on an artificial diet at 25 °C under a 16-hr light and 8-hr dark photocycles. 4th instar day 3 larvae were subjected to heavy ion beam irradiation.

Ion beam irradiation

We used carbon ion beams (¹²C⁵⁺, 220 MeV, 18.3 MeV/u, range in water=1.2 mm) provided from the AVF-cyclotron in TIARA. As described in the previous paper¹⁾, we made several holes (5 mm in diameter) on an acrylic resin plate (2 mm in thickness) for selective irradiation, and through the hole the imaginal wing disc attached with the hemopoietic organ was selectively exposed to the ion beams at dose of 100 Gy.

Observation by electron microscope

The hemopoietic organs of day 2 and day 6 larvae were fixed at 4°C in 2.5% glutaraldehyde in 0.13 M phosphate buffer at 7.4 for about 1 hr. Fixed samples were washed in phosphate buffer and post-fixed in 1% osmium tetroxide buffered to pH 7.4 for 1 hr. After fixation the tissue was

embedded in Epon 812 by routine methods. The sections were stained for 30 min in 70% ethanol saturated with uranyl acetate and then for a few minutes in lead citrate. The grids were examined with Japan Electron Optic JEM electron microscope.

3. Results and Discussion

All of the 4th instar larvae whose right thoracic regions were irradiated with carbon ions (100 Gy) ecdyed into the 5th instar ($n=18$), and developed normally as the non-irradiated control larvae did. They began to wander on day 5. Normal hemopoietic organ consists of spherical islets or cysts in which many cells are packed, and they are covered by acellular sheath^{3,4}. Observation of the irradiated hemopoietic organs from day 2 larvae revealed that the organs lose most of acellular membrane covering the islets, and a lot of cells showed typical features of melt-necrosis (Fig.1). Thus, it is clear that the irradiation of carbon ions (100 Gy) causes serious damage to the hemopoietic organs. However, it is noteworthy that there are a few cells with normal morphology in the irradiated hemopoietic organs. We suppose that those hemocytes might be derived from the circulating hemocytes and they function as phagocytosis of the dead cells produced by necrosis after irradiation.

On the other hand, the irradiated organs of day 6 larvae showed actively proliferating features. The organs are composed of free hemocytes and typical islets in which there are many immature or mature hemocytes. In addition, the organs are again surrounded by acellular sheath (Fig.2), and

adhere to the trachea invaded. From these results it is concluded that regeneration occurred in the hemopoietic organs even after the irradiation of 100 Gy carbon ions.

There is no doubt that carbon ions passed through the whole hemopoietic organ, because beam depth (range in water = 1.2 mm) is enough long to reach the organ which lies within 0.3 mm underneath from the surface of the cuticle in the 4th instar. In addition, 100 Gy of carbon ions is enough high to induce complete deletion of adult wings when irradiated at larval stages¹. Why does regeneration occur in the irradiated hemopoietic organs? We are now investigating the source and fate of the cells with normal morphology observed in the irradiated organs of day 2 larvae, with special reference to the mechanism of regeneration in the hemopoietic organs after the selective irradiation of heavy ion beams.

References

- 1) Tu, Z.-L., Yamasaki, S., Shirai, K., Kanekatsu, R., Kiguchi, K., Kobayashi, Y., Taguchi, M., and Watanabe, H. (1999a) *J. Seric. Sci. Jpn.* 68, 443-453.
- 2) Tu, Z.-L., Shirai, K., Kanekatsu, R., Kiguchi, K., Kobayashi, Y., Taguchi, M., and Watanabe, H. (1999b) *J. Seric. Sci. Jpn.* 68, 491-500.
- 3) Akai, H., and Sato, S. (1971) *J. Insect Physiol.* 17, 1665-1676.
- 4) Han, S.-S., Lee, M.-H., Kim, W.-K., Wago, H., and Yoe, S.-M. (1998) *Zool. Sci.* 15, 371-379.

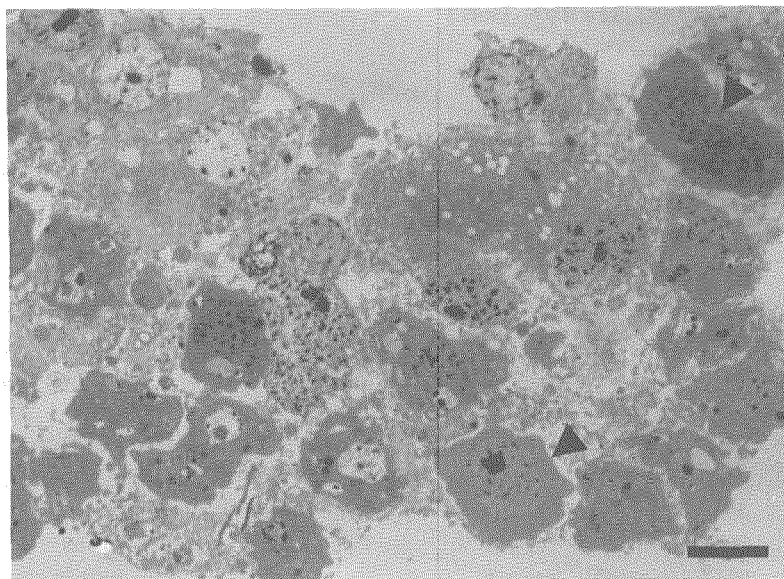


Fig. 1 The hemopoietic organ of 5th instar day 2 larva which has been irradiated with carbon ions (100 Gy) at the 4th instar premolting stage. Most cells show typical features of melt-necrosis. Note that there are a few cells with normal morphology in the organ. Scale bar =7 μ m

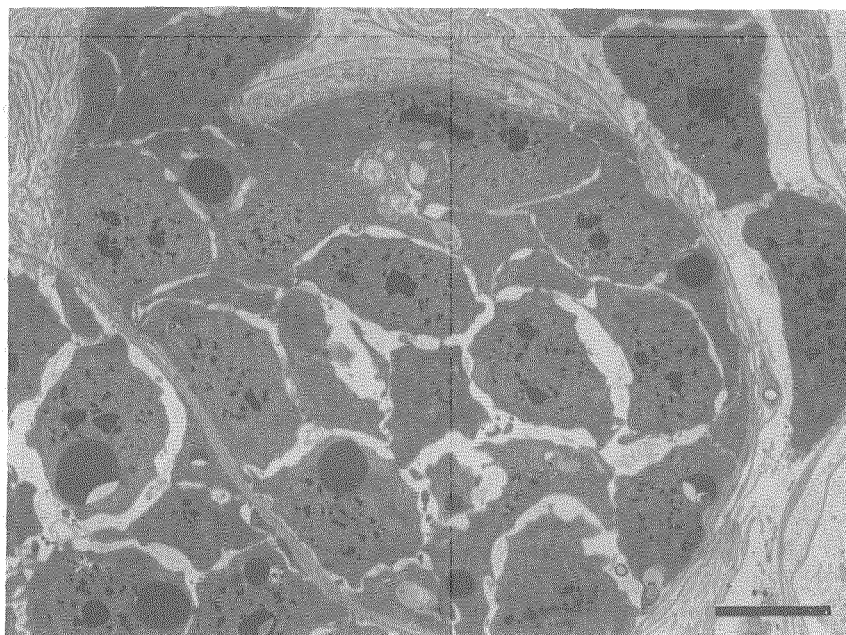


Fig. 2 The hemopoietic organ of 5th instar day 6 larva which has been irradiated with carbon ions (100 Gy) at the 4th instar premolting stage. The organ is filled with many cells and surrounded with acellular sheath, suggesting that regeneration occurs after the irradiation. Scale bar =5 μ m

2.22 Mechanism of Bystander Effect Induced by Precise-Numbered Heavy Ions

Y. Furusawa^{*}, C. Shao^{*}, M. Aoki^{*}, S. Wada^{**}, T. Funayama^{**}, and Y. Kobayashi^{**}

Heavy Ion Radiobiology Research Group, NIRS^{*}, Department of Radiation Research for Environment and Resources, JAERI^{**}

1. Introduction

Considerable evidences have recently been accumulated in support of the existence of a "bystander effect" which cells having received no irradiation show biological consequences from their neighbor irradiated cells. Previously studies have shown that the number of sister chromatid exchange (SCE) in fibroblast cells greatly exceeded the statistical number of the cells having sustained a traversal by an α -particle track¹⁾. It has been reported that some soluble factors, such as reactive oxygen species (ROS) and transforming growth factor β 1 (TGF- β 1), generated from irradiated cells were involved in the medium-mediated bystander effect. ROS might also contribute to the mutation production when the cytoplasm of mammalian cell was irradiated by precise numbered α -particles²⁾. Most recently, we found that nitric oxide could be released from irradiated HSG cells so that plating efficiency and cell proliferation were increased as well that micronucleus (MN) was induced in unirradiated neighbor cells^{3,4)}.

On the other hand, a lot of evidences showed that gap junctional intercellular communication (GJIC) was an important mediator to radiation-induced bystander effect. The bulk researches concerning bystander effect are in the field of gene therapy of which the gene product of transfected DNA can travel through gap junction from transfected cells to neighboring cells. Recently, cell-cell communication has been thought to be relevant to radiation-induced effect. Cells with microcolonies where cell-cell interactions occurred were demonstrated to be more sensitive than single cells when they were irradiated with a dose less than 2 Gy. With a three-dimensional tissue culture model, it was also proved that GJIC played a role in enhancing cell damage and so reducing the survival of unirradiated neighbor V79 cells. In addition, Azzam *et al* found that TP53 and CDKN1A were over expressed, associated with

a G1-phase arrest, in the confluent human fibroblast cell population exposed to α particles with a very low dose, and these expressions were effectively reduced when GJIC was inhibited by lindane⁵⁾.

Therefore, two different manifestations, medium-derived factors and GJIC, of a radiation-induced bystander effect have previously been demonstrated. However, it is largely unknown which one has a dominative role or whether they just have a parallel role in the bystander effect. With present study, it was believed that GJIC likely played an essential role, although ROS also had an obvious effect, in the radiation-induced bystander effect by using PMA to inhibit GJIC and using DMSO to scavenge ROS.

2. Experimental

2.1 Cell Culture and Treatments

AG1522 normal human-diploid skin fibroblasts purchased from the Coriell Cell Repositories were cultured at 37°C in humidified atmosphere of 95% air and 5% CO₂ with Eagle's minimum essential medium (E-MEM, Sigma M5650) supplemented with 2.0 mM L-Glutamine and 18% fetal bovine serum (FBS, Lenexa) plus 100 μ g/ml streptomycin and 100 units/ml penicillin. Cells destined for heavy-ions irradiation were seeded in 35 mm plastic dishes with 8.5 μ m-thick replaceable Kapton film bottoms at a density of 2×10^5 cells per dish 4 days before irradiation and were fed on the days 2. At the time of irradiation the cells were in full confluence. In some flasks, cell culture medium was changed with that containing 10^{-9} M PMA (4 β , 9 α , 12 β , 13 α , 20-pentahydroxytiglic-1, 6-dien-3-one 12 β -myristate 13-acetate, 10^{-6} M prepared in DMSO) 1 h before irradiation; in this case, 0.1% DMSO was contained in the culture medium. As a control of the PMA treatment, the culture medium was replaced with one containing 0.1% of DMSO in some flasks also 1 h before irradiation.

2.2 Cells Irradiation

A microbeam facility of TIARA at Takasaki Institute of JAERI was used to provide precise-numbered heavy-ions, 13.0 MeV/u $^{20}\text{Ne}^{7+}$ (~430 keV/ μm) and 11.0 MeV/u $^{40}\text{Ar}^{13+}$ (~1260 keV/ μm). The particles were detected by a plastic scintillator and photomultiplier tube (PMT) after traversing through cell sample. Before irradiation, the culture medium was removed but the cell layer was covered with a Kapton film in order to keep cells in wet during irradiation. Cells were irradiated by two ways; on the one hand, 1 to 121 spots with a matrix distribution of 11x11 mm² in the center area of the cell film dish were precisely traversed by 1 particle per spot; on the other hand, 49 matrix-distributed spots in the cell film dish were respectively irradiated by 1 to 4 particles. After irradiation, the cells were subsequently cultivated for approximate 15 h in 2 ml medium where 5×10^{-10} M PMA or 0.05% of DMSO was contained with respect to the PMA- or DMSO-treated cells, respectively.

2.3 MN Assay

The formation of MN in the irradiated cell layer was assayed by using the cytokinesis-block technique developed by Fenech and Morley⁶⁾. Briefly, a portion of the harvested cells was incubated in 2 ml of growth medium in the presence of 2.5 $\mu\text{g}/\text{ml}$ cytochalasin-B. After 48 h, the cells were collected and suspended in a 0.075 M KCl hypotonic solution for 10 min at 37°C, and finally fixed by methanol at -30°C for overnight. For the observation, the fixed cells was placed on a glass slide and stained with 10 $\mu\text{g}/\text{ml}$ acridine orange for 5 min. MN in binucleated (BN) cells was checked by a fluorescence microscopy and morphologically identified by the criteria method. At least 1000 BN cells were scored at each dose point for MN measurement of three separately experiments.

3. Results and Discussion

Fig. 1 illustrates the frequency of MN production in the heavy ion irradiated cell layer. When each selected cell was precisely traversed by one $^{40}\text{Ar}^{13+}$ particle, the MN yield biphasically increased with the number of irradiated cells. It was found that even only one cell in the dish was hit by only one particle the yield of

MN could be obviously increased to about 2-fold of the control, therefore, MN was produced in other hundreds of non-hit cells since a bystander effect. When the hit cell number increased from 4 to 121, the MN yield continually increased but with a slope lower than the original one when the hit cell number was less than 4.

When the cells were pretreated by PMA, the MN yield in the $^{40}\text{Ar}^{13+}$ ion irradiated-cell layer was extensively reduced to a very low level near to the control without any treatment. This decrease in MN induction might result from PMA and its solvent DMSO. To investigate the influence of DMSO to the PMA treatment experiment, we detected the MN induction in 0.1% DMSO treated cell layer that has been hit by $^{40}\text{Ar}^{13+}$ ions, and found that this treatment could partly decrease the MN induction (see Fig. 1).

Because PMA is an effective inhibitor of gap junctional cellular communication (GJIC) and DMSO is a scavenger of reactive oxygen species (ROS), the results in Fig. 1 indicate that both GJIC and ROS are involved in the radiation-induced bystander effect and GJIC may have an essential role in this bystander effect.

To explore the dose effect of the bystander effect, we irradiated 49 matrix-distributed cells in a dish with 1 to 4 particles. It was found that no significant difference in the MN induction existed in the cell population irradiated by 1 to 4

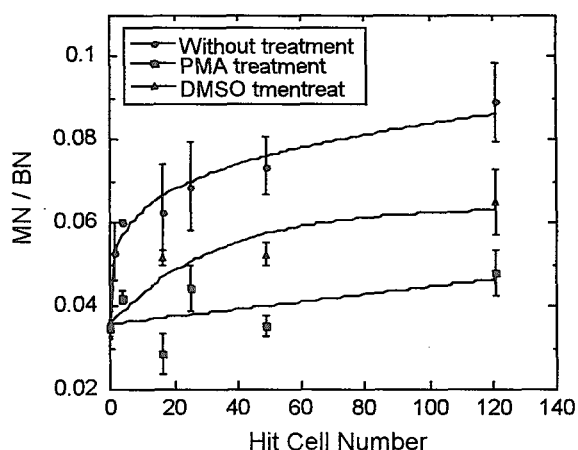


Fig. 1 Yield of MN production in the $^{40}\text{Ar}^{13+}$ particles irradiated cell population. Cells with a matrix distribution in confluent cell layer were hit by one particle per cell. The cells were pretreated by 10^{-9} M PMA or 0.1% DMSO for 1 h before irradiation or were not treated.

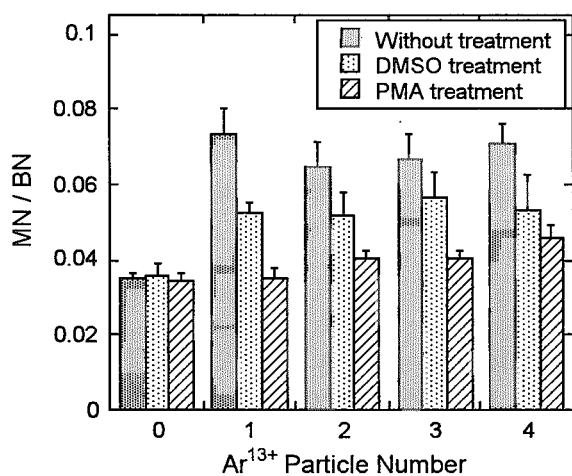


Fig. 2 Yield of MN production in the $^{40}\text{Ar}^{13+}$ particles irradiated cell population. 49 cells with a matrix distribution in confluent cell layer were hit by 1 to 4 particles per cell. The cells were pretreated by 10^{-9} M PMA or 0.1% DMSO for 1 h before irradiation, or were not treated.

particles per cell (Fig. 2). Again, the treatment of DMSO and PMA partly and extensively reduced this MN yield, respectively.

On the other hand, we measured the MN induction in $^{20}\text{Ne}^{7+}$ particle irradiated cell layer with the same way as the above, and found that the yield of MN was not influenced by the LET of radiation (data not shown).

4. Conclusion

Considering the results in Fig. 1 and Fig. 2, it is suggested that the hit cell number as well as the damage degree of the hit cell are not the main reason of the MN production in other hundreds of non-irradiated cells. In fact, the maximum number of irradiated cells, 121, only has a very small portion ($\sim 0.015\%$) of the cells in the dish. This small fraction is not enough to contribute the measured MN induction. Therefore, these traversed cells may have another important effect, i.e. triggering a series of bystander effect via the GJIC pathway and medium-mediated pathway.

References

- 1) Nagasawa H and Little JB (1992) Induction of sister chromatid exchanges by extremely low doses of alpha- particles. *Cancer Res* **52**, 6394-6396.
- 2) Wu LJ, Randers-Pehrson G, Xu A, Waldren CA, Geard CR, Yu Z and Hei TK (1999) Targeted cytoplasmic irradiation with alpha particles induces mutations in mammalian cells. *Proc Natl Acad Sci U S A* **96**, 4959-4964.
- 3) Shao C, Aoki M and Furusawa Y (2001) Medium-mediated Bystander Effects on HSG Cells Co-cultivated with Cells Irradiated by X-rays or a 290 MeV/u Carbon Beam. *J. Radiat. Res.* **42**, 305-316.
- 4) Shao C, Furusawa Y, Aoki M, Matsumoto H and Ando K (2002) Nitric oxide-mediated bystander effect induced by heavy-ion radiation in human salivary gland neoplastic cells. *International Journal of Radiation Research*, in press.
- 5) Azzam EI, de Toledo SM and Little JB (2001) Direct evidence for the participation of gap junction-mediated intercellular communication in the transmission of damage signals from alpha -particle irradiated to nonirradiated cells. *Proc Natl Acad Sci U S A* **98**, 473-478.
- 6) Fenech M and Morley AA (1986) Cytokinesis-block micronucleus method in human lymphocytes: effect of in vivo ageing and low dose X-irradiation. *Mutat Res* **161**, 193-198.

2.23 The Effect to Mammalian Nucleus by Irradiation of Heavy Ion Beams.

S.Wada^{*,**}, M.Natsuhori^{*}, N.Ito^{*}

Y.Kobayashi^{**}, T.Funayama^{**}, K.Yamamoto^{**}

Department of Veterinary Medicine, Kitasato University^{*}

Biotechnology Lab., JAERI- Takasaki^{**}

1.Introduction

In space environment high LET heavy ions at low fluence are a component of cosmic rays. Extended mission above atmosphere of the earth put humans at an inherent risk due to exposure to cosmic rays. For cells exposed to high LET heavy charged particles DNA double strand breaks (dsbs) have an important role in biological effects. Adequate assessment of this risk will lead to an improved understanding of the biological response to heavy ion radiation. At present there are many studies with regard to the measurements of DNA dsbs induced by the heavy ions that deposit energy at very high LET. Previously the classical sucrose gradient centrifugation method was used for detection of DNA dsbs. Recently filter elution, conventional electrophoresis and pulsed-field gel electrophoresis were used. The quantitative analysis of every approach relies on the assumption that ions hit randomly to the cells and Poisson statistics was applied. However the biological effect of one charged particle to cell can not be calculated with the analysis of these

methods. To estimate the number of ions traversing cells and to evaluate the radiation damage induced by one or precise number of ions, we established the method of simultaneous detection of ions traversing the cellular nuclei and DNA damage in the individual cells. We compared the number of ions traversing the cell and the DNA damage detected with the comet assay.

2.Materials and methods

CHO-K1 cells were grown in Ham's F12 medium supplemented with 10% serum (Nichirei, Tokyo) and 0.1 mg/ml kanamycin in 10 cm diameter culture dishes. Cells were incubated at 37°C in humidified atmosphere of 5% carbon dioxide and 95% air.

Cells were harvested after incubating for 12 hr with medium containing 1 mM Hydroxyurea. Then cells were attached on the CR-39 plate that is particle track detector. Accelerated heavy ion of 17.3 MeV/u $^{12}\text{C}^{5+}$, 15.7 MeV/u $^{20}\text{Ne}^{8+}$, 10.4 MeV/u $^{20}\text{Ne}^{7+}$ and 6.9 MeV/u $^{40}\text{Ar}^{13+}$ were provided by the AVF cyclotron at TIARA JAERI-Takasaki.

Immediately After irradiation the

CR-39 plate on the which cells were attached was placed in chilled PBS. The CR-39 was placed on the slide glass and then was embedded in 1% agarose-LGT GP-42 (Nacalai Tesque, Kyoto, Japan). Finally 100 μ l of 1% agarose GP-42 (Nacalai Tesque, Kyoto, Japan) was quickly layered. The slide glasses were placed immediately in a chilled nucleus lysing solution (pH 10) of 2.5 M NaCl, 100 mM Na₂EDTA, 1% sarkosyl, 10% DMSO, and 1% Triton X-100 and kept at 4°C in the dark for 60 min. Under the neutral condition for comet assay the slides were placed on a horizontal gel electrophoresis platform and covered with chilled neutral solution made up of 90 mM Tris, 2 mM Na₂EDTA and 90 mM boric acid (pH 8) for 1 hour. Electrophoresis was conducted at 4°C in dark for 30 min at 25 V (0.89 V/cm).

The slide glasses were wash with 300 mM NaOH and 1 mM Na₂EDTA and then rinsed gently with 400mM Tris (pH 7.5) to neutralize the excess alkali. After air drying the CR-39 plate was take off from the slide glass. the agarose gel on the CR-39 was stained with 50 μ l of 0.4 μ g/ml ethidium bromide and the opposite side of the CR-39 plate was etched with KOH-ethanol solution at 37°C. Using a fluorescence microscope equipped with a green filter (Olympus, Tokyo) we examined about cells on one slide at 400 magnification. The comet image was stored using CCD camera. Then the microscope was focused on the image of pits etched on the CR-39, and the image was also

stored using CCD camera. Because the area of cellular nucleus was identified with the area of high fluorescent intensity of comet image, the number of ions traversing individual cellular nuclei was counted by merging both images. The comet image was analyzed using a Komet software (Komet 4.0, Kinetic imaging, LTD, UK). The parameter used as an index of DNA damage was tail moment, which combines a measure of the length of comet tail and the proportion of DNA to migrate into the tail.

3.Result and Discussion

The number of ions traversing the cellular nuclei and DNA damage in the individual cells was detected simultaneously. The DNA damage induced in the heavy ion irradiated cells was detected by comet assay. The comet image of cell attached on the CR-39 was observed using fluorescence microscope. Moreover, the image of etched ion pits was observed at the opposite side of cells attached on the CR-39 by changing the focus. When both images were merged, the number of pits etched was detected on the area of cellular nuclei that is the area of high fluorescent intensity of the comet image. Thus the number of ions traversing the cellular nuclei can be estimated.

DNA dsbs induced by heavy ion irradiation was evaluated as tail moment that generally used for evaluating DNA damage with comet assay. Tail moment increased with the number of ions traversing the cellular nuclei. Fig. 1 shows the relationship

between tail moment and the number of ion hits with four different LET values. Those data was fitted by linear regression. The slope of the fitted curves indicated the induction of DNA damage per a particle in CHO-K1 cell, thus reflecting the effectiveness of the accelerated ions. Table 1. shows parameters of the particle ion used in this study and the slope of the fitted linear regression. In figure 2, the slopes calculated from the fitted plots of tail moment and ion traversals were plotted as a function of LET of irradiated heavy ions. The slopes increased with the LET values of ions. This result indicated that the amount of DNA damage induced by one particle depended on the its LET.

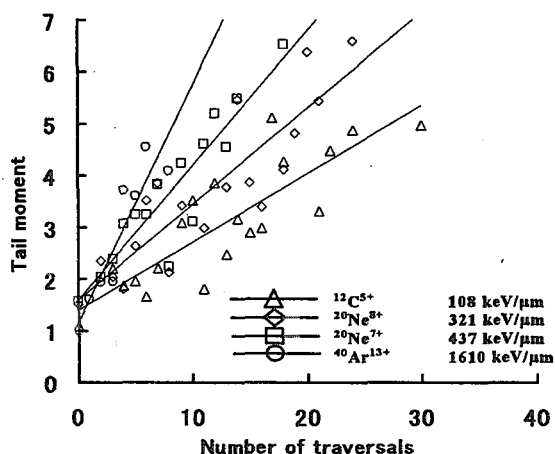


Fig. 1 Relationship between tail moment and the number of ions traversing the cellular nucleus. The cells were irradiated with ion beams having LET values of 108, 321, 437 and 1610 keV/μm.

Table 1 Parameter of used and the slopes from fitted plots of the tail moment and traversed particle number.

	Energy (MeV/u)	LET (keV/μm)	Slope (Tail moment/particle)
C ⁵⁺	17.3	108	0.136±0.004
Ne ⁸⁺	15.7	321	0.17±0.01
Ne ⁷⁺	10.4	437	0.23±0.03
Ar ¹³⁺	6.9	1610	0.41±0.03

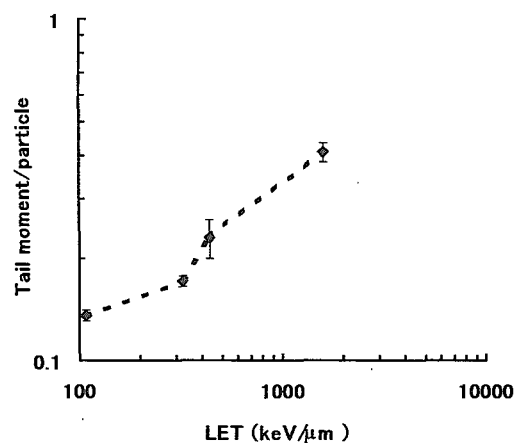


Fig. 2 The slopes from fitted plots of tail moment and ion traversals as a function of LET values.

2.24 Dynamical study on influence of the CO₂ enrichment to the photoassimilate transportation using positron imaging

S. Matsushashi, S. Watanabe, N. S. Ishioka, C. Mizuniwa, T. Ito and T. Sekine

Department of Ion-Beam-Applied Biology, JAERI

Introduction

It is generally known that plants cultivation under CO₂ enrichment condition introduces increase of fruit harvest¹⁾. CO₂ enrichment plays as if it was extra manure, and causes change of regulations related to photoassimilate efflux from a leaf and/or their transportation through phloem in a plant. However the mechanism of increasing fruit harvest is not clear yet. The objective of the present study is to understand the regulation of photoassimilate transportation in a plant under CO₂ enrichment condition. For this purpose, we have been using a positron emitting tracer imaging system (PETIS) to observe the transportation of photoassimilates which are labeled with a positron-emitting tracer. Previously, we reported our first experiments on the influence of CO₂ enrichment to behavior of photoassimilates in a broad bean plant using ¹¹C-labeled carbon dioxide (¹¹CO₂)²⁾. The present paper reports behavior of the photoassimilate efflux from a leaf and the photoassimilate transportation in a plant when high-CO₂-concentration air is fed to different areas of a leaf of a broad bean plant.

Experiment

Seeds of broad bean (*Vicia faba*) were immersed in a water flow until a radicle (embryonic root) broke through testa (seed coat). The seeds were transplanted to a vermiculite bed after germination. After a shoot appeared on the soil, the plant was transplanted again to a plastic cultivation pot filled with vermiculite. The beds and pots were kept in an illuminated incubator. A commercial nutrient solution (HYPONeX 8-12-6, HYPONeX Japan Co.) was fed to the

plants every week. A broad bean with the 6th under-growing foliage leaf on the plant was selected for the present experiment.

For positron imaging measurement, the plant was placed in a chamber conditioned at 350-ppm CO₂. A small acrylic cell with inside dimensions of 0.9 cm in diameter and 2 cm in height was fixed on the center of the reverse side of the 4th foriage leaflet using a dental filling, and connected to a ¹¹CO₂ gas circulating system. In another experiment, the 4th foliage leaves were inserted into a quvet for feeding ¹¹CO₂, which is a clear acrylic box with inside dimensions of 12 cm in length, 8 cm in width and 1 cm in depth. The quvet was sealed at the petiole of the 4th foliage leaves with a dental filling, and connected to the ¹¹CO₂ gas circulating system.

The CO₂ concentration in the cell or the quvet was controlled at 350- or 1000-ppm CO₂ by introducing fresh air or a CO₂ standard gas containing 1000-ppm CO₂, respectively, at a flow rate of 60 ml/min. Immediately, after the ¹¹CO₂ gas was supplied to the cell or the quvet for 1-2 minutes³⁾, measurement with the PETIS was started⁴⁾. After the ¹¹CO₂ gas was drained from the cell or the quvet, fresh air was sent to it. Three hours later, the CO₂ concentration in the cell or the quvet was changed from 350-ppm to 1000-ppm, and kept at the same CO₂ concentration for approximately 2 hours. The next PETIS measurement was done by labeling the same area of the leaf or the same leaves with ¹¹CO₂ gas, followed by supplying a 1000-ppm CO₂ standard gas until the end of the measurement.

Results and discussion

Figure 1 shows time-course changes of the amount of ^{11}C -labeled photoassimilates translocation from a small area of the 4th foliage leaf of a broad bean plant for the two different CO_2 concentrations. When the CO_2 concentration inside of the small cell was 350 ppm, the ^{11}C -labeled photoassimilates took 5 minutes for reaching the base of the 4th foliage leaves through the petiole. The amount of the ^{11}C -labeled photoassimilates increased until 20 minutes, and became to equilibrium. The same time-course change of ^{11}C -labeled photoassimilate translocation was observed under the 1000-ppm CO_2 condition. As seen from Fig. 1(b), the ^{11}C -labeled photoassimilates reached the stem between the 2nd and 3rd nodes 8 minutes after labeling with $^{11}\text{CO}_2$ under the 350-ppm CO_2 condition, and then the ^{11}C count increased to more than 7000 cps after 35 minutes. The time-course change of ^{11}C -labeled photoassimilates transportation under the 1000-ppm CO_2 condition observed at the same place of the stem was similar to that under the 350-ppm CO_2 condition, but the maximum ^{11}C count was lower than that under the 350-ppm CO_2 condition. The results suggest that high-concentration- CO_2 treatment of a small area of a leaf has no effect on the photoassimilate translocation from the leaf.

Figure 2 shows time-course changes of the amount of ^{11}C -labeled photoassimilates that were exported from a pair of the 4th foliage leaves. At 350-ppm CO_2 , the ^{11}C -labeled photoassimilates took 5 minutes to reach the base of the 4th foliage leaves. The maximum ^{11}C count was 90 cps 25 minutes after labeling with $^{11}\text{CO}_2$. At 1000-ppm CO_2 , the arrival time was the same as that at 350-ppm CO_2 . However, the amount of ^{11}C -labeled photoassimilates vastly increased and reached to more than 600 cps of ^{11}C 22 minutes after labeling with $^{11}\text{CO}_2$. This value was approximately 7 times higher than that under the 350-ppm CO_2 condition. At the stem between the 4th and 5th nodes, near the terminal bud of the

plant, only 10 cps of ^{11}C were observed 20 minutes after labeling with $^{11}\text{CO}_2$ at 350-ppm CO_2 . In comparison with this, at 1000-ppm CO_2 , more than 150 cps of ^{11}C were observed. The fact that photoassimilates exported from a leaf increased by high-concentration CO_2 treatment to the leaf, is consistent with the results obtained previously²⁾.

A terminal bud of a plant is a sink organ that uses photoassimilates as a nutrient and an energy source for growing, and is one of the major consumers of the photoassimilates. But the other organs also consume photoassimilates. Therefore, Figure 2(b) shows the photoassimilate amount remaining after interception by other organs during the photoassimilate transportation. The ratio of the photoassimilate amount exported from leaves, given in Figure 2(a), to that transported to the terminal bud, given in Figure 2(b), was 6.7 to 1 at 350-ppm CO_2 . However the ratio was 3.5 to 1 under the 1000-ppm CO_2 condition. This difference suggests that the efflux amount of photoassimilates from each leaf or the photoassimilate concentration in phloem can be changed by high-concentration- CO_2 treatment to a broad bean plant even for a few leaves, not for all leaves.

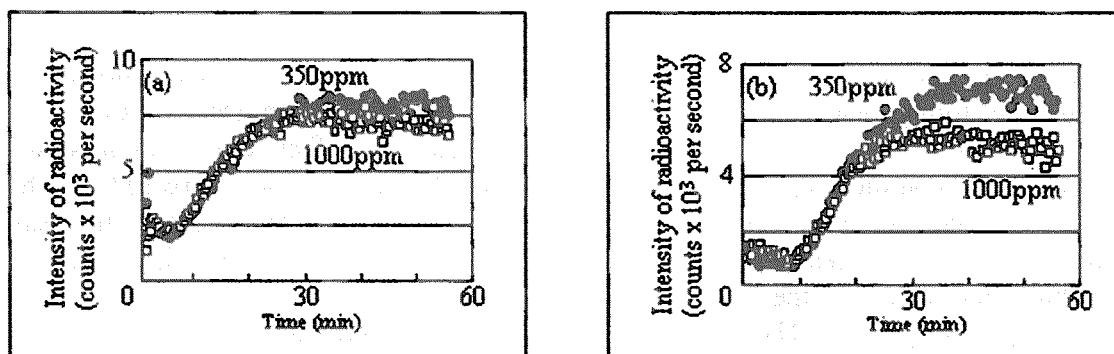


Fig. 1. Time-course study of the translocation of ¹¹C-labeled photoassimilates from a small area of the 4th foliage leaflet kept in the air of different CO₂ concentrations. (a) The analysis at the base of the 4th foliage leaves. (b) The analysis at the stem between the 2nd and 3rd foliage leaves.

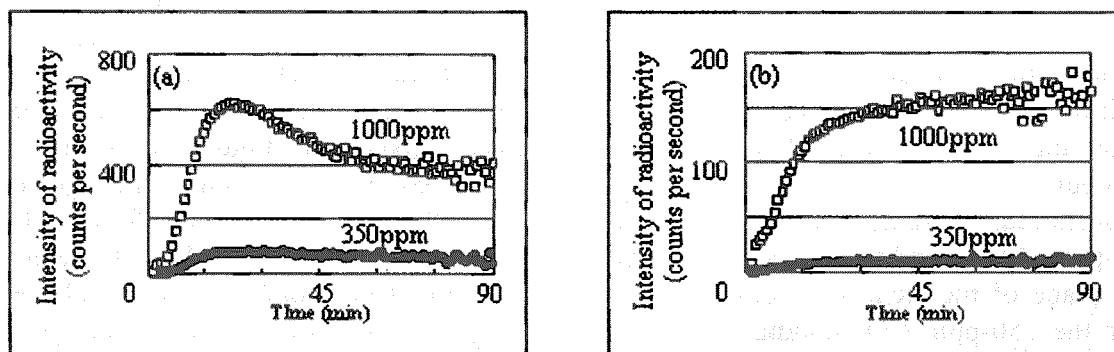


Fig. 2. Same as Fig. 1, except that the 4th foliage leaves were kept in the air of different CO₂ concentrations.

References

1. T. Sakashita, *Annual Report of Agricultural Research Center*, (1997) 42-43.
2. S. Matsuhashi, S. Watanabe, N. S. Ishioka, C. Mizuniwa, T. Ito, T. Sekine, *TIARA Annual Report 2000, JAERI-Review 2001-039* (2001) 90-92.
3. N. S. Ishioka, H. Matsuoka, S. Watanabe, A. Osa, M. Koizumi, T. Kume, S. Matsuhashi, T. Fujimura, A. Tsuji, H. Uchida, T. Sekine, *Journal of Radioanalytical and Nuclear Chemistry*, **239** (1999) 417-421.
4. H. Uchida, T. Omura, T. Suzuki, A. Tsuji, T. Yamashita, T. Fujimura, S. Matsuhashi, T. Kume, *Radiation and Industries*, **80** (1998) 6-10.

2.25 Effect of Atmosphere Gas Conditions on Soybean (*Glycine Max* L.) $^{13}\text{N}_2$ Fixation Activity

N. Ohtake, T. Ohyama, K. Sueyoshi., H. Fujikake, N. S. Ishioka*, S. Matsuhashi*, S. Watanabe*, T. Sekine*, H. Uchida** and A. Tsuji**

Faculty of Agriculture, Niigata University, * Department of Ion-Beam-Applied Biology, JAERI, ** Hamamatsu Photonics Co.

1. Introduction

Nodulated leguminous crops assimilate both gaseous nitrogen by root nodules and combined nitrogen from roots for their growth. In soybean plants, the nitrogen fixed in root nodules is metabolized mainly into ureides (allantoin and allantoic acid). Studies on the assimilation of N_2 fixed in nodules has been reported in detail, while the transport and utilization of fixed N in shoot organs is not fully understood. Recently we could detect ^{13}N distribution in plants in real-time by PETIS. In the present study we tried to establish a method for $^{13}\text{N}_2$ feeding to soybean nodules.

2. Experimental Procedure

2.1 Plant material

Soybean plants, cv. Williams, and its supernodulating mutant (cv. Nod 1-3) were inoculated with *Bradyrhizobium japonicum* strain USDA 110 and were hydroponically cultivated with N free medium. Thirty-five days after sowing, these plants were used for $^{13}\text{N}_2$ feeding experiment in TIARA.

2.2 Production of $^{13}\text{N}_2$

$^{13}\text{N}_2$ was produced with the $^{12}\text{C}(\text{d}, \text{n})^{13}\text{N}$ reaction by bombarding 80 mL of the CO_2 containing 10% He with a 20 MeV deuterium ion beam from the TIARA AVF cyclotron. Using a beam current of 5 μA for 10 min, about 165 MBq of $^{13}\text{N}_2$ was produced. Pressured by Ar gas, this radioactive gas was transferred into a 300 mL stainless bomb. The final pressure in the bomb was about 0.4-0.6 MPa.

2.3 Experimental set up for $^{13}\text{N}_2$ feeding to an intact soybean plant

The $^{13}\text{N}_2$ feeding system for soybean root nodules is shown in Fig. 1 (Left). The plant was sealed by silicone base (OPTASIL, Heraeus Inc). The flow system is shown in Fig. 1 (right). The $^{13}\text{N}_2$ flow rate was fixed at 30 or 40 mL min^{-1} . Before $^{13}\text{N}_2$ feeding to the plant, air was mixed at a rate of 1 mL min^{-1} . The distribution of radioactivity in the plant shoot was observed by PETIS, and then the radioactivity in the whole plant was detected by BAS.

Results

In preliminary experiments, the

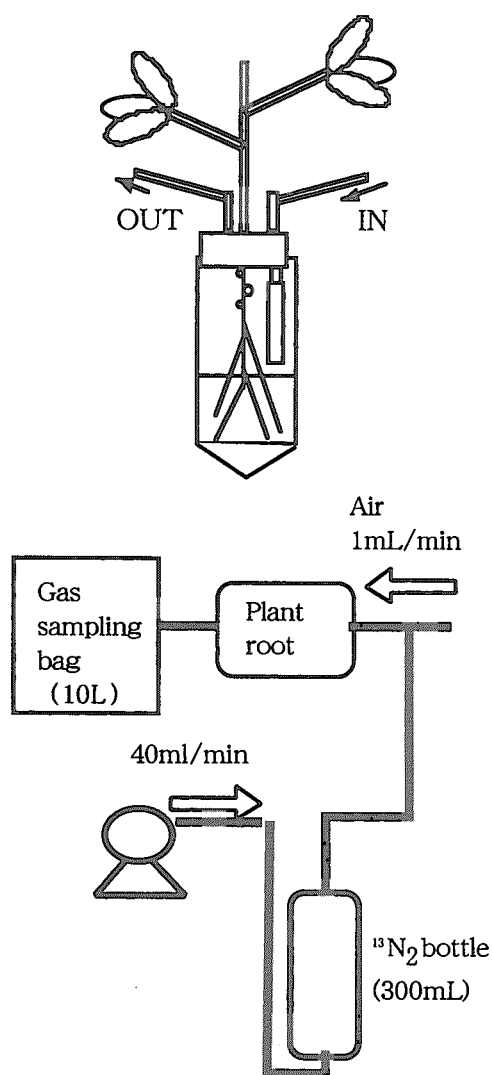


Fig. 1 Schematic $^{13}\text{N}_2$ Application to soybean plant root nodules (upper) and the $^{13}\text{N}_2$ flow system (lower).

$^{13}\text{N}_2$ -containing target gas was collected in a 40 mL pipe by its self-pressure or by high-pressure Ar gas. The gas was applied to the soybean nodulated root position. No ^{13}N signal, however, could be observed by PETIS or BAS in this experiment. Because the $^{13}\text{N}_2$ was made from the mixed gas of 90% CO_2 and 10% He, the applied gas was

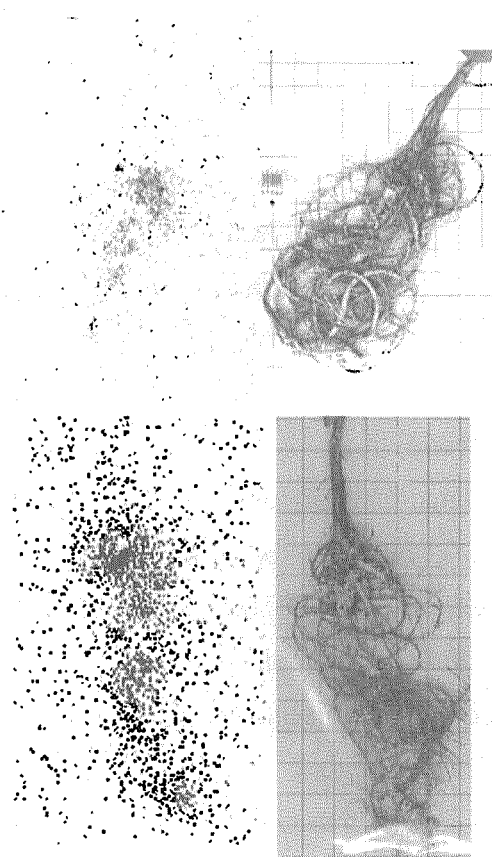


Fig. 2 BAS images of radioactivity in nodulated roots. Upper : Williams, Lower : Nod 1-3 (supernodulation mutant of Williams).

almost CO_2 .

It is known that the amount of N_2 fixed in nodule is proportional to oxygen concentration at least until 20%¹⁾. Therefore a cold experiment was performed to determine a limitation of O_2 concentration in our experiment that is a main factor inhibiting N_2 fixation. The N_2 fixation activity was estimated from the measurement of the acetylene-reducing activity. The results showed that 20% O_2 could not alleviate the inhibition in N_2 fixation under 70% CO_2 and 10% C_2H_2 root

atmosphere condition. We supposed that the presence of high-concentration CO_2 might disturb nitrogen fixation directly or indirectly. The root environmental gas changed into CO_2 , including 10% C_2H_2 for fixation assay, led complete inhibition of N_2 fixation. By investigating optimum conditions for N_2 fixation with the presence of CO_2 , N_2 fixation was found to recover to about 60% of the maximum activity by replacing 10% of the gas with air.

From the results obtained above, the present experiment was designed as described in Experimental Procedure. In this procedure, the irradiated target gas (80 mL) was diluted 5 -7 times by Ar. When the mixed gas was supplied to a plant (40 mL min^{-1}), air was also supplied at 1 mL min^{-1} . Using this method ^{13}N accumulation in nodules could be visualized as a BAS image (Figure 2), while that in a plant shoot could not still be detected by PETIS.

Discussion

Symbiotic relationship between legume crop and rhizobia has been studied for a long time. Wilson (1940) first reported the effect of environmental gas condition on nitrogen fixation activity. He showed that the $p\text{N}_2$ supporting half-maximum fixation was about 0.05 atm N_2 . In this experiment, helium was used as dilution gas to bring the pressure in the bottle to one atmosphere, while hydrogen was used as dilution gas on

the logical assumption that it would be inert in the nitrogen-fixing reaction²⁾. Nowadays the phenomenon has been recognized that H_2 inhibits N_2 fixation in an ordered sequential reaction in which H_2 binds to nitrogenase before N_2 bind³⁾. On the other had, there are few reports about negative CO_2 effect on the nitrogen fixation to our knowledge. Further experiment was necessarily to improve the $^{13}\text{N}_2$ supplying method for soybean nodules without inhibition of nitrogenase.

References

- 1) Ohyama T. and Kumazawa K., 1979. Soil Sci. Plant Nutri. 25, 9-19.
- 2) Wilson P. W., 1940. Madison, Wis. (USA): University of Wisconsin Press.
- 3) Guth J. H., Burris R. H., 1983. Biochemistry 22: 511-5122.

2.26 Absorption and transfer of the iron (^{52}Fe) in the iron absorption maize mutant '*ys1*'

T. Tsukamoto*, S. Kiyomiya*, H. Nakanishi*, H. Uchida***,
S. Watanabe**, N. Ishioka**, S. Matsushashi**, T. Sekine**,
and S. Mori*

Department of Applied Biological Chemistry, The University of Tokyo*,

Department of Ion-Beam-applied Biology, JAERI**,

Central Research Laboratory, Hamamatsu Photonics K.K.***

1. Introduction

Iron is required for many functions in plants, including heme and chlorophyll biosynthesis, photosynthesis, and as a component of iron-sulfur cluster containing enzymes. Although iron exists in large quantities in the environment, plants cannot absorb iron easily in high pH soil because of the low solubility of the oxidized form of iron, $\text{Fe}(\text{OH})_3$. Therefore, plants have developed evolutionally efficient mechanisms of iron acquisition that are directed at solubilizing iron. As a mechanism of this kind, graminaceous monocots release $\text{Fe}(\text{III})$ -chelating compounds, mugineic acid family phytosiderophore (MAs) into the rhizosphere. MAs solubilize inorganic $\text{Fe}(\text{III})$ -compounds by chelation.

Very recently it was reported that the $\text{Fe}(\text{III})$ -MAs complexes are taken up through $\text{Fe}(\text{III})$ -MAs transporter '*YS1*' in the root plasmamembrane.⁷⁾ Although the ability of *YS1* was shown in a growth test (complementation) in a yeast iron uptake mutant, and from the effect of Fe starvation on *ys1* gene expression in maize roots, it is not shown whether *YS1* works actually to absorb $\text{Fe}(\text{III})$ -MAs in plants.

Here we used the positron-emitting ^{52}Fe , and, using the PETIS method,^{1-6, 8)} traced the time-course of ^{52}Fe translocation in maize plant, which is a family of

graminaceous monocots.

2. Material and methods

The maize (*Zea mays* L. cv. Alice) yellow *stripe1* (*ys1*) mutant which is defective in $\text{Fe}(\text{III})$ -MAs transporter '*YS1*'⁶⁾ and wild type plants were grown hydroponically in absence of iron for 2 weeks after germination.

Figure 1 shows pictures of plants used in the experiment. In the *ys1* mutant, chlorosis was observed for all the leaves other than the 1st leaf.

The production and the radiochemical separation of $^{52}\text{Fe}(\text{III})$ was carried out with a method described by Watanabe et al.³⁾ The separated $^{52}\text{Fe}(\text{III})$ was chelated with deoxymugineic acids.

The roots of a single plant were placed in a polyethylene bag that contained 15 mL of culture solution without iron. $^{52}\text{Fe}(\text{III})$ -deoxymugineic acid (DMA) was supplied to the culture solution. We analyzed ^{52}Fe absorption from roots using the PETIS method.

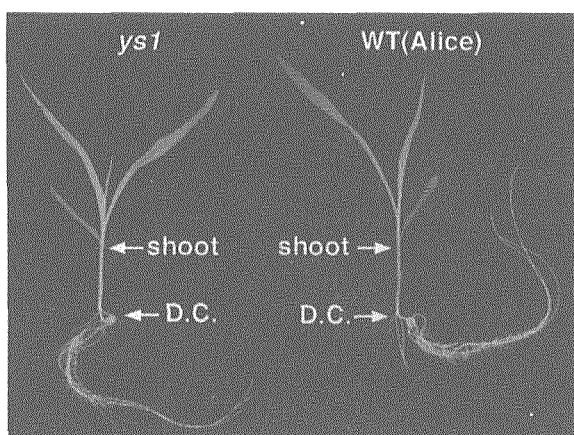


Fig.1 Pictures of the *ys1* mutant (left) and wild type (right) used in the present experiment. Arrows indicate the positions where time-course analysis of ^{52}Fe radioactivity was carried out.

3. Results and discussion

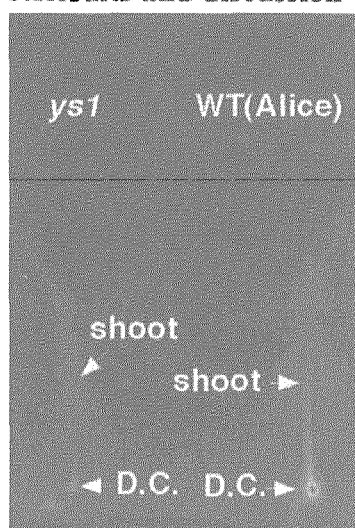


Fig.2 Images of the accumulated ^{52}Fe radioactivity with PETIS

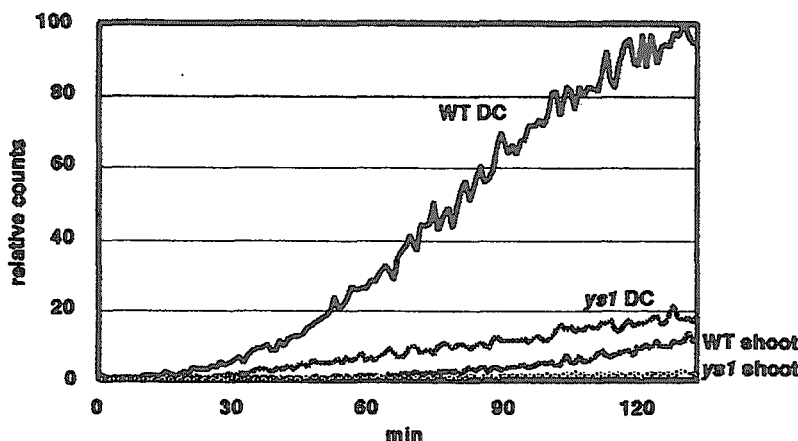


Fig.3 Time-course of ^{52}Fe translocation in maize plants at the positions DC and shoot, indicated in Fig.1.

WT : wild type (Alice)

ys1 : Fe(III)-MAs

transporter mutant

Figure 2 shows the distributions of the accumulated ^{52}Fe radioactivity picture obtained with PETIS. Although ^{52}Fe translocation was suppressed in the *ys1* mutant in comparison with the wild type plant, the ^{52}Fe accumulated slightly at the basal part of the leaf 'discrimination center (DC)'. Figure 3 shows the time-course of ^{52}Fe translocation at DC and the portion of the ground part indicated with 'shoot' in Fig. 1. In the wild type plant, ^{52}Fe radioactivity was detected at the DC about 10 min after the supply of ^{52}Fe , and in the *ys1* mutant, it took about 15 min. Furthermore, in the *ys1* mutant ^{52}Fe translocation at the DC was suppressed to about 20% of that of the wild type plant. ^{52}Fe translocation at the ground part was similarly suppressed.

In the present experiment, YS1 affected the ^{52}Fe translocation to the ground part, as expected. It was actually shown with the PETIS method for the first time that YS1 works to absorb Fe(III)- MAs in maize plants.

Moreover, we have made an animation of the PETIS images obtained in this experiment at the following site:
<http://park.itc.u-tokyo.ac.jp/pmp/>

References

- 1) H. Nakanishi et al., *Journal of Experimental Botany* 50: 637-643 (1999)
- 2) S. Mori et al., *Soil Science and Plant Nutrition* 46: 975-979 (2000)
- 3) N. Bughio et al., *Planta* 213: 708-715 (2001)
- 4) S. Kiyomiya et al., *Plant Physiology* 125: 1743-1754 (2001)
- 5) S. Kiyomiya et al., *Physiologia Plantarum* 13: 359-367 (2001)
- 6) S. Mori et al., *Soil Science and Plant Nutrition* 48: in press (2002)
- 7) C. Curie et al., *Nature* 409: 346-349 (2001)
- 8) S. Watanabe et al., *Radiochimica Acta* 89: 853 (2001)

2.27 Effects of cold stress on ^{11}C distribution in rice plants detected by PETIS detector

H. Hayashi*, H. Mano*, N. Suzui*, S. Matsushashi**, C. Mizuniwa**,
T. Ito**, N. Ishioka**, T. Watanabe**, T. Sekine**, H. Uchida***, A. Tsuji***
Department of Applied Biological Chemistry*,
Univ. Tokyo, Department of Ion-Beam-Applied Biology, JAERI**,
Central Research Laboratory, Hamamatsu Photonics Co.***

1. Introduction

Sieve tubes are the main routes for long distance transport of photoassimilates, such as sucrose and amino acids, in plants. This phloem transport process of photoassimilates is affected by the surrounding conditions, such as temperature and light conditions. To date, many experiments were performed to show the effects of cooling translocation pathways on the photoassimilate partitioning. Cooling treatments of translocation pathways may physically block a phloem transport transiently and this effect was genotype dependent⁽¹⁾. This inhibition was observed for a temperature drop of only 2.5 °C⁽²⁾ and for even a slowly cooling treatment (25°C to 1 °C in 40 min)⁽³⁾. These results suggested that the effects of cooling a phloem path were very fine and the phloem transport process was well regulated.

To know the cooling effects on the phloem transport in rice plants more deeply, we have

established the experiments for detailed analysis of phloem transport, such as speed of translocation and photoassimilate-partitioning patterns, by a positron-emitting tracer imaging system (PETIS).

As for the rice production, cooling stress is one of the severest problems in Japan. It is very important to understand the fine effects of cooling the rice plants on the photoassimilate partitioning for the stable rice production.

2. Experiments

Rice plants (*Oryza sativa* L. var. Nipponbare) were grown in a complete nutrient solution. The plants of the 9th-leaf stage were used for the experiments.

Around 100 MBq of $^{11}\text{CO}_2$ was applied to the small absorption chamber containing the tip of 7th leaf blade of rice plant for 10 min. Just after the absorption started, the ^{11}C -compounds distribution was detected by PETIS at the leaf

sheath position. To detect the effects of cooling, a basal part of the leaf blade was cooled down to 5 °C by a cooling block before (before-cooling treatment) or after (after-cooling treatment) $^{11}\text{CO}_2$ absorption by the leaf blade to the end of experiments.

3. Results and discussion

Phloem transport of ^{11}C -compounds measured by PETIS is very useful to discuss the effects of environmental stress on the long distance phloem transports of photoassimilates, specially the rate of transport and the pattern of photoassimilate distributions. In this experiment, the rate of phloem transport was calculated directly based on the data by PETIS.

Figure 1 shows the PETIS images of the absorption and translocation of ^{11}C -compounds during experiments. The absorbed ^{11}C -compounds at the leaf blade were transported only to the leaf sheath direction, namely to the leaf sheath, roots and other leaves, not to the tip of the leaf blade. Absorbed $^{11}\text{CO}_2$ was metabolized at the leaf blade and translocated to the bottom of the leaf sheath within 16 min in control plant (Figure 1 Control, Position A). Activities in positions B and C in the control plant started to increase at 12 min after ^{11}C application start and reached to a plateau at 30 min after application. In case of before-cooling treatment, ^{11}C reached to the position A within 14 min after ^{11}C application start, 2 min earlier than control plant. This acceleration of phloem

transport rate by this cooling treatment was clearer when the treatment was done after $^{11}\text{CO}_2$ application (Figure 1 cool 2). In this after-treatment, radioactivity was detected at the bottom of leaf sheath at 8 min after $^{11}\text{CO}_2$ application start. Total amount of translocated ^{11}C -compounds from leaf blade was severely decreased by the after-cooling treatment, not before-cooling treatment.

These results obtained by PETIS showed the reversible effects of cooling on the phloem transport in rice plants. Namely once the plant body was cooled down for a long time, the long distance transport process through sieve tubes could recover the performance. However, just after cooling, the phloem transport was severely affected. Unexpectedly, phloem transport rate was accelerated by the cooling treatments. Decreased amount of translocation may be compensated by the acceleration of phloem transport rate.

References

- 1) H. A. Hannah, M. J. Iqbal and F. E. Sanders, *Journal of Experimental Botany* 52 (2001) 1123-1127.
- 2) P. E. H. Minchin and M. R. Thorpe, *Journal of Experimental Botany* 34 (1983) 529-536
- 3) M. A. Grusak and P. E. H. Minchin, *Journal of Experimental Botany* 40 (1989) 215-223

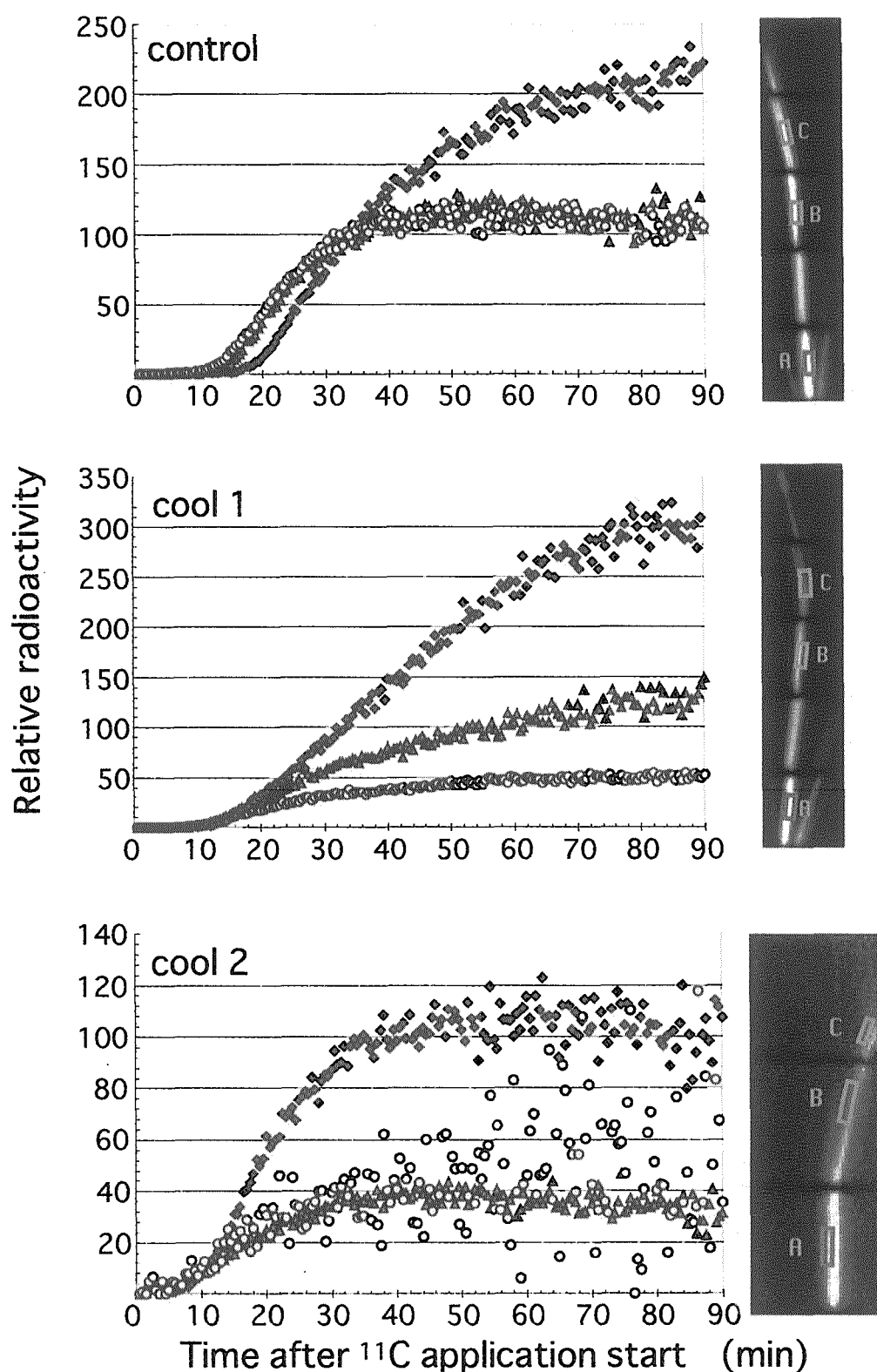


Figure 1 ^{11}C translocation pattern affected by cooling in rice plants. PETIS pictures showed the accumulation patterns of ^{11}C for 90 min. Changes in the relative radioactivity at the positions A(\diamond), B(Δ) and C(\circ) were plotted. Control: Control plant. Cool 1: Cooling treatment at the basal part of leaf blade was started before ^{11}C application. Cool 2: Cooling was started at the same position after ^{11}C application. $^{11}\text{CO}_2$ was applied for 2 min to the leaf blade.

2.28 Water and Trace Element Behavior in a Plant

T.M.Nakanishi*, J.Furukawa*, K.Tanoi*, M.Yokota*, S.Ueoka*, N.Ikeue*, Y.Hayashi*
 N.S.Ishioka**, S.Watanabe*, T.Sekine**, T.Ito**, T.Mizuniwa**, S.Matsushashi**,
 H.Uchida*** and A.Tsuji***

Graduate School of Agricultural and Life Sciences, The University of Tokyo*

Department of Ion-Beam-Applied Biology, JAERI**

Central research Laboratory, Hamamatsu Photonics K.K.***

1. Introduction

Since real-time movement of chemicals in living plant is expected to provide new information in plant physiology, the authors measured the absorption and translocation of water in a soybean plant. Until last year, we used $^{18}\text{F}\text{-H}_2\text{O}$ for tracing the water behavior in a soybean as well as in a cowpea plant. However, there was always a problem whether $^{18}\text{F}\text{-H}_2\text{O}$ really traces water movement itself. Therefore, we tried to produce $^{15}\text{O}\text{-H}_2\text{O}$ and compared the behavior of the tracer with that of ^{18}F .

The other objective of the research for this year was to compare the water uptake manner when supplied from the bottom part of the stem with that from the root. We also tried to study whether the water uptake was inhibited by the addition of Al in culture solution.

2. Experimental

Soybean plants after about two weeks in water culture were used for the experiment. To prepare the tracers, $^{18}\text{F}\text{-H}_2\text{O}$ was produced by $^{16}\text{O}(\alpha, \text{pn})^{18}\text{F}$ at Takasaki Establishment of JAERI and $^{15}\text{O}\text{-H}_2\text{O}$ by $^{14}\text{N}(\text{d}, \text{n})^{15}\text{O}$ reaction, at Hamamatsu Photonics, Co. About 10MBq/10ml of $^{18}\text{F}\text{-water}$ and 1GBq/10ml of $^{15}\text{O}\text{-water}$ were prepared and supplied to the plant. Because of the short half-lives of the nuclides, ^{15}O and ^{18}F , the absorption experiment was performed for 20min. and the uptake manner of the tracers were

compared. The tracers were supplied in two ways, from root and from the bottom part of the stem, where the root was cut off. The measurement was performed both by PETIS (Positron Emitting Tracer Imaging System) and luminography as we reported last year. Then 200 μM of AlCl_3 solution was prepared and the uptake manner of the tracers was measured in the same way.

3. Results and Discussion

When the uptake manner of the tracers were compared, $^{18}\text{F}\text{-H}_2\text{O}$ was found to be taken up much faster than $^{15}\text{O}\text{-H}_2\text{O}$. Since the determination of the water amount measured by PETIS was not able to be performed yet, we present the luminography of the plants (Fig. 1). In both cases, the tracers were supplied for 5 min and the plants were exposed to the imaging plates for 5 min. In the figure, the corrections due to the different half-lives of the nuclides were not performed. When $^{18}\text{F}\text{-H}_2\text{O}$ was supplied, ^{18}F was found to be translocated to the leaves as well as the stem. However, in the case of $^{15}\text{O}\text{-H}_2\text{O}$, though most of the radioactivity decayed out, not a trace of activity was found in leaves. The activity of ^{15}O was found only at the bottom part of the stem. When Al was supplied, it was found that the uptake amount was decreased not only for $^{18}\text{F}\text{-H}_2\text{O}$ but also for $^{15}\text{O}\text{-H}_2\text{O}$.

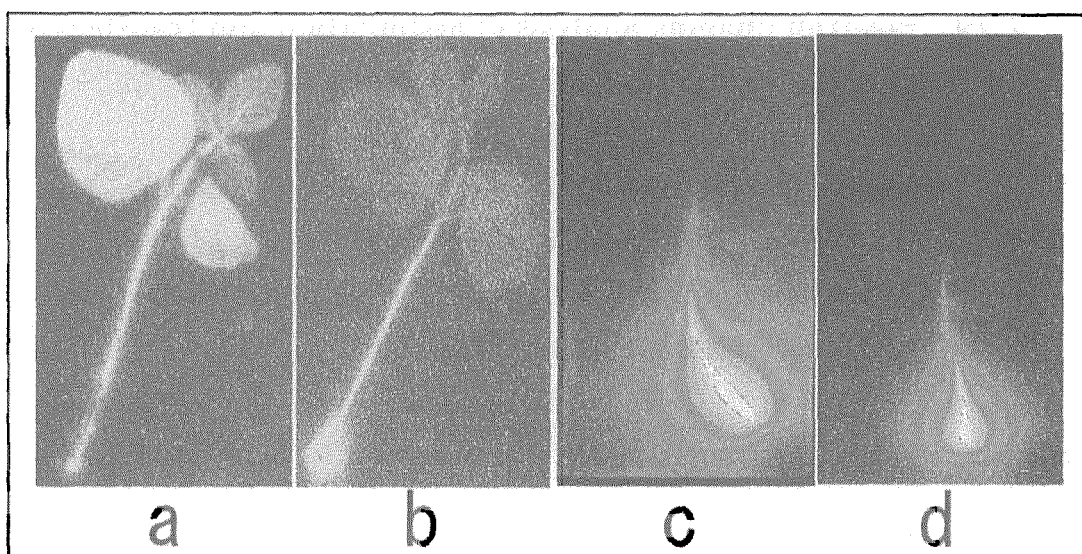


Fig. 1 Luminography of $^{18}\text{F}\text{-H}_2\text{O}$ (a and b) and $^{15}\text{O}\text{-H}_2\text{O}$ (c and d) taken up by soybean plants. The tracers were supplied from the bottom part of the stem with (b and d) or without (a and c) the addition of $200\ \mu\text{M}$ of AlCl_3 in solution.

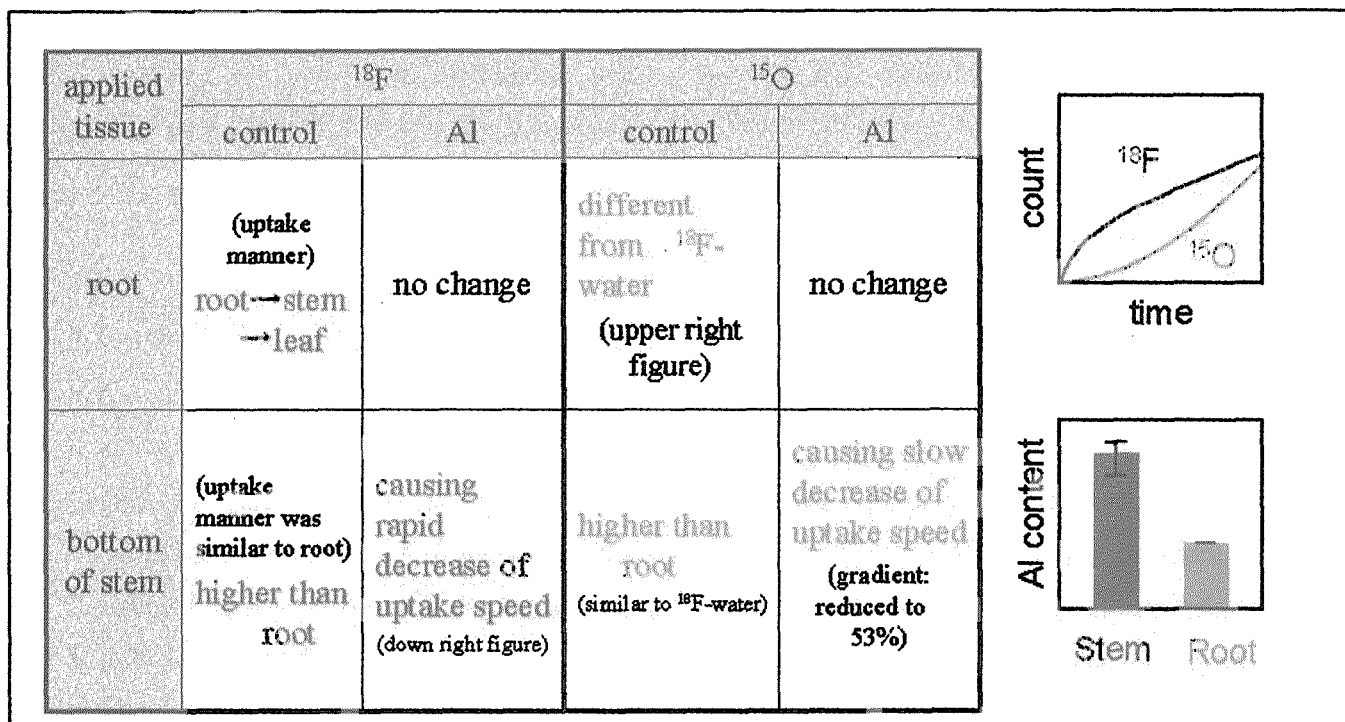


Fig.2 Schematic illustration to compare $^{18}\text{F}\text{-H}_2\text{O}$ and $^{15}\text{O}\text{-H}_2\text{O}$ uptake

The summary of the experiment of this year was illustrated in Fig.2. As shown in two figures in the right, the uptake speed of $^{15}\text{O}\text{-H}_2\text{O}$ was much slower than that of $^{18}\text{F}\text{-H}_2\text{O}$. The amount of Al accumulated at the bottom part of the stem was lower than that when supplied

from the root.

References

- 1) J.Furukawa et al. J.Radioanal. Nucl. Chem. 249 (2001) 495-498.
- 2) T.M.Nakanishi et al. *ibid*, 249 (2001) 503-507

2.29 Positron imaging analysis of assimilation and translocation of carbon and nitrogen sources in rice plant

S. Otsuki, Y. Sonoda, S. Saiki, S. Matsushashi*, S. Watanabe*,

N. S. Ishioka*, T. Sekine* and J. Yamaguchi

Graduate School of Division of Biological Sciences, Hokkaido University,

*Department of Ion-Beam-Applied Biology, JAERI

Introduction

Leaf photosynthesis is known to be affected by the levels of environmental nitrogen where the plants are grown¹⁾. It is also known that Nitrogen assimilation needs a carbon source to produce amino acid ²⁾. Thus, interaction between carbon assimilation and nitrogen assimilation is one of the most important factors regulating plant growth, in particular under elevated CO₂ conditions. The suppression of photosynthesis by CO₂ enrichment is associated with a decrease in total leaf nitrogen content¹⁾. This suggests that the elevated CO₂ condition may affect the assimilation and translocation of carbon and nitrogen sources.

It has been impossible to conduct dynamical studies in translocation and partitioning of fixed carbon as sugars and taken nitrogen as amino acids. Use of Positron Emitting Tracer Imaging System (PETIS) can visualize the real-time movement of these compounds and biosynthetic products ^{2),3)}. Here we report the results of two experiments for rice plants: effects of nitrogen supply to soil water on

¹⁵NO₃⁻ and ¹⁵NH₄⁺ uptake; translocation of ¹⁴CO₂, ¹⁵NO₃⁻ and ¹⁵NH₄⁺ under elevated CO₂ conditions.

Experiments

Rice (*Oryza sativa* L. cv. Nipponbare) seeds were germinated in water and cultured hydroponically in a growth chamber with a 14-h light (25°C) / 10-h dark (20 °C). The procedure for production of ¹⁵NO₃⁻, ¹⁵NH₄⁺ and ¹⁴CO₂ was described elsewhere³⁾.

1) Effects of nitrogen supply to soil water on ¹⁵NO₃⁻ and ¹⁵NH₄⁺ uptake

¹⁵NH₄⁺ was fed to the roots of rice plants cultivated for a month under distinct conditions: control; 4-day nitrogen deficiency; pretreatment with 0.3 mM NH₄⁺ for 2 h after 4-day nitrogen deficiency. Meanwhile, ¹⁵NO₃⁻ was fed to the roots pretreated with 0.3 mM NO₃⁻ for 2 h after 4-day nitrogen deficiency.

2) Translocation of ¹⁴CO₂, ¹⁵NO₃⁻ and ¹⁵NH₄⁺ under elevated CO₂ conditions

After rice plants were cultured on tap water for 3 weeks, half of the group was transferred to ambient (40 Pa) conditions, and the other

half to elevated CO_2 (140 Pa) conditions for 4 weeks. $^{15}\text{NO}_3^-$ and $^{15}\text{NH}_4^+$ were fed to the roots, and $^{14}\text{CO}_2$ was supplied at the middle part of the newest and second newest leaves through a

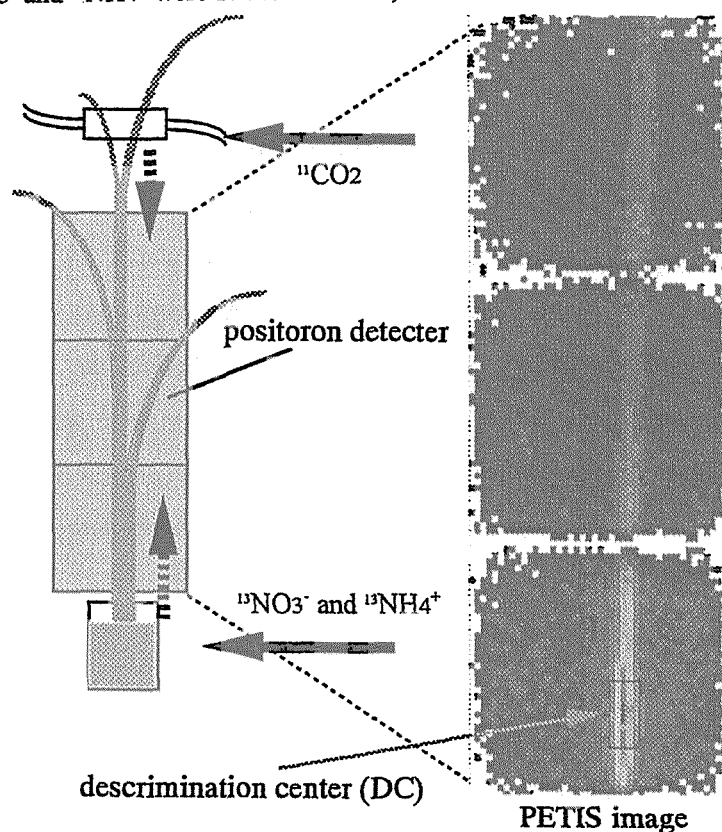


Fig. 1 Schematic of the present positron imaging experiment for a rice plant (left) and a resulting PETIS image (right).

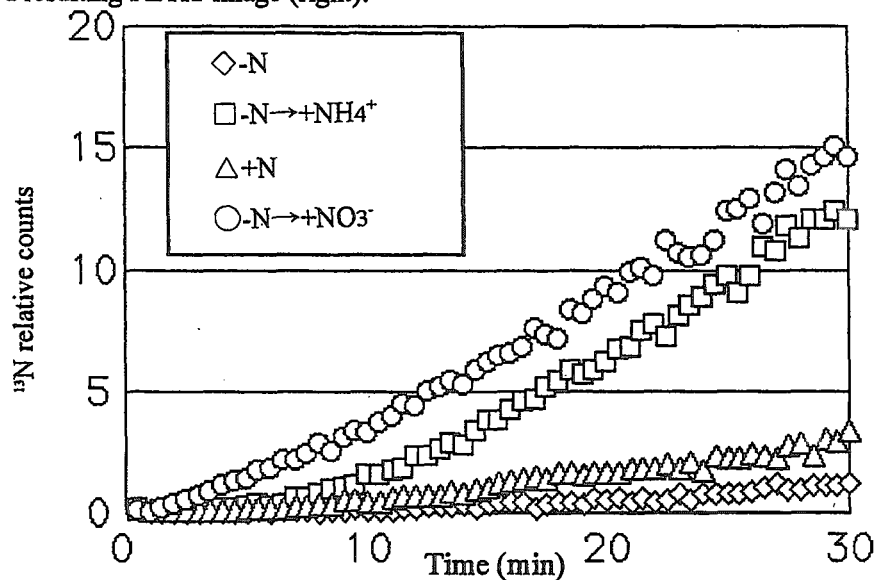


Fig. 2 ^{15}N translocation from roots to the discrimination center. Curves show the accumulated of radioactivity at the DC for different cultivation conditions: control (Δ); 4-day nitrogen deficiency (\diamond); pretreatment with 0.3 mM NH_4^+ for 2 h after 4-day nitrogen deficiency (\square); pretreatment with 0.3 mM NO_3^- for 2 h after 4-day nitrogen deficiency (\circ).

quvet to feed $^{14}\text{CO}_2$ ⁴⁾. PETIS measurements were performed in the same CO_2 conditions as at the foregoing cultivation stage.

Results and discussion

1) Effects of nitrogen supply to soil water on $^{15}\text{NO}_3^-$ and $^{15}\text{NH}_4^+$ uptake: Figure 1 shows a PETIS image obtained for $^{15}\text{NH}_4^+$. From these imaging data, the time-course of ^{15}N radioactivity at the discrimination center (DC) ²⁾ was obtained for the different pretreatment conditions, as shown in Fig. 2. This revealed that the pretreated rice with 0.3 mM NH_4^+ for 2 h after 4-day nitrogen deficiency and the pretreated rice plant with 0.3 mM NO_3^- for 2 h after 4-day nitrogen deficiency absorbed more amounts of ^{15}N throughout the experiment than the control plant and the plant cultivated in a 4-day nitrogen deficiency condition. This suggests that uptake of nitrogen sources from roots is induced by an increase of the nitrogen content around the roots.

It is possible that this induction of NH_4^+ uptake is caused by high affinity NH_4^+ transporter (*OsAMT1;2*) which is induced in NH_4^+ -treated rice roots after nitrogen deficiency ³⁾. Analysis of mutant and transgenic rice of *OsAMT1; 2* gene will verify the hypothesis.

The observed uptake delay between $^{15}\text{NO}_3^-$ and $^{15}\text{NH}_4^+$ at the DC may result from the fact that NO_3^- is translocated directly without metabolism, whereas NH_4^+ needs to be

assimilated into glutamine at the roots²⁾.

2) Translocation of $^{14}\text{CO}_2$, $^{15}\text{NO}_3^-$ and $^{15}\text{NH}_4^+$ under elevated CO_2 conditions

The results of this PETIS analysis detected no difference in translocation of $^{15}\text{NO}_3^-$, $^{15}\text{NH}_4^+$ and $^{14}\text{CO}_2$ between the rice plants cultivated in the ambient and elevated CO_2 conditions (data not shown). Although the elevated CO_2 condition may not affect the translocation of these compounds during a period of time as short as one hour, further experiments will be needed to confirm this phenomenon.

References

- 1) H. Nakano, A. Makino, T. Mae, Plant Physiology 115 (1997) 191-198.
- 2) S. Kiyomiya, H. Nakanishi, H. Uchida, A. Tsuji, S. Nishiyama, M. Ftatsubashi, H. Tsukada, N. S. Ishioka, S. Watanabe, T. Ito, C. Mizuniwa, A. Osa, S. Matsuhashi, S. Hashimoto, T. Sekine, S. Mori, Plant Physiology 125 (2001) 1743-1754.
- 3) N. S. Ishioka, H. Matsuoka, S. Watanabe, A. Osa, M. Koizumi, T. Kume, S. Matsuhashi, T. Fujimura, A. Tsuji, H. Uchida, T. Sekine, Journal of Radioanalytical and Nuclear Chemistry 239 (1999) 417-421.
- 4) S. Matsuhashi, S. Watanabe, N. S. Ishioka, C. Mizuniwa, T. Ito, T. Sekine, TIARA Annual Report (2001) 90-93.
- 5) Y. Sonoda, A. Ikeda, J. Yamaguchi, Rice Genetic Newsletter 17 (2000) 89-92.

2.30 Uptake of ^{18}F FDG and ^{13}N O_3^- in Tomato Plants

A. Tsuji, H. Uchida, T. Yamashita, S. Matsushashi*, T. Ito*, C. Mizuniwa*,
N.S. Ishioka*, S. Watanabe* and T. Sekine*

Central Research Lab., Hamamatsu Photonics K.K.,

*Department of Ion-Beam-Applied Biology, JAERI,

1. Introduction

Conventionally, observation of the movement or distribution of chemical compounds in plant bodies has been mainly carried out by using static methods such as autoradiography. We have developed a dynamic imaging method using positron emitting nuclides, which allows us to investigate biological functions of higher plants from a new angle.

The Positron Emitting Tracer Imaging System (PETIS) which we have developed is comprised of two planar detectors with position sensitivity to detect positron-electron-annihilation γ -rays. This measurement method visualizes dynamic movements of substances within a plant, without touching it, as a series of two-dimensional images.

In the present work, PETIS is used to study movements of nutrients or assimilation products introduced into a leafstalk in which those compounds are considered to be vigorously translocated. Behavior of ^{13}N O_3^- as a nutrient and ^{18}F FDG as an assimilation product in a tomato plant was studied with PETIS.

2. Experiments

The PETIS used in this experiment consists of two-dimensional block detectors one of which is composed of a $\text{Bi}_4\text{Ge}_3\text{O}_{12}$ scintillator array coupled to a position sensitive photomultiplier tube (PS-PMT; Hamamatsu R3941-2). The mosaic BGO array is formed of 22(X) x 23(Y)

BGO scintillators, placed with a 2.2 mm pitch, each of which is 2 mm square in cross section and 20 mm in depth.

^{18}F FDG and ^{13}N O_3^- were produced by using the TIARA AVF cyclotron.

Tomato plants were grown from seed in vermiculite at 27°C in a controlled environmental chamber. The plants cultivated for 4~6 weeks (about 40 cm in height) were used for the experiment.

The water containing ca. 10 MBq/ml of ^{18}F FDG or 10 MBq/ml of ^{13}N O_3^- was fed to a scratched leafstalk of a plant or a cut leafstalk, which naturally loses its leaf. Furthermore, a part of a leafstalk was heated with a heater to make the phloem tissue in the part lose its function as a translocation pipe for assimilation products.

3. Results and discussion

When ^{13}N O_3^- was fed onto a cut leafstalk, the ^{13}N O_3^- taken was found to be translocated to the main stem. But, the ^{13}N O_3^- taken from a scratched leafstalk, with its leaf attached, showed no such movement. Since the translocation of water depends on leaves' activity in photosynthesis and transpiration, it was anticipated that, when a leaf was removed, a taken radioactive tracer may be translocated in a countercurrent water flow.

When a part of a leafstalk without the leaf was heated, ^{13}N O_3^- and ^{18}F FDG were found to be translocated from the cut leafstalk to the main

stem, as shown in Figs. 1 and 2. This behavior was almost the same as that observed in the experiments without heating (data not shown).

The fact that the heat treatment had no effect to the tracer movement suggests that the tracers were mainly taken into xylem vessels, not into phloem. This speculation also fits the result that the tracers were not translocated towards the

stem in the case of the leafstalks with the leaves attached in which transpiration may actively occur.

The present work has shown that PETIS is useful for studying translocation of nutrients and assimilation products from various parts of a plant.

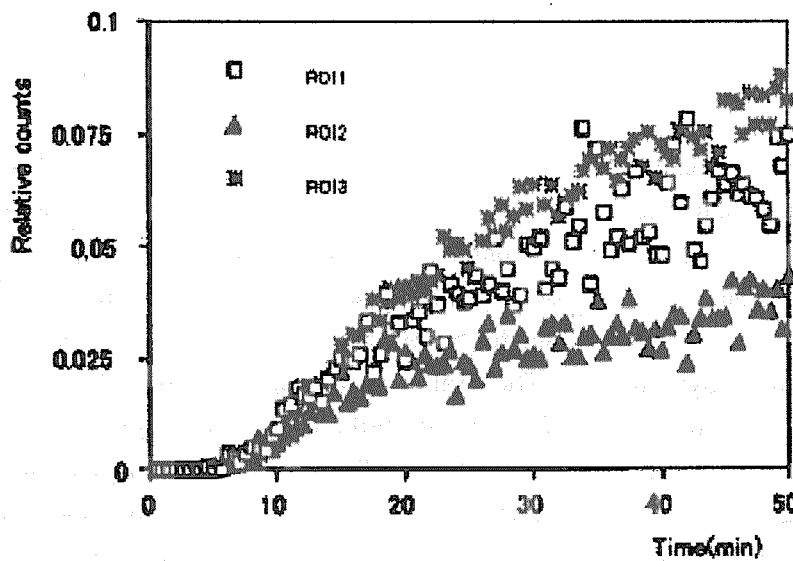


Fig. 1 Time course study of ^{18}F FDG uptake from a cut leafstalk of a tomato plant at three positions in the leafstalk. ROI1 was at the top of the leafstalk, and ROI3 at the bottom of the leafstalk. ROI2 was between ROI1 and ROI3, and this part was heated.

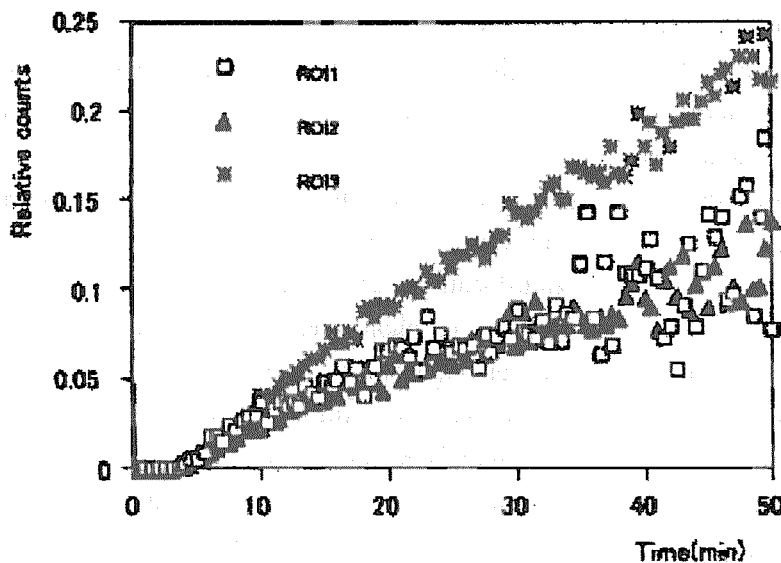


Fig. 2 Same as Fig. 1, except for $^{13}\text{NO}_3^-$ uptake.

2.31 Utilization of Ion Beam-irradiated Pollen in Plant Breeding

S. Kitamura**, Y. Yokota*, M. Inoue*, Y. Hase** and A. Tanaka**

Faculty of Agriculture, Kyoto Prefectural University*, Department of
Radiation Research for Environment and Resources, JAERI**

1. Introduction

Pollen is indispensable to sexual reproduction in different plant species. Previously, we found a unique phenomenon, "leaky pollen", in which internal substances leaked through an opening in outer membrane of tobacco pollen grain exposed to He ion^{1),2)}. This phenomenon was specific for the ion beam exposure, and seemed to be resulted from physical lesions induced in outer wall of pollen. If exogenous DNA can be incorporated into pollen cell through the opening cleavage and transferred to egg cell, pollen can be used as a gene vector in combination with crossing.

When tobacco pollen exposed to C ion was suspended in the medium with pCH and used for pollination, several survival seedlings were obtained in the medium with hygromycin. However, corresponding band of hygromycin-resistance gene was not detected in them⁵⁾. On the other hand, it was found that nuclease activity was high in mature pollen, resulting in the degradation of exogenous plasmid DNA suspended in the medium⁴⁾. To establish the gene transfer system using the pollen exposed to ion beam, it is necessary to

reduce the nuclease activity during the period of the pollen incubation in the medium with exogenous DNA.

In the present experiment, we examined the procedure for removing nuclease in tobacco pollen.

2. Materials and Methods

Nicotiana tabacum L. cv. Bright Yellow 4 was used. All treatments were carried out at room temperature.

Mature and dry pollen was suspended in a pollen germination medium with 10% sucrose, 100 μ g/ml boric acid and 0.7 % agar during different periods, and washed with the same medium. Then, they were incubated in the medium with 50 μ g/ml pCH plasmid, 10 % sucrose and 100 μ g/ml boric acid, and subjected to electrophoresis in a 1.0 % agarose gel. Germination rate was also determined 24 hr after setting in the germination medium under 25 °C-dark condition.

3. Results and Discussion

Nucleases were released from tobacco pollen and their activities were very high^{6),7),8)}.

In this experiment, different treatments in combination with the period of the

pollen suspension and number of washing cycles prior to the pollen incubation in the medium with pCH were performed. As shown in Fig.1, the degradation of plasmid DNA was observed in the pollen without pre-treatment 5 min after the beginning of incubation (Lane 16). Over 30 min of incubation (Lane 11-15), plasmid DNA was completely degraded. On the other hand, in the case of the pre-treated pollen, the degradation was slightly reduced by the suspension for 10 (Lane 7), 30 (Lane 10) and 60 min (Lane 4). However, pre-treatment had no effect on the removal of nucleases and the reduction of their activities.

Pollen germination was remarkably reduced by pre-treatment, although 25.7 % of germination rate was retained in the pollen suspended for 1 hr, as compared with 63.2 % in non-treated pollen.

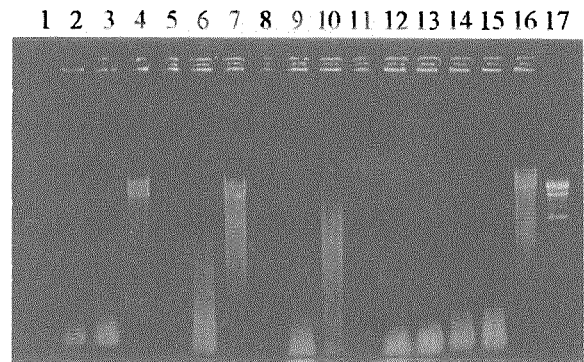


Fig. 1 Degradation of plasmid DNA after pre-treatment.

Each lane number is the same as shown in Table 1.

Furthermore, the nuclease activity could not be reduced by pre-treatment at 0 °C and the EDTA application in the suspension medium (data not shown).

Again, it is confirmed that nuclease released from pollen is a big obstacle for the gene transfer system using the pollen exposed to ion beam. Another procedure should be developed for dealing with nucleases.

Table 1 Pollen germination rate after different pre-treatments

Number	Pre-treatment		Incubation period	Pollen germination rate (%)
	suspension period (min)	Number of cycles		
1	-	-	-	63.2 ± 3.0 ¹⁾
2	60	1	3 hr	25.7 ± 3.3
3	60	1	1 hr	28.5 ± 1.2
4	60	1	30 min	32.4 ± 1.5
5	10	3	3 hr	21.4 ± 1.4
6	10	3	1 hr	33.8 ± 1.4
7	10	3	30 min	39.5 ± 1.4
8	30	1	3 hr	26.4 ± 0.8
9	30	1	1 hr	31.4 ± 3.6
10	30	1	30 min	42.7 ± 1.2
11	-	-	12 hr	
12	-	-	6 hr	
13	-	-	3 hr	
14	-	-	1 hr	
15	-	-	30 min	
16	-	-	5 min	
17	pCH			

1) mean ± S. D.

References

- 1) M. Inoue, H. Watanabe, A. Tanaka and A. Nakamura, TIARA Annual Report 2 (1992) 50-52.
- 2) A. Tanaka, H. Watanabe, S. Shimizu, M. Inoue, Y. Kikuchi, Y. Kobayashi and S. Tano, Nuc. Instr. Meth. Phys. Res. B129 (1997) 42-48.
- 3) M. Inoue, S. Kitamura, Y. Toda, H. Watanabe, A. Tanaka and Y. Hase, JAERI-Review 99-025 (1999) 80-81.
- 4) Y. Hase, Y. Toda, A. Tanaka, M. Inoue and H. Watanabe, JAERI-Review 99-025 (1999) 82-83.
- 5) Y. Toda (1998), Thesis of Master Degree, Kyoto Prefectural University.
- 6) M. Vischi and S. Marchetti, Theor. Appl. Genet. 95 (1997) 185-190.
- 7) J. Matousek and J. Tupy, Plant Sci. Lett. 30 (1983) 83-89.
- 8) I. Negrutiu, E. H. Bors and I. Potrykus, Biotechnology and Ecology of pollen, Springer Verlag (1986) pp.65-70.

2.32 Study on the apoptosis induction by a local damage using penetration controlled ion-beam exposure

Y. Hase* and S. Wada**

Department of Radiation Research for Environment and Resources, JAERI*

Department of Veterinary Medicine, Kitasato University**

Introduction

Apoptosis is known to be induced by the damage on DNA. Some evidence suggests that the damage on cell membrane is also involved in the apoptosis induction¹⁾. In this experiment, we measured the fraction of apoptosis induced cells following ion beam exposure with different penetration depth, in order to examine whether the damage on cell membrane is involved in the apoptosis induction.

Materials and Methods

Chinese hamster ovary (CHO) cells grown on a kapton film (8- μ m thick) were exposed to the carbon ions at the distance of 26, 27 and 28 mm from the beam window using the penetration controlled irradiation apparatus for cell²⁾. The initial fluence of carbon ions was counted using the CR-39 track detector to be 1×10^7 p cm⁻¹. Apoptosis induction was detected by the TUNEL assay.

Results and Discussion

The fraction of the TUNEL-positive cells was about 45% at the distance of 26 and 27 mm but it decreased to 18.8% at the distance of 28 mm (Figure 1). The fraction was 6.7% in the control. When CR-39 track detector was irradiated at the distance of 26, 27 and 28 mm from the beam window, etch pit could not be found only in the case of 28 mm. This indicates that the range of carbon ions was shorter than the detection limit

when it was irradiated at the distance of 28 mm. These results may indicate that the damage on cell membrane is also involved in the apoptosis induction. We are going to examine the damage on nuclear DNA.

References

- 1) I.R.Radford Int. J. Radiat Biol. 25 (1999) 521-528.
- 2) A.Tanaka et al. Nucl. Instru. and Meth. in Phys. Res. B 129 (1997) 42-48.

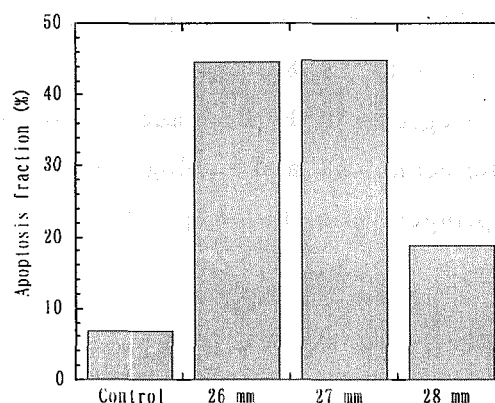


Figure 1. Apoptosis fraction of cells exposed to carbon ions at different distances from beam window. Apoptosis induction was detected by the TUNEL assay.

3. Radiation Chemistry / Organic Materials

3.1	Preparation of Functional Nano-porous Membranes	111
	M. Asano, H. Koshikawa, Y. Maekawa, M. Yoshida and K. Ogura	
3.2	Preparation of Copper Nanowires using Ion Track Membranes.	113
	H. Koshikawa, Y. Maekawa, M. Asano and M. Yoshida	
3.3	Nano-wire Formation and Selective Adhesion on Substrates by Single Track Gelation of Polysilanes	115
	S. Seki, S. Tsukuda, Y. Yoshida, S. Tagawa, M. Sugimoto, N. Morishita and S. Tanaka	
3.4	Oxidation Product Yields of Phenol along Heavy Ion Trajectory in Aqueous Solution : Differential G-value.	117
	M. Taguchi, N. M. Thu, T. Kojima	
3.5	Crosslinking of Polymers in Heavy Ion Tracks	119
	H. Koizumi, M. Taguchi, Y. Kobayashi and T. Ichikawa	
3.6	Primary Process of Radiation Chemistry Studied by Ion Pulse Radiolysis	121
	Y. Yoshida, S. Seki, A. Saeki, S. Tagawa, M. Taguchi, T. Kojima and H. Namba	
3.7	Dosimetry for 3-45 MeV/u Ion Beams using Thin Film Dosimeters	123
	T. Kojima, H. Sunaga, H. Takizawa, H. Hanaya and H. Tachibana	

This is a blank page.

3.1 Preparation of functional nano-porous membranes

M. Asano*, H. Koshikawa*, Y. Maekawa*, M. Yoshida*
and K. Ogura**

Department of Material Development, JAERI*

College of Industrial Technology, Nihon University**

1. Introduction

If the membrane of poly(ethylene terephthalate) (PET) and poly(diethyglycol-bis-arylcarbonate)(PDEGAC) is etched after ion irradiation, the pore will be formed along the ion path. The shape and the diameter size of the pore can be controlled according materials, ions, accelerated energies, and etching conditions. Based on this method, membranes, which have uniform pore sizes, are applied to the separation of fission product elements. The ion porous membranes which have nano-scale pore resulting from ion irradiation and etching treatment, have been used to test their performance for the separation of polyethylene glycol with various molecular weight as well as the separation of albumin and γ -globulin from the mixture solutions¹⁾. Gas

and liquid generally flow smoothly through such porous separation membranes. In current work, the shape of the pores in the membranes has been controlled by combination of ion irradiation and etching treatment. In this paper, we report the two step etching method to prepare the membranes that possess pores with the funnel shape (horizontally spread) at the surface, connected by the cylindrical pore at the center of the membrane.

2. Experimental

The PET(38 μ m) films(Diafoil®) used in this study were obtained from Diafoil Hoechst Co., Ltd.. The PDEGAC(38 μ m) film was

prepared according to a conventional cast polymerization with 3 wt-% of diisopropylperoxydicarbonate as a radical initiator at 70°C for 24 hours. The films were irradiated with ⁴⁰Ar ion (150MeV), ³⁸Ar ion (195MeV), ⁸⁴Kr ion (322MeV), and ¹²⁹Xe ion (450MeV) in the densities of 3x10⁶ ions/cm² using TIARA cyclotron. The following solution (PEWx) was used as etching solution in the first step of etching treatment.

PEWx = 15wt-% KOH + x wt-% C₂H₅OH + (85-x)wt-% H₂O

Then, 0.1N-0.3N NaOH aqueous solutions were used as etching solutions in the second step. The pores size was confirmed by electron conductivities through the membranes. The shapes and sizes of ion pores were confirmed by using scan electron microscope(SEM).

3. Results and Discussion

Fig.1 shows the effect of PEWx solution concentration on the V_b of PET before irradiation. From the figure, it is clear that higher the x of PEWx solutions, as well as C₂H₅OH concentrations, higher the V_b. In addition, when the treatment is done in high temperature, V_b will be high. However, the etching sensitivity S, which is expressed as V_t/V_b, will be low when the treatment is done in high concentration of C₂H₅OH and high temperature. When etching sensitivity is small, the etch pit will horizontally formed and spread, and then based on this characteristic, the pore

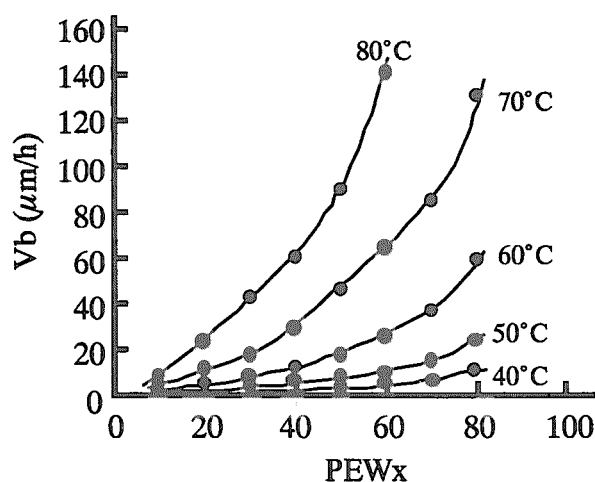


Fig. 1 Concentration effect of PEWx the Vb of PET films at different etching temperatures

part of the filter can be designed relation to the first step of etching treatment.

Fig. 2 shows the changes of the pore diameter of the PET film surface when the etching was treated with 0.1N-0.3N NaOH solutions at 70°C after Xe ion irradiation. It is understood that the pore diameter increased with the increase of etching time and concentration of NaOH aqueous solution. In addition, it is understood that a circle shape of etch pit (the shape of the pore) is formed when the etching sensitivity S of each system (Q value at 0.1N:185, 0.2N:497, 0.3N:382) is high. Furthermore, based on this treatment, cylindrical pores at the middle of the membrane can be designed in nano scale at the second step of the etching treatment.

Fig.3 shows the SEM photograph of the surface of the etched porous membrane resulting from second step etching treatment. From this figure, it is clear that the membrane possesses the pores with the funnel shape of $0.5\mu\text{m}$ diameter at the surface and the cylindrical shape of $0.1\mu\text{m}$ diameter at the middle of the membrane.

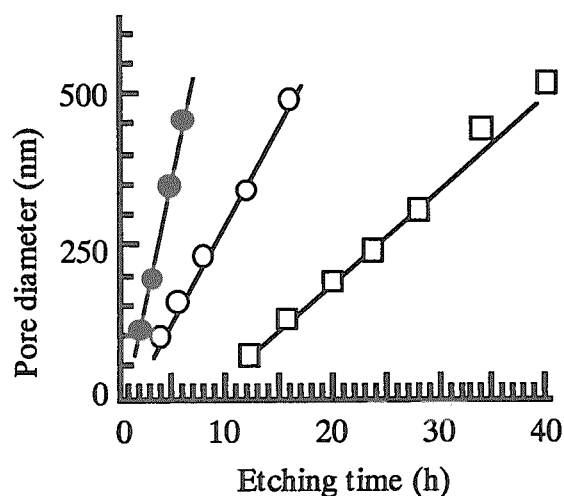


Fig. 2 Pore diameters plotted as a function of etching time at different etchant concentrations ; (\square) 0.1 N, (\circ) 0.2N, (\bullet) 0.3N. Ion beam : $^{129}\text{Xe}(450\text{MeV})$

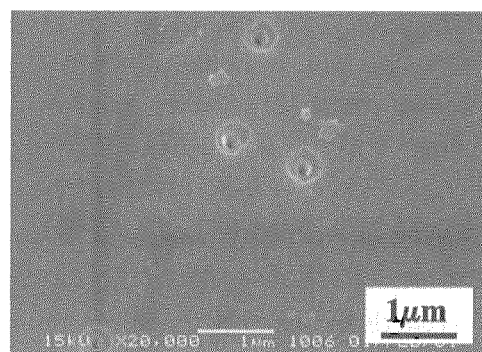


Fig. 3 SEM observation of PET film obtained by two steps etching: (1) PEW50 at 70°C for 30sec and (2) 0.2N NaOH at 70°C for 4h. Ion beam : $^{129}\text{Xe}(450\text{MeV})$

References

- 1) M. Asano, H. Koshikawa, Y. Maekawa, M. Yoshida, T. kume, and K. Ogura, TIARA-Annual Report 2000, 118